Bilel Kallel

Design of Inductive Power Transmission System for Low Power Application with Movable Receiver and Large Air Gap

Scientific Reports on Measurement and Sensor Technology

Volume 12

Prof. Dr.-Ing. Olfa Kanoun (Editor)

Bilel Kallel

Design of Inductive Power Transmission System for Low Power Application with Movable Receiver and Large Air Gap

TECHNISCHE UNIVERSITÄT
CHEMNITZ

Universitätsverlag Chemnitz
2019

Impressum

Bibliografische Information der Deutschen Nationalbibliothek

Die Deutsche Nationalbibliothek verzeichnet diese Publikation in der Deutschen Nationalbibliografie; detaillierte bibliografische Angaben sind im Internet über http://www.dnb.de abrufbar.

Titelgrafik: Chemnitz School of Metrology
Satz/Layout: Bilel Kallel

Technische Universität Chemnitz/Universitätsbibliothek
Universitätsverlag Chemnitz
09107 Chemnitz
https://www.tu-chemnitz.de/ub/univerlag

readbox unipress
in der readbox publishing GmbH
Am Hawerkamp 31
48155 Münster
http://unipress.readbox.net

ISSN 2509-5102 print - ISSN 2509-5110 online

ISBN 978-3-96100-083-8

http://nbn-resolving.de/urn:nbn:de:bsz:ch1-qucosa2-329759

TECHNISCHE UNIVERSITÄT
CHEMNITZ

Design of Inductive Power Transmission System for Low Power Application with Movable Receiver and Large Air Gap

Von der Fakultät für Elektrotechnik und Informationstechnik

der

Technischen Universität Chemnitz

genehmigte Dissertation

zur Erlangung des akademischen Grades

DOKTOR-INGENIEUR

(Dr.-Ing.)

vorgelegt

von M. Sc. Bilel Kallel

geboren in Sfax, Tunesien

Gutachter:

Univ.-Prof. Dr.-Ing. Olfa Kanoun (Technische Universität Chemnitz)

Univ.-Prof. Dr.-Ing. Hamadi Ghariani (National Engineering School of Sfax)

Univ.-Prof. Dr.-Ing. Roman Gruden (DHBW Stuttgart)

Tag der Einreichung: 08. Oktober 2018

Tag der Verteidigung: 18. Dezember 2018

Abstract

Inductive power transmission is very useful, not only for systems where energy transfer should take place in hazardous, humid and wet areas, but also for mobile and very small systems. It finds today a widespread use in several fields, such as industry, automotive, medicine and smart buildings. For a good efficiency and a high-power transmission, the sending and the receiving coils should be perfectly aligned and close to each other. A misalignment between the sender and the receiver becomes unavoidable especially for systems with movable parts.

This thesis aims to improve the transmitted power, the mutual inductance, the power at the load, and consequently the power transmission efficiency in case of lateral misalignment between the sending and receiving coils and at large coil-to-coil distance. For this purpose, we adopt a multi input single output (MISO) coil system able to orientate the issued magnetic field to the receiving coil by powering the neighbouring sending coils of the active ones with a weak current in the opposite direction. Furthermore, an analytical model of the used coils and an accurate three-dimensional model of the system have been developed to calculate the induced voltage, the induced current, and the equivalent mutual inductance. Both simulation and experimental results prove that the proposed multi-coil inductive system having an hexagonal arrangement and the sending coils, which have the half diameter of the receiving coil, is able to improve significantly the transmitted power in case of lateral misalignment and big air gap. The novel MISO system reaches better efficiency beginning with an air gap of 50% of the sending coil diameter, and a misalignment of 28% of the sending coil diameter. It reaches the double of the transmitted power of the conventional two-coil inductive system at 50 mm air gap (corresponding to 166% of the sending coil diameter) and at 10 mm lateral misalignment (corresponding to 33% of the sending coil diameter).

In order to improve the equivalent mutual inductance between the primary and secondary sides and to avoid energy losses, we propose a receiver detection method using the sending coils themselves as detectors. Thereby, only the sending coils, under the receiver,

are activated and the others remain switched off. For that, the peak of the AC current of the sending coils, is measured and then compared to a detection threshold. The excitation strategy of the active sending coils is optimized corresponding to the receiving coil position. The novel excitation strategy increases the mutual inductance by 85% and the induced voltage by 13% at perfect alignment and by 30% and 10% respectively at 10 mm lateral misalignment, in comparison to the MISO system without a receiver detector and coil-excitation strategy.

In order to increase the transmitted power by resonance, different system topologies have been investigated, such as series-series SS, series-parallel SP, parallel-series PS, and parallel-parallel PP topologies for different levels of load impedance. The results show that a multi-coil inductive system with parallel-parallel PP topology realizes a higher transmitted power than the other topologies for both high and low load impedance values.

The proposed multi-coil inductive system is suitable for low-power systems, such as wireless sensors and biomedical implants, but can be also applied to higher range of power at a flexible position of the receiver.

Keywords: Inductive power transmission, multi-coil systems, lateral misalignment, large air gap, movable receiver, equivalent mutual inductance, detection method, excitation strategy, energy management, topologies.

Kurzfassung

Die induktive Energieübertragung ist interessant, nicht nur für Systeme, bei denen die Energieübertragung in rauen, feuchten und nassen Bereichen erfolgen soll, sondern auch für mobile und sehr kleine Systeme. Diese Art von Energieübertragung findet heute eine breite Anwendung in verschiedenen Bereichen, wie z.B. Industrie, Automobil, Medizin und intelligente Gebäude. Um eine gute Effizienz und eine hohe Energieübertragungsleistung zu realisieren, sollten die Sende- und Empfangsspulen perfekt ausgerichtet und nahe beieinander sein. Insbesondere bei Systemen mit beweglichen Teilen ist jedoch eine Fehlausrichtung zwischen Sender und Empfänger unvermeidlich.

Diese Arbeit zielt darauf ab, die übertragene Leistung, die gegenseitige Induktivität, die Leistung an der Last und damit den Wirkungsgrad der Leistungsübertragung im Falle einer seitlichen Fehlausrichtung zwischen Sende- und Empfangsspule und bei großem Abstand von Spule zu Spule zu verbessern. Zu diesem Zweck wird ein Multi-Input Single-Output (MISO)-Spulensystem vorgeschlagen, das in der Lage ist, das ausgegebene Magnetfeld auf die Empfangsspule auszurichten, indem die benachbarten Spulen der aktiven Sendespulen mit einem schwachen Strom in der entgegengesetzten Richtung versorgt wird. Darüber hinaus wurde ein analytisches Modell für die verwendeten Spulen und ein genaues dreidimensionales Modell für das System entwickelt, um die induzierte Spannung, den induzierten Strom und die äquivalente gegenseitige Induktivität zu berechnen. Sowohl die Simulation als auch die experimentellen Ergebnisse belegen, dass das vorgeschlagene induktive Mehrfachspulensystem mit hexagonaler Anordnung und die Sendespulen, die den halben Durchmesser der Empfangsspule haben, in der Lage sind, die Sendeleistung bei lateraler Fehlausrichtung und großem Luftspalt deutlich zu verbessern. Das neuartige MISO-System erreicht einen besseren Wirkungsgrad, beginnend mit einem Luftspalt von 50% des Sendespulendurchmessers und einer Fehlausrichtung von 28% des Sendespulendurchmessers. Sie erreicht bei 50 mm Luftspalt (entspricht 166% des

Sendespulendurchmessers) und bei 10 mm seitlichem Versatz (entspricht 33% des Sendespulendurchmessers) das Doppelte der Sendeleistung des herkömmlichen Zwei-Spulen-Induktivsystems.

Um die äquivalente gegenseitige Induktivität zwischen Primär- und Sekundärseite zu verbessern und Energieverluste zu vermeiden, schlagen wir ein Verfahren zur Detektion des Empfängers vor, bei dem die Sendespulen selbst als Detektoren verwendet werden. Dabei werden nur die Sendespulen unter dem Empfänger aktiviert und die anderen bleiben ausgeschaltet. Dazu wird der Scheitelwert des Wechselstroms der Sendespulen gemessen und mit einem vorgegebenem Schwellenwert verglichen. Die Anregungsstrategie der aktiven Spulen wird entsprechend der Position der Empfangsspule optimiert. Die neuartige Anregungsstrategie erhöht die gegenseitige Induktivität um 85% und die induzierte Spannung um 13% bei perfekter Ausrichtung und um 30% bzw. 10% bei 10 mm seitlichem Versatz, im Vergleich zum MISO-System ohne Empfängerdetektor und Spulenanregungsstrategie.

Um die übertragene Leistung durch Resonanz zu erhöhen, wurden verschiedene Systemtopologien untersucht, wie z.B. Serien-SS, Serien-Parallel-SP, Parallel-Series-PS und Parallel-Parallel-PP-Topologien für verschiedene Stufen der Lastimpedanz. Die Ergebnisse zeigen, dass ein MISO System mit parallel-paralleler PP-Topologie eine höhere Sendeleistung realisiert als die anderen Topologien für hohe und niedrige Last-Impedanzen.
Das vorgeschlagene induktive Mehrspulensystem eignet sich für Systeme mit geringer Leistung, wie drahtlose Sensoren und biomedizinische Implantate, kann aber auch flexibler Position des Empfängers in einen höheren Leistungsbereich angewendet werden.

Schlagworte: Induktive Kraftübertragung, Mehrspulensysteme, seitlicher Versatz, großer Luftspalt, beweglicher Empfänger, äquivalente Gegeninduktivität, Detektionsschaltung, Erregungsstrategie, Energiemanagement, Topologien.

Content

List of abbreviations and symbols

ADC	Analogue-to-digital converter
AC	Alternating current
CCD	Coil to coil distance
CET	Contactless energy transfer
CPT	Capacitive power transmission
DAC	Digital-to-analogue converter
DC	Direct current
EMF	Electromagnetic field
FEM	Finite element method
emf	Electromotive force
IC	Integrated circuit
IPT	Inductive power transmission
ICNIRP	International commission on non-ionizing radiation protection
IRPA	International radiation protection association
LDR	Light dependent resistor
MIMO	Multi input multi output
MISO	Multi input single output
MIT	Massachusetts institute of technology
NIR	non-ionizing radiation
PP	Parallel-series topology
PS	Series-parallel topology
RF	Radio frequency
RFID	Radio frequency identification
SAR	Specific energy absorption rate
SHM	Structural health monitoring
SIMO	Single input multi output
SISO	Single input single output
SOA	State of the art
SP	Series-parallel topology

SS	Series-series topology
WPT	Wireless power transmission
a	Winding's wire radius
a_i	Radius of a single circular loop
b	Coil length
C	Capacitance
C_L	Coil self-capacitance
D	Coil diameter
d	Coil to coil axial distance
$E( )$	Complete elliptic integral of the second kind
f	Frequency
I	Electric current
I_{ind}	Induced current
k	Coil coupling factor
$K( )$	Complete elliptic integral of the first kind
L	Coil self-inductance
Leq	Equivalent inductance
M	Mutual inductance
Meq	Equivalent mutual inductance
m	Number of layers of the coil
m_i	Modulus of the complete integral
N	Number of turns of the coil
P	Power
P_S	Source power of the primary circuit
P_{RL}	Power at the load
P_t	Transmitted power from the primary to the secondary side
Q	Coil quality factor
q_{enc}	Amount of charge contained within a closed surface
R	Resistance
r	Coil mean radius

R_{coil}	Coil resistance
Req	Equivalent resistance
R_L	Load
r_o	Coil outer radius
r_I	Coil inner radius
S	Power density
V	Voltage
V_{ind}	Induced voltage
V_{ref}	Reference voltage
X	Impedance amplitude
Z	Impedance
Z_r	Reflected impedance from the secondary to the primary side
$\vec{B}$	Magnetic field
$\vec{E}$	Electric field
ε_0	Electric permittivity of vacuum
Δ	Lateral misalignment
ω	Angular frequency
ϕ	Impedance phase
η	System efficiency
τ	Factor describing the proportion of the sending coil's diameter over the coil-to-coil vertical distance
Φ	Magnetic flux
μ_0	Vacuum permeability

In loving memory of my father

Ameur Kallel

My first source of inspiration and motivation

My mother

Mahbouba

No words can describe her sacrifices.

Her endless support and encouragement enable me to reach my goals

My wife

Fatma

and

My brothers

Akram & Hedi

Thanks for supporting me and being always by my side.

Bilel Kallel

Acknowledgement

This dissertation was carried out in the chair for Measurement and Sensor Technology (MST) at Technische Universität Chemnitz, Germany in cooperation with Computer, Electronic & Smart Engineering systems design (CES) laboratory at the National Engineering School of Sfax (ENIS), Tunisia.

First, I would like to express my deep appreciation to my supervisor, Professor Olfa Kanoun at Technische Universität Chemnitz, Germany for her continuous support and encouragement along my PhD phases, her contributions of times and her generous guidance.

I would like to express my special thanks to my supervisor, Professor Hafedh Trabelsi at National Engineering School of Sfax, Tunisia for his guidance and encouragement that help me to make my PhD.

I would like to thank all my colleagues in the energy autonomous sensors group at MST Lab, especially Dr. Thomas Keutel, Dr. Christian Viehweger, Slim Naifar, Sonia Bradai, Issam Chaour and Ghada Bouattour for their fruitful discussions.

My special thanks to Dhouha El Houssaini, Sabrine Khriji and again Ghada Bouattour for their efforts and support during the submission phase of the dissertation.

Special thanks go to my family members and friends for their advices and continuous help.

I appreciate also the financial supports from the German academic exchange service (DAAD) and the exchange program InProTUC offred by Technische Universität Chemnitz during my Ph.D. and my research visit to Eindhoven University of technology.

Chapter 1

Introduction

Wireless power transmission is getting more attention since the end of 19th century as an alternative, energy efficient power energy supply for contactless and wireless systems. This was in 1891, when Nicolas Tesla demonstrated that the transmission of electrical energy without wires depends on electrical conductivity [1]. Afterwards, in 1893, Tesla succeeded in the illumination of vacuum bulbs, wirelessly, for power transmission during the World Columbian Exposition in Chicago. Despite its success, Tesla's experiment didn't find a commercial implementation because it was judged to be not environmentally friendly, cost effective and low efficiency. Tesla's experiments pushed researchers to investigate deeply alternative wireless power solutions and thus, they focused more on wireless technology due to their interesting advantages, such as sending power to movable devices, underwater applications, inflammable environment and micro and nano devices.
Starting from the last decades, the use of wireless power transmission technology has been growing increasingly, to include many important applications, such as electric vehicles, aerospace, oil field, industrial robotics, military, wireless sensor networks, medical devices, automotive, underwater operations, smart buildings and many other applications. This is why, more studies and investigations should be attributed to wireless power transmission as an alternative solution for powering wireless systems.

1.1 Motivation

1.1.1 Wireless power transmission

In this context, different methods are available to wirelessly transfer the power to the desired system. Based on the state of art, four main methods can be adopted: Lasers [2-5], electromagnetic waves (including radio frequency "RF") [6-9], electrostatic induction (capacitive link) [10, 11] and electromagnetic induction (inductive link) [12-14]. These

techniques can be categorized based on their fundamental mechanisms, power ratings, and transmission range. Thus, two main classes of wireless power transmission can be identified with consideration of the distance transfer between the transmitter and the receiver, which are far field methods and near field methods (see Fig. 1.1). In the case of far field transmission, laser and electromagnetic waves have their advantages. Where, in case of near field transmission methods, capacitive and inductive links are possible.

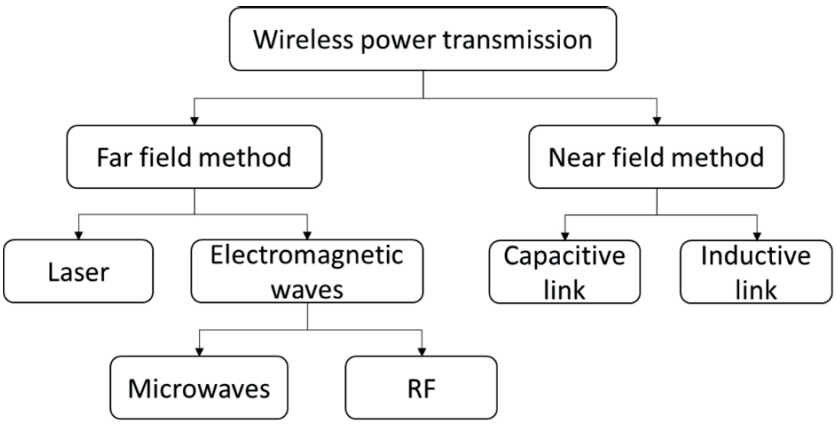

Fig. 1.1: Classification of wireless power transmission techniques

The main differences between wireless energy transmission methods, which are decisive for their practical use, are the typical level of transmitted energy and the power transmission distances.

Table 1.1: Typical transmitted energy and power transmission distance for different wireless power transmission techniques [1-50]

Type of WPT		**Typical transmitted Energy**	**Typical transmission distance**
Electromagnetic waves & Radio Frequency	LF	1 W – few kW	< 50 cm
	HF	30 - 40 W	up to 2 m
	UHF	1 - 3 W	3.5 m - 10 m
	Microwave	up to 30 kW	up to 1.54 km
Laser		530 W	30 – 200 m
Capacitive link		up to 1 - 3 W	< 5 mm
Inductive link		1 mW - few kW	< 2 m

Table 1.1 compares wireless energy transmission methods based on these properties. The results show that, capacitive and inductive power transmission systems have in general higher power transmission efficiency comparing to the other types.

Wireless systems with different requirements need appropriate wireless power transmission techniques. For this, investigating the properties of each method is important to choose the suitable technique to power a certain targeted system.

Table 1.2: Overview of wireless power transmission techniques [1-50]

Technique	Advantages	Disadvantages	Typical applications
Laser	- High energy transmission distance - No radio frequency interference to existing radio communication	- Line-of-sight necessity - Difficult energy transfer to movable devices - Strict human safety issues even at low power level - Low energy conversion efficiency (high losses)	- Military applications - Aerospace applications
Electrom-agnetic waves	- Energy transmission over high distances - Possible energy transfer to movable devices - Direction change of energy transfer	- Strict human safety issues - Sensitivity to interferences - Challenging power management - Low power transmission efficiency	- Wireless sensor networks - RFID - Underwater applications - Mines
Capacitive link	- Insensitive to magnetic flux - No heat generation - Necessity of high voltage - Wide charging area	- Short energy transmission distance necessary - Necessity of alignment between the primary and the secondary plates - Low energy level	- Battery recharging of small electronic devices
Inductive link	- Safe energy transfer - Possible energy transfer to movable devices - Possible energy transfer to micro and nano devices - High energy transfer surface in comparison to other methods	- Energy losses due to flux leakage - Heating losses - Eddy currents in metallic parts in the environment of the sending coils - Dependency of the efficiency on lateral and vertical distances	- Battery recharging of electrical vehicles - RFID transponders - Biomedical implants - Portable consumer electronic products

Table 1.2 gives an overview of available wireless power transmission methods, where advantages, limitations and examples of typical applications are illustrated. Based on Table 1.2, the choice of the appropriate power transmission method should respect the level of needed power and the distance separating the sending side and the receiving side. It should also respect the application's environment, where the system is implemented.

1.1.2 Inductive power transmission systems

In general, for inductive power transmission systems, energy transfer takes place between two or more coupled coils via electromagnetic induction. The transfer mechanism is similar to the transformer principle. An alternating current supplies the primary and sending sides, which can be composed by one or more coils. This produces a changing magnetic field, which reaches the receiving side, which can be also composed by one or more coils. The receiving coils are flooded by the magnetic field and this leads to an induced voltage and a current flow through the connected load. The induced voltage in the receiving coil is in the opposite direction of the voltage at the sending coil.
Inductive power transmission has many advantages compared to other methods. Indeed, this power transmission technique is robust and is not sensitive surrounding external factors such as, the dirt and moisture, due to the use of galvanic isolation. It is considered as a relative safe energy transfer methods through which, power can be sent to mobile receivers. Also, the generated power can be sent to micro and nano devices [15, 16]. Referring to Table 1.1, wireless power transmission via inductive link has a wide range of applications. It is used for high, medium and low power ranges including battery recharge of electrical vehicles [17-22], biomedical implants [23-26], portable electronic devices [27-30], wireless sensors [31-34] and other various applications [35 - 41].

1.2 Problem statement

Despite that, inductive power transfer offers various advantages, this technique shows in the same time some critical limitations, mainly related to the distance between the receiver and transmitter and the strong dependency of the power transmission efficiency on both vertical (axial) and lateral distances. In fact, for inductive wireless transmission, a good

efficiency can be reached at small vertical distance, which is smaller than the sending coil diameter, and in case of a perfect alignment between the sending and receiving coils axis. Otherwise, there is a high magnetic flux leakage and consequently only a very low power is transmitted (see figure 1.2).

Placing the sending and the receiving coils in a perfect position is a challenging task, which is not realistic in every application scenario. In fact, lateral misalignment of coils is persistent, an important decrease of the energy transmission efficiency of the system occurs. Thus, the placement of the receiving and sending coils is critical for the performance of the whole system.

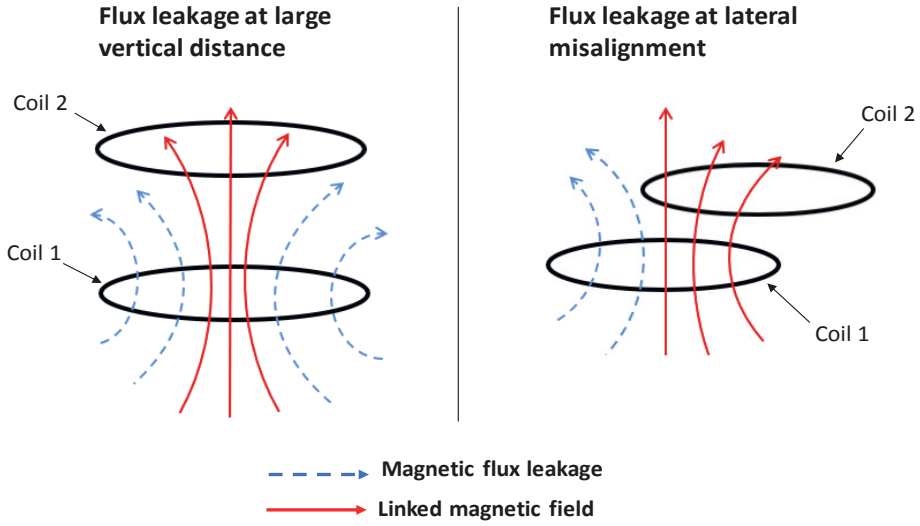

Fig. 1.2: Magnetic flux leakage in IPT systems

In order to choose and set the adequate parameters of the used coils and to optimize, in general, the inductive system, it is necessary to have an accurate and simple analytical model. Nevertheless, most of the analytical models presented in the state of the art are more complicated or dedicated to the conventional two-coil systems. Therefore, having a simplified and accurate analytical model for a multi-coil inductive system is highly requested.

Furthermore, inductive systems with multiple senders present an important level of power consumption and a high emission of magnetic field to uncoupled regions caused by the fact of powering all employed sending coils at the same time. This leads to high energy

losses and thereby, decreases the power transmission efficiency of the system. Therefore, a position detector of the receiver must be implemented to activate only the sending coils, which are under the receiver and keep the other sending coils switched off. For that, an additional sensor is required, thereby increasing its complexity and cost. So, an alternative solution to reduce the cost and the complexity of the system must be implemented.

1.3 Research objectives

This thesis focuses on the design of an efficient multi-coil inductive system that solves the problems of large air-gap misaligned coils systems with movable receiver, which are described in section 1.2. In this work, we aim to improve the transmitted power, the mutual inductance, the power at the load, and consequently, the power transmission efficiency of the inductive system in case of lateral misalignment between the sending and receiving sides and at large coil-to-coil vertical distance. In this context, several objectives are defined:

1- Proposing a simple and accurate analytical model for circular air-core coils constructed by copper wires, so that the use of finite element modelling could be avoided and the calculations could be simplified.
2- Design and implementation of a multi input single output MISO coil system configuration with optimized coil's size and arrangement in case of a large air-gap misalignment between the sending side and the receiving side.
3- Developing a novel detection method for movable receiving coil in order to switch off inactive sending coils and power only the coils underneath it independently of the receiver's position and speed.
4- Developing a novel coil excitation strategy to maintain a uniform magnetic field distribution and high equivalent mutual inductance between the active sending coils and the receiving coil along the coil matrix.
5- Energy management of the multi-coil inductive system by studying possible system topologies and load impedance values to realize the resonance and to increase thereby, the power transmission efficiency of the system.

1.4 Thesis overview

This thesis is structured in eight chapters (Fig. 1.3). Chapter 1 is devoted to the general introduction of the thesis. In the first part, an overview of wireless power transmission techniques is presented. The inductive power transmission systems and their typical applications are also introduced. In the second part, the limitations of the inductive power transmission systems, the contribution, and the research objectives are presented.

Chapter 2 covers the fundamental laws of electromagnetism that are applied to analyse and model the inductive system. The mutual parameters applied for the inductive system are then, presented, which are the mutual inductance and coupling factor. The last part is devoted to some safety guidelines for limiting the exposure to electromagnetic field.

In chapter 3, a literature review about multi-coil inductive systems and receiver detection techniques are presented. A classification of different inductive system is proposed and thoroughly explained. This chapter also, presents a comparison of the performance of some inductive systems in terms of power transmission efficiency, which considers the type, size and shape of the used coils. In the second part, we present some examples of the detection techniques applied to multi-coil inductive systems. The thesis proposal and the followed approach are presented in the last part of the chapter.

Chapter 4 focuses on the modelling of circular air-core coils used in experiments. Important parameters such as self-inductance, resistance, quality factor and coupling factor are estimated. The simplicity and the accuracy of the mathematical model of the coils are needed to provide guidelines in the choice of design parameters, system performance indices as well as for the efficiency optimization of the inductive power transmission systems. The second part of this chapter covers some rules for the choice of coil's properties in order to improve the power transmission efficiency.

In chapter 5, a multi-coil inductive system with oriented magnetic field is presented. This system presents a potential solution for large air gap misaligned system. An analytical model and a three-dimensional model for the studied system are proposed followed by both simulations and experimental verifications. The second part of this chapter is addressed to the investigation of different system topologies in case of multi-coil inductive

system. Hence, the expression for compensation capacitors, transmitted power and system efficiency are explored.

Chapter 6 is devoted to the study and implementation of different receiver detection. Some of them are based on the use of additional sensors to the circuit and others without adding any sensors. In the second part, a suitable activation (excitation) strategy for primary coils is described in order to decrease the magnetic field losses increasing thereby the coupling between the coils and consequently the system efficiency.

Chapter 7 addresses the energy management of the multi-coil inductive system. The aim is to realise the resonance by setting the appropriate topologies of the primary and the secondary circuits in order to improve the transmitted power and reduce losses. Simulations and experimental investigations of different system topologies are carried out. The second part of this chapter is addressed to the study of the effect of the load impedance value on the transmitted power for different system topologies.

Chapter 8 includes the general conclusions from the simulation and experimental results of the previous chapters.

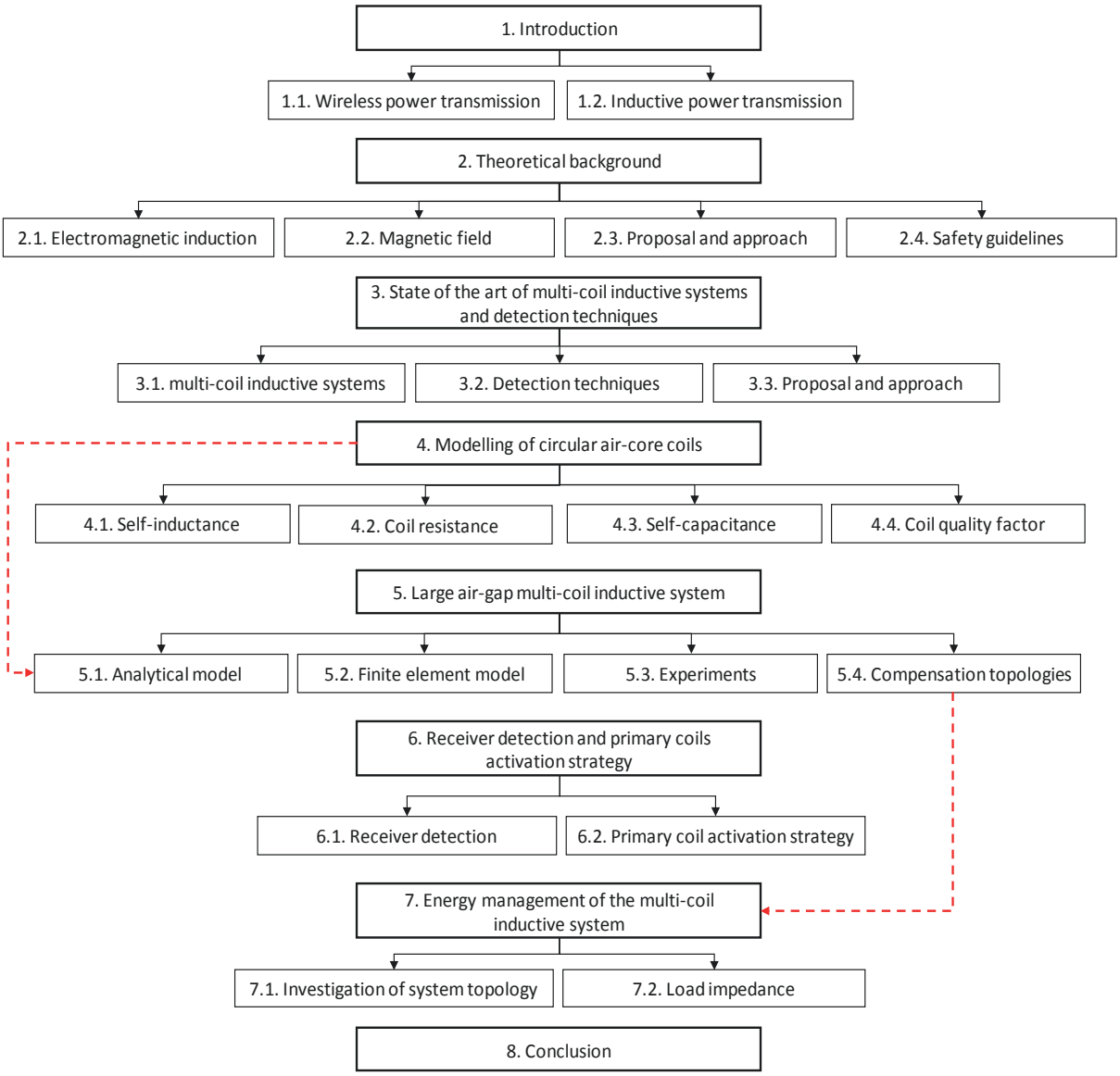

Fig. 1.3: Thesis overview

Chapter 2

Theoretical background

Inductive power transmission consists of the transfer of energy between two or more coupled coils in order to provide power to a load. It is also known as electromagnetic induction. The involved mutual parameters between the sending and the receiving coils are the magnetic field, the mutual inductance and the coupling factor. For the modelling of the inductive systems, fundamental laws of electromagnetism are applied. As all wireless power transmission systems, the use of inductive systems has some safety rules limiting the exposure of the human body to time-varying electric and magnetic fields.

The first part of this chapter covers the fundamental laws of electromagnetism, which are applied to analyse and model the studied inductive power transmission system. We present also the mutual parameters applied for the inductive system. In the second part, the safety guidelines for limiting exposure to electromagnetic field are presented.

2.1 Electromagnetic induction

A changing magnetic field produced by a coil induces an electric field in the other coil. Similarly, a changing electric field circulating in a coil produces a magnetic field issued from this coil. These phenomena are expressed mathematically through Maxwell's equations.

Faraday's law [42] states that a changing magnetic flux through a surface A induces an electromotive force (emf) in any boundary path of that surface, and a changing magnetic field $\vec{B}$ induces a circulating electric field $\vec{E}$:

$$\oint_C \vec{E}\, d\vec{l} = -\frac{d}{dt}\int_S \vec{B}\, d\vec{A} \tag{2.1}$$

Where C is a conductor loop, $d\vec{l}$ is an incremental segment of path C, $d\vec{A}$ is the differential of surface area, and $\vec{E}$ is the induced electric field at each segment $d\vec{l}$ of the path.

The differential form of the Faraday's law is given by:

$$\vec{\nabla} \times \vec{E} = -\frac{\partial \vec{B}}{\partial t} \tag{2.2}$$

It states that a circulating electric field is produced by a magnetic field that changes with time.

The Ampere-Maxwell law states that a magnetic field is produced along a path if any current is enclosed by the path or if the electric flux through any surface bounded by the path changes over time.

$$\oint_C \vec{B}\, d\vec{l} = \mu_0 \left(I + \varepsilon_0 \frac{d}{dt} \int_A \vec{E}\, d\vec{A} \right) \tag{2.3}$$

Where, μ_0 is the vacuum permeability, I is the enclosed electric current, ε_0 is the electric permittivity of vacuum.

The differential form of the Ampere-Maxwell law is:

$$\vec{\nabla} \times \vec{B} = \mu_0 \left(\vec{J} + \varepsilon_0 \frac{\partial \vec{E}}{\partial t} \right) \tag{2.4}$$

Where, $\vec{J}$ is the total electric current density.

Equation 2.4 states that by an electric current and by an electric field that changes with time, a circulating magnetic field is produced [42].

In inductive system, the conductor loop is a circular air core coil. The alternating current in the sending coil produces a changing magnetic field and induced an electric field in the receiving coil.

The Gauss's law for electric fields states that electric charge produces an electric field and the flux of that field passing through any closed surface is proportional to the total charge contained within that surface. The integral form is generally expressed as follows

$$\oint_S \vec{E}\, d\vec{A} = \frac{q_{enc}}{\varepsilon_0} \tag{2.5}$$

Where: q_{enc} is the amount of charge contained within the closed surface.

The Gauss's law for magnetic field states that the total magnetic field flux passing through any closed surface is zero. The integral form of Gauss's law is generally expressed as follows:

$$\oint_C \vec{B}\, d\vec{A} = 0 \tag{2.6}$$

That does not mean that zero magnetic field lines penetrate the surface, it means that for every closed surface it must be a magnetic field line leaving that volume.

2.2 Magnetic field

2.2.1 Biot-Savart's law

The Biot-Savart's law [42] allows the determination of the magnetic field vector $\vec{B}$ due to wire-shaped conductors of arbitrary geometry. Referring to Fig. 2.1, the contribution at a specific point P from a small element of electric current is given by:

$$d\vec{B} = \mu_0 \frac{I\, d\vec{l} \times \hat{r}}{4\pi r^2} \tag{2.7}$$

Where I is the current, $d\vec{l}$ is a vector with the length of the current element and pointing in the direction of the current, $\hat{r}$ is a unit vector pointing from the current element to the point P at which the field is calculated and r is the distance between the current element and P.

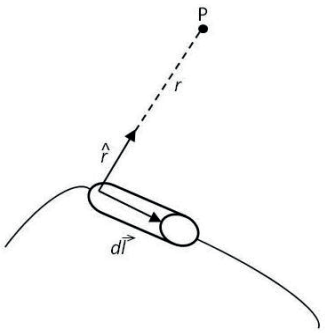

Fig. 2.1: Biot-Savart's law geometry [42]

2.2.2 Magnetic field produced by a circular current loop

Figure 2.2 depicts a circular loop of radius R carrying a current I. In Cartesian coordinates, $\vec{r}'$ is expressed as follows:

$$\vec{r}' = R(\cos\phi'\hat{i} + \sin\phi'\hat{j}) \tag{2.8}$$

Consequently, the differential current element $I\vec{dl}$ in Eq.2.7 can be written as,

$$I\,d\vec{l} = I(d\vec{r}'/d\phi')d\phi' = IRd\phi'(-\sin\phi'\,\hat{i} + \cos\phi'\,\hat{j}) \tag{2.9}$$

The relative vector position $\vec{r}$ of the field point *P,* which is located at the axis of the loop at a distance z is given by

$$\vec{r} = \vec{r}_p - \vec{r}' = -R\cos\phi'\,\hat{i} - R\sin\phi'\,\hat{j} + z\,\hat{k} \tag{2.10}$$

Using Eq. 2.10, the distance between point *P* and the differential current is given by

$$r = \left|\vec{r}\right| = \sqrt{(-R\cos\phi')^2 - (R\sin\phi')^2 + z^2} = \sqrt{R^2 + z^2} \tag{2.11}$$

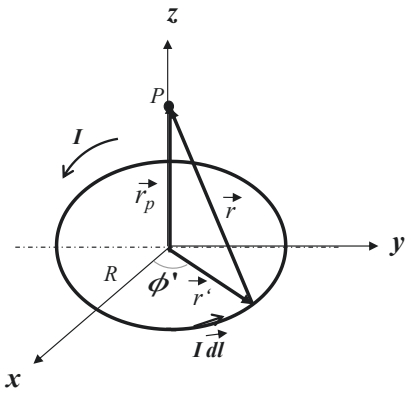

Fig. 2.2: Circular current loop

Then, the unit vector pointing from the current element to the point P at which the field is calculated can be written as

$$\hat{r} = \frac{\vec{r}}{r} = \frac{\vec{r}_p - \vec{r}'}{\left|\vec{r}_p - \vec{r}'\right|} \tag{2.12}$$

Referring to the Biot-Savart's law, the contribution at a specific point P from a small element of electric current is given by

$$d\vec{B} = \frac{\mu_0 I}{4\pi}\frac{d\vec{l}\times\hat{r}}{r^2} = \frac{\mu_0 I}{4\pi}\frac{d\vec{l}\times\vec{r}}{r^3} = \frac{\mu_0 I}{4\pi}\frac{d\vec{l}\times(\vec{r}_p - \vec{r}')}{\left|\vec{r}_p - \vec{r}'\right|^3} \tag{2.13}$$

Note that, the cross product $d\vec{l}\times(\vec{r}_p - \vec{r}')$ can be written as

$$d\vec{l}\times(\vec{r}_p - \vec{r}') = Rd\phi'(-\sin\phi'\,\hat{i} + \cos\phi'\,\hat{j})\times(-R\cos\phi'\,\hat{i} - R\sin\phi'\,\hat{j} + z\,\hat{k})$$

$$= Rd\phi'(z\cos\phi'\,\hat{i} + z\sin\phi'\,\hat{j} + R\,\hat{k}) \tag{2.14}$$

Substituting Eq. 2.14 in Eq. 2.13, we obtain

$$d\vec{B} = \frac{\mu_0 I}{4\pi} \frac{d\vec{l} \times (\vec{r}_p - \vec{r}')}{\left|\vec{r}_p - \vec{r}'\right|^3} = \frac{\mu_0 IR}{4\pi} \frac{z\cos\phi'\,\hat{i} + z\sin\phi'\,\hat{j} + R\,\hat{k}}{(R^2 + z^2)^{3/2}} \tag{2.15}$$

Finally, the magnetic field at point *P* equals

$$\vec{B} = \frac{\mu_0 IR}{4\pi} \int_0^{2\pi} \frac{z\cos\phi'\,\hat{i} + z\sin\phi'\,\hat{j} + R\,\hat{k}}{(R^2 + z^2)^{3/2}} d\phi' \tag{2.16}$$

The x and y components of the magnetic field can be shown to equal zero,

$$B_x = \frac{\mu_0 IRz}{4\pi(R^2 + z^2)^{3/2}} \int_0^{2\pi} \cos\phi'\, d\phi' = \left[\frac{\mu_0 IRz}{4\pi(R^2 + z^2)^{3/2}} \sin\phi' \right]_0^{2\pi} = 0 \tag{2.17}$$

$$B_y = \frac{\mu_0 IRz}{4\pi(R^2 + z^2)^{3/2}} \int_0^{2\pi} \sin\phi'\, d\phi' = \left[-\frac{\mu_0 IRz}{4\pi(R^2 + z^2)^{3/2}} \cos\phi' \right]_0^{2\pi} = 0 \tag{2.18}$$

However, the z component of the magnetic field is different from zero and it is equal to

$$B_z = \frac{\mu_0}{4\pi} \frac{IR^2}{(R^2 + z^2)^{3/2}} \int_0^{2\pi} d\phi' = \frac{\mu_0}{4\pi} \frac{2\pi\, IR^2}{(R^2 + z^2)^{3/2}} = \frac{\mu_0 IR^2}{2(R^2 + z^2)^{3/2}} \tag{2.19}$$

In this work, coils are modelled as the sum of multiple circular loops of radius *r* carrying a current *I*. Referring to Biot-Savart's law, the magnetic field equation for a circular coil placed in the xy plane, at a distance z along the z-axis is given as follows:

$$\vec{B} = \frac{\mu_0\, N I r^2}{2\sqrt{\left(r^2 + z^2\right)^3}} \hat{z} \tag{2.20}$$

Where: *N* and *r* are the number of turns and the radius of the coil, respectively.

2.3 Mutual parameters

2.3.1 Mutual inductance

Inductive links are strongly dependent on the mutual inductance between the sending and the receiving coils. Many researchers proposed different direct methods to compute the mutual inductance of circular coils. The most important expression is given by Neumann's formula [46]. Figure 2.3 depicts the considered configuration.

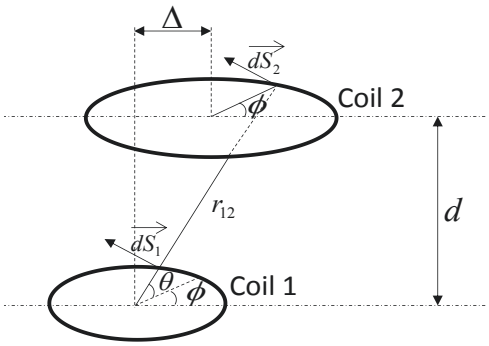

Fig. 2.3: Inductive system with misaligned coils

For two coils in parallel planes with number of turns N_1 and N_2 respectively, separated by a distance d and having a lateral misalignment Δ, the mutual inductance is given as follows:

$$M = \frac{\mu_0}{4\pi} N_1 N_2 \oint\oint \frac{dS_1 \,.\, dS_2}{r_{12}} \tag{2.21}$$

$$dS_1 = r_1 d\phi \tag{2.22}$$

$$dS_2 = r_2 d\theta \tag{2.23}$$

$$r_{12} = \sqrt{r_1^2 + r_2^2 + d^2 + \Delta^2 - 2\Delta r_1 \cos\theta + 2\Delta r_2 \cos\phi - r_1 r_2 \cos(\phi - \theta)} \tag{2.24}$$

After defining the parameters, Eq. 2.21 takes the form:

$$M = \frac{\mu_0}{4\pi} N_1 N_2 r_1 r_2 \oint d\phi \oint \frac{\cos\theta \, d\theta}{r_{12}} \tag{2.25}$$

After simplification of the double integral by means of trigonometric manipulations as demonstrated in [46], the mutual inductance expression becomes as follows:

$$M = \frac{\mu_0 N_1 N_2 r_1 r_2}{\sqrt{r_1 (r_2 + \Delta)}} G(h) \tag{2.26}$$

Where:
$$h = \sqrt{\frac{4 r_1 (r_2 + \Delta)}{(r_1 + r_2 + \Delta)^2 + d^2}} \tag{2.27}$$

$$G(h) = \left(\frac{2}{h} - h\right) K(h) - \frac{2}{h} E(h) \tag{2.28}$$

K(h) and *E(h)* are the complete elliptic integral of the first and the second kind, respectively [47].

Using Eq. 2.26, the mutual inductance between two coils could be estimated with an error less than 10% of the exact value. Similar formulas are presented in [48].

Figure 2.4 depict the mutual inductance between a sending coil with 3 cm diameter and 4 turns and a receiving coil with 6 cm diameter and 8 turns. The axial and lateral distances vary from 1 cm to 5 cm and from 0 cm to 2.5 cm, respectively.

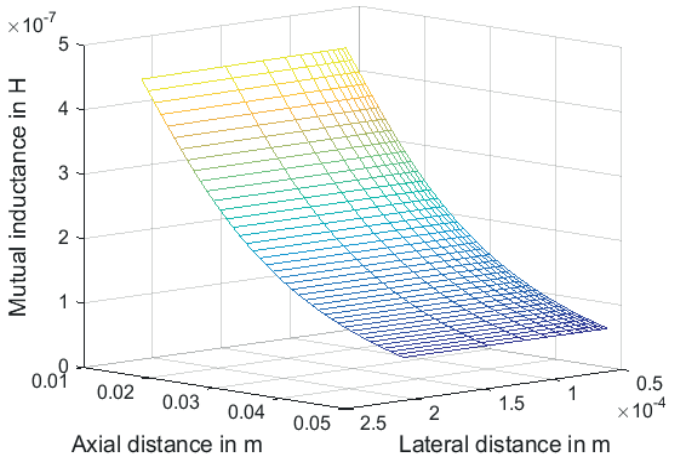

Fig. 2.4: Mutual inductance for variable axial and lateral distances

2.3.2 Coupling factor

The coupling factor '*k*' is defined as the amount of magnetic flux penetrating the receiving coil compared to the whole generated flux. It could be measured by the following expression:

$$k = \frac{M}{\sqrt{L_1 L_2}} \tag{2.29}$$

Here M is the mutual inductance between two coils having respectively self-inductances L_1 and L_2. The coupling factor depends on the axial distance separating the two coils as well as on the lateral misalignment between them. Figure 2.5 depicts the coupling factor between a sending coil with a radius of 15 mm and a receiving coil with a radius of 30 mm.

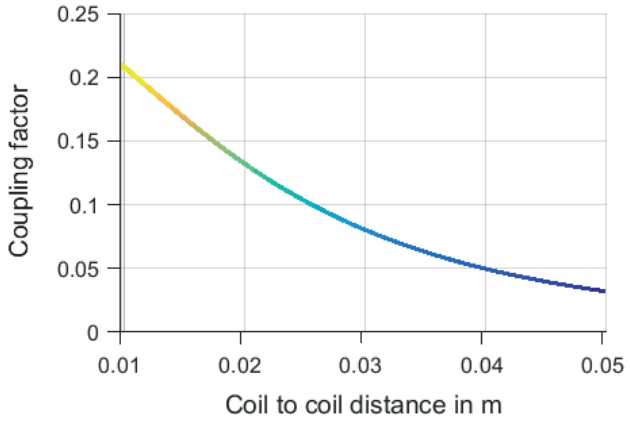

Fig. 2.5: Coupling factor for different coil to coil distances

2.4 Safety guidelines limiting the exposure

Applications with wireless systems via electromagnetic induction should comply with certain safety norms (basic restrictions) because there are both direct and in indirect effects with the human body while dealing with time-varying electric, magnetic, and electromagnetic fields. These restrictions were issued by several organizations such as the International Radiation Protection Association (IRPA) and the International Commission on Non-Ionizing Radiation Protection (ICNIRP) [49, 50].

Human's body is directly interacted to time-varying electric and magnetic fields through different coupling mechanisms known as: Coupling to electric fields, coupling to magnetic fields and absorption of energy from electromagnetic fields.

2.4.1 Effect of electric fields

The exposure of the human body to time-varying electric fields leads not only to the issue of electric charges (induced currents) in the body but also to the reorientation of electric dipoles that are already present in the tissue. These effects are dependent generally on the electrical conductivity and the permittivity of the body, which vary from person to person, with the frequency of the applied field and the type of body tissue. They also depend on the shape, the size, and the position of the body in the field.

2.4.2 Effect of magnetic fields

The exposure of the human body to time-varying magnetic fields leads to both induced electric fields and flowing electric currents. The amplitudes of the induced electric field and the current density are proportional to coil's radius, the electrical conductivity of the body tissue, and the amount and amplitude of the magnetic flux density.

2.4.3 Energy absorption from electromagnetic fields

The physical interaction of electric and magnetic fields with human body at low frequencies results in very low energy absorption and no increase of temperature measured in the body. However, a physical interaction of electric and magnetic fields with human body at frequencies above 100 kHz leads to important energy absorption and a remarkable increase of temperature in the body. Referring to Durney et al. 1985 [51], the absorption of energy from electromagnetic fields can be divided as shown in Table 2.1.

Table 2.1: Energy absorption from electromagnetic fields [51]

Frequency range	**Energy absorption**
100 kHz - 20 MHz	High absorption in the trunk and possible absorption in the neck and legs
20 MHz – 300 MHz	Absorption in whole body, higher values in the head
300 MHz – 10 GHz	Non-uniform absorption
More than 10 GHz	Absorption occurs at the body surface

Table 2.2 presents the basic restrictions for general public exposure to time varying electric and magnetic fields for frequencies up to 300 GHz. These restrictions on current density and specific absorption rate SAR are destined to protect against intense exposure effects on central nervous system. As can be seen, strict limitations are imposed for higher frequencies.

Table 2.2: Energy absorption from electromagnetic fields [49, 50]

Frequency range	Magnetic flux density (mT)	Current density (mA/m^2)	Whole body average SAR (W/Kg)	Localized SAR (head and trunk) (W/Kg)	Localized SAR (Limbs) (W/KG)	Power density (W/m^2)
0 Hz	40	-	-	-	-	-
>0-1 Hz	-	8	-	-	-	-
1-4 Hz	-	8/f	-	-	-	-
4-1000 Hz	-	2	-	-	-	-
1-100 kHz	-	f/500	-	-	-	-
0.1-10 MHz	-	f/500	0.08	2	4	-
0.01-10 GHz	-	-	0.08	2	4	-
10-300 GHz	-	-	-	-	-	10

2.4.4 Reference Levels

The reference levels are derived from the basic restrictions by mathematical investigations and referring to some experimental results done in laboratory at specific frequencies. They are presented for the condition of maximal coupling of the field to the exposed body, consequently providing the highest protection. A summary of reference levels is provided in Table 2.3.

Table 2.3: Reference levels for general public exposure to time-varying electric, magnetic and electromagnetic fields [49, 50]

Frequency range	E-field strength (V/m)	H-field strength (A/m)	B-field (μT)	Equivalent plane wave power density (W/m^2)
0-1 Hz	-	3.2×10^4	4×10^4	-
1-8 Hz	10 000	$3.2 \times 10^4/f^2$	$4 \times 10^4/f^2$	-
8-25 Hz	10 000	4000/f	5000/f	-
0.025-0.8 KHz	250/f	4/f	5/f	-
0.8-3 KHz	250/f	5	6.25	-
3-150 KHz	87	5	6.25	-
0.15-1 MHz	87	0.73/f	0.92/f	-
1-10 MHz	$87/\sqrt{f}$	0.73/f	0.92/f	-
10-400 MHz	28	0.073	0.092	2
400-2000 MHz	$1.375\sqrt{f}$	$0.0037/\sqrt{f}$	$0.0046\sqrt{f}$	f/200

Chapter 3

State of the art of multi-coil inductive systems and detection techniques

Multi-coil systems have been investigated to maximize the transmitted power, to supply movable devices, to enlarge the misalignment tolerance, and to increase, in several cases, the system efficiency. We can classify the multi-coil systems to two categories:
Stationary multi-coil systems where the receiver is not moving during the power transmission phase (operation), and dynamic multi-coil system where the receiver is in movement or it has a variable position during the power transmission phase.
The high emission of the magnetic field, caused by powering all sending coils at the same time, leads to high energy losses and decreases thereby the power transmission efficiency of the multi-coil inductive systems. Therefore, a position detector of the receiver must be implemented to activate only the sending coils under the receiver and keep the other sending coils switched off.
The first part of the chapter covers some examples from the literature of multi-coil inductive systems and their limitations. In the second part, we present some detection techniques used for the detection of the receiver. The last part is devoted to the proposal and approach.

3.1 State of the art of multi-coil inductive systems

Based on literature, different types of multi-coil system are studied. Some of them are the three-coil systems, others are the four-coil systems and the rest are just called multi-coil systems and they could be noted as MISO (Multi-Input Single-Output), SIMO (Single-Input Multi-Output) and MIMO (Multi-Input Multi-Output).

3.1.1 Three-coil systems

A multi-coil system was proposed by MIT [52] consisting of adding a third coil that resonates at the same resonance frequency of the traditional two-coil system. The sending and receiving coils are placed vertically and don't have a direct magnetic coupling between them. However, they transfer energy through the intermediate coil as shown in Fig.3.1 (a). The added coil has a strong coupling with both sides. Investigation shows that the added coil improves two times the transfer efficiency from 29% to 61.2% [52].

A similar three-coil system is proposed in [53] and shown in Fig. 3.1 (b). The additional coil (coil 2) improves the transfer efficiency when the distance and the angle θ between the sending coil 1 and the receiving coil are increased. Here, the out-of-phase excitation, in which the two sending coils are excited in opposite direction, leads to a good efficiency.

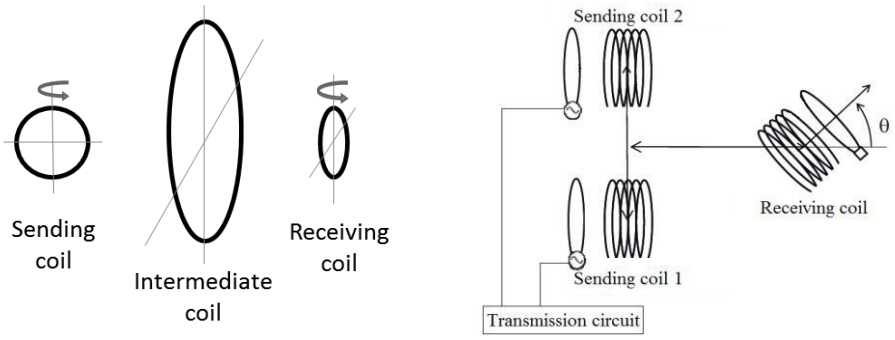

Fig. 3.1: Examples of three-coil systems with intermediate coil [52, 53]

Another three-coil system is studied in [54]. Authors proposed a method to extend the misalignment tolerance of inductive charging system by adopting two receiving coils placed orthogonally as shown in Fig. 3.2.

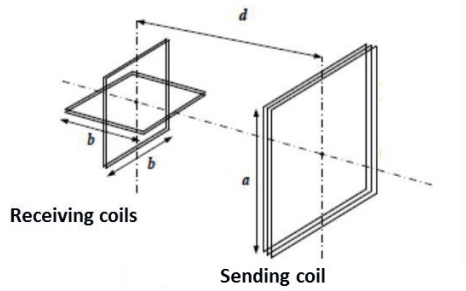

Fig. 3.2: Three-coil system consisting of 2 receiving coils placed orthogonally [54]

This solution improves the misalignment tolerance in a limited extent. However, it increases the coil manufacturing difficulty and controlling complexity of the inductive system.

3.1.2 Four-coil systems

Many studies focused on the four-coil systems. In [55] a four-coil concentric system (see Fig. 3.3 (a)) consisting of two sending and two receiving coils is designed to improve the transfer efficiency through an axial distance of 10 to 20 mm. Here, a low coupling coefficient between driver and load coils, caused by the increase of the operating distance, is compensated by using two compensation coils of 64 mm diameter having a high-quality factor. The driver coil and the load coil have both a diameter of 22 mm, where the driving frequency of the link equal to 700 kHz. Investigation shows that by using a four-coil system, the power-transfer efficiency is improved by the double of the conventional two-coil system.

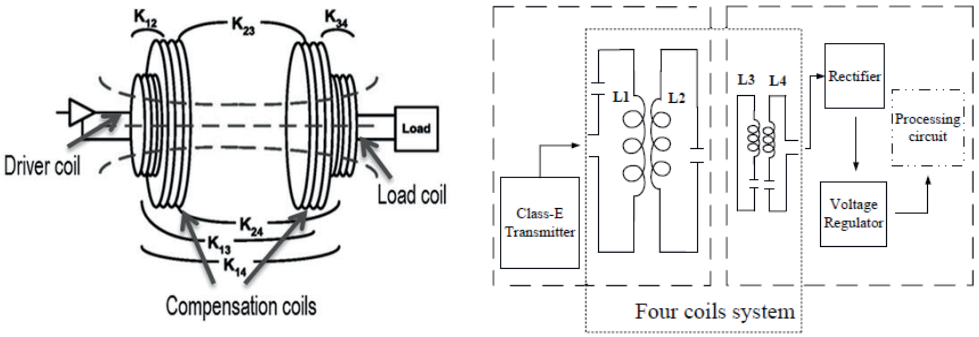

(a) (b)

Fig. 3.3: Examples of four-coil systems [55, 56]

A similar four coil system is investigated in [56] and shown in Fig. 3.3 (b). Here, Li et al. proved that the power transfer efficiency of a micro implantable medical device is improved by adding magnetic enhanced resonators. The diameter of the two primary coils (L1 and L2) and the two secondary coils (L3 and L4) equal respectively to 34 mm, 36 mm, 14 mm and 16.5 mm. The operation frequency equals to 742 kHz. Obtained results show that the efficiency of the four-coil system at the distance of 1.5 cm is 1.9 times higher than the efficiency achieved by the two-coil system.

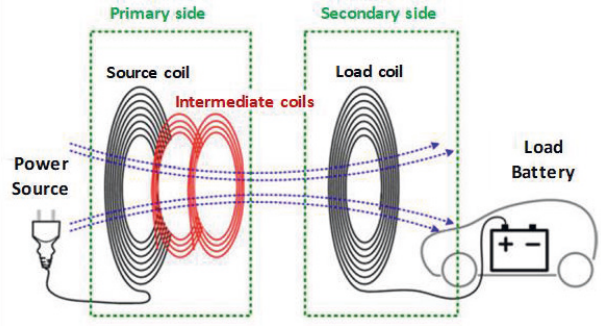

Fig. 3.4: Asymmetric four-coil system [57]

An asymmetric four-coil system, shown in Fig. 3.4, is proposed by Moon et al. [57]. The primary side consists of three sending coils: One source coil and two intermediate coils. These coils are placed in the same plane. The idea behind the design of this system is to improve the coupling coefficient, have a longer transfer distance and to provide a wide operation frequency range.

Table 3.1: Efficiency comparison between two-coil and four-coil systems [57]

Load condition	**1.1 kW**	**2.2 kW**	**3.3 kW**
Conventional two-coil system efficiency in %	89.80	90.31	90.45
Asymmetric four-coil system efficiency in %	95.63	96.21	96.56
Improvement in %	6.00	6.13	6.32

Referring to Table 3.1, it is clear that the asymmetric four-coil system has better efficiency than the conventional two-coil system. It reaches an improvement of more than 6% for all load conditions.

3.1.3 Multi-coil systems

A multi-coil system presented in [58] consists of a sending side composed by multiple coils, where each one has a ferrite core and the receiving has a ferrite plate. The idea is to guarantee that at any direction of the receiving coil, it encloses at least one small transmitter coil that should be able to provide enough energy to the load. For those reasons, the receiving coil should be larger than the sending ones. This system is able to

provide power to the receiving coil having different shapes such as rectangular, oval or hexagonal. Figure 3.5 depicts the proposed multi-coil system.

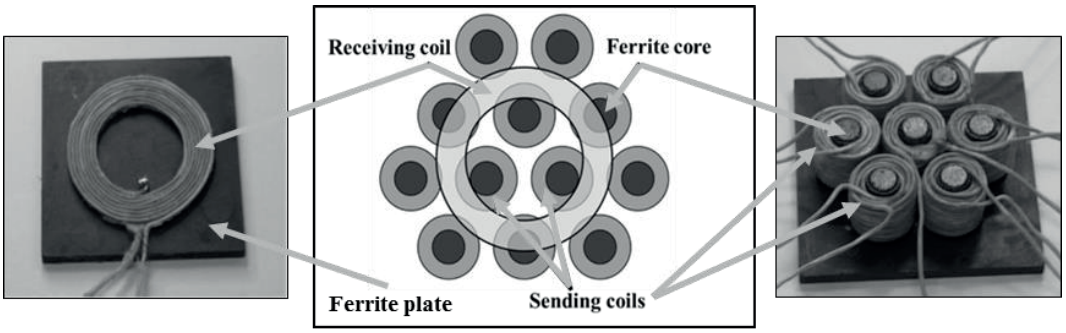

Fig. 3.5: Multi-coil system with ferrite core and plates [58]

A multi-coil system studied in [59] deals with multiple transmitter and/or receiver coils (multi input single output "MISO", single input multi output "SIMO" or multi input multi output "MIMO"). Here, the authors investigated the impact of the coupling between the sending coils and/or between the receiving coils on the driving frequency yielding to the maximum efficiency.

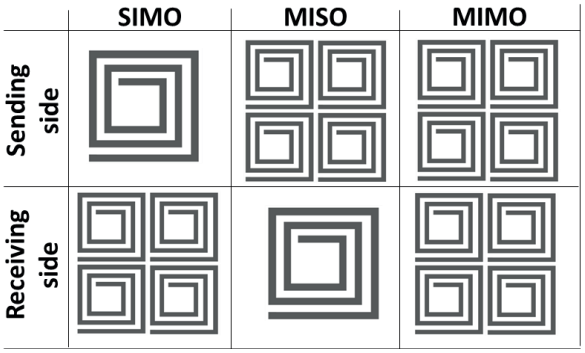

Fig. 3.6: Different multi-coil system configurations

The authors show that the systems with multiple sending or receiving coils have higher transferred power and efficiency than two-coil systems. Additionally, they show that in case of SIMO or MIMO coils systems, the coupling between receiving coils reduces the driving frequency and consequently the maximum efficiency, which was also reported in [29, 60]. However, the coupling between sending coils in MISO coils system doesn't have any significant influence on the required driving frequency that leads to the maximum efficiency.

In [61, 62], a multi input single output “MISO” coils system composed by three layers of the sending printed coils has been studied. At each layer, coils are placed in a hexagonal arrangement as shown in Fig.3.7. This structure guaranties, at each position of the receiver, three small sending coils underneath it and contributing to energy transmission.

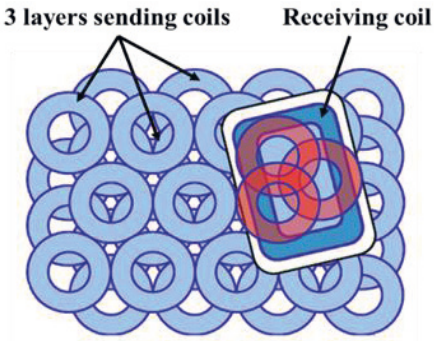

Fig. 3.7: Multi-coil system with three layers of sending coils [61, 62]

Single input multi output “SIMO” coils systems have been investigated in [63] by applying a coil array to a receiving coil instead of a conventional single coil to improve the wireless power transmission efficiency in case of coils misalignment. They propose the study of 2×2 and 3×3 coil arrays as shown in Fig. 3.8 (a). Experimental results of Fig.3.8 (b) show that the highest efficiency was reached by a 3×3 coil array. Here, the WPT efficiency was improved by 56.45% as compared with the conventional two-coil system (1×1).

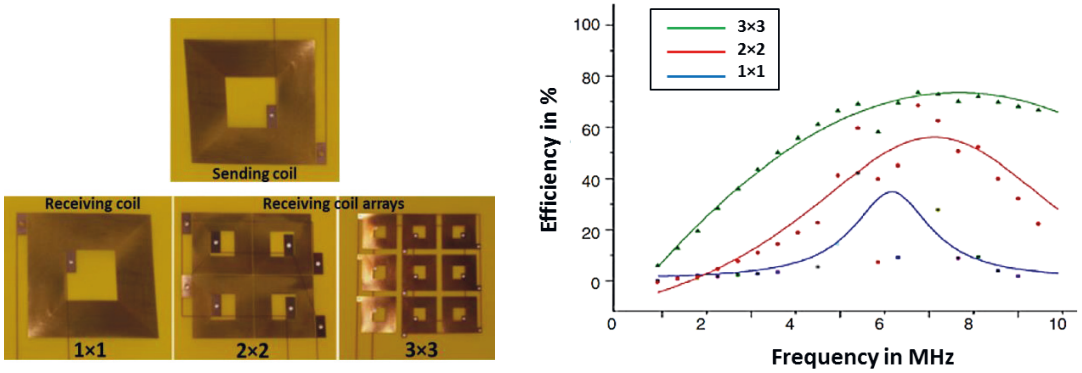

(a) (b)

Fig. 3.8: Examples for SIMO coils systems [63]

A similar SIMO coil system is investigated in [64]. The designed system consists of a single circular sending coil with a ferrite core and an array of circular receiving coils, also with a ferrite core. The two sides are very close to each other. The system serves for charging electric vehicles at a small air gap and over a wide range of coils' displacement (see Fig. 3.9).

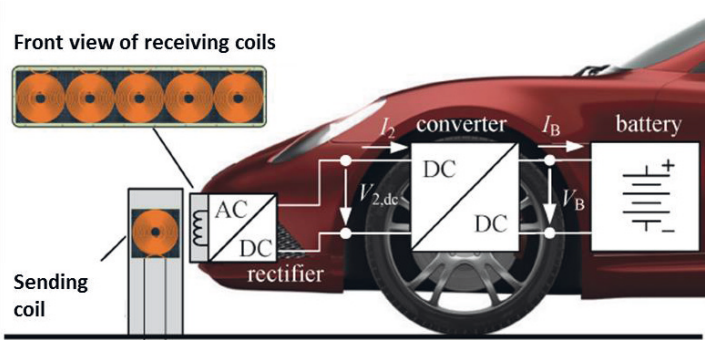

Fig. 3.9: Multi-coil system for charging electric vehicles [64]

A MISO coil system with vertical-and-horizontal secondary coil was proposed in [65]. The sending side consists of a matrix of air core circular coils having an alternate winding design as shown in Fig. 3.10. Each coil has a diameter of 150 mm and a height of 8 mm. The receiving coil is composed by both horizontal and vertical windings. The length and the height of the vertical windings equal to 65.5 mm and 22.5 mm, respectively. Besides, the length and the height of the horizontal windings equal to 58 mm and 15 mm, respectively.

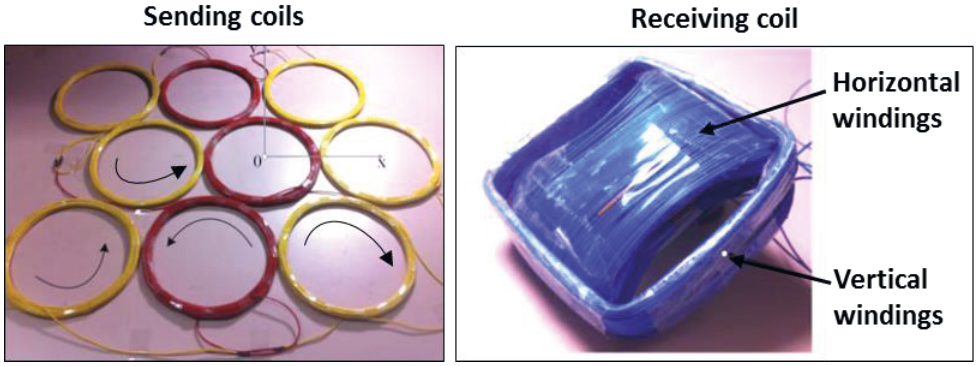

Fig. 3.10: MISO coil system with vertical-and-horizontal secondary coil [65]

In addition to the continuous powering method for movable target, the proposed multi-coil system first, increases the magnetic field density (see Fig. 3.11) and consequently, the

capability of transferring power to the secondary side and, secondly, the acquisition of energy especially in the region above coils' gap.

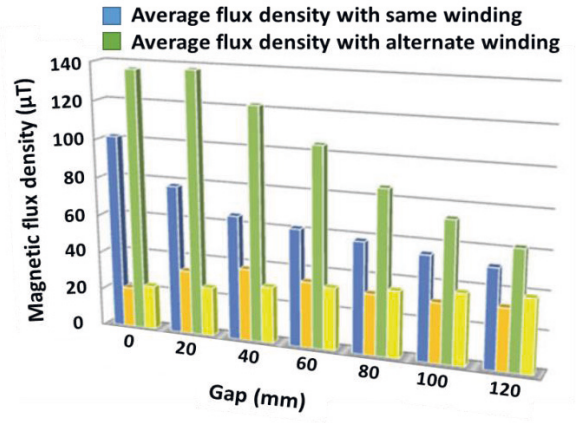

Fig. 3.11: Magnetic field density [65]

In [63], a multi-coil system is designed to power wireless sensors installed in a conveyor element. The sending side is composed by an array of sending air core coils connected in series and excited in the same direction. The receiving coil is in movement above the sending coils in a parallel plane. It has a constant speed, so its position is known at each time interval.

Fig. 3.12 depicts the studied system. The system provides a permanent powering for wireless sensors over a 30 mm coil to coil distance.

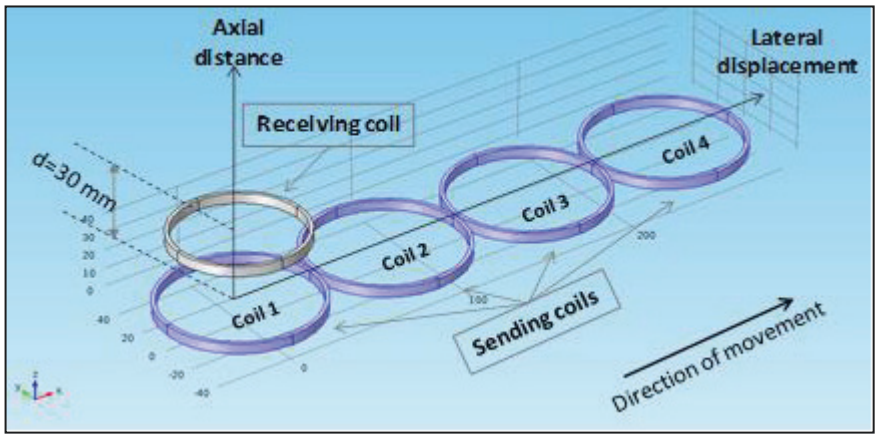

Fig. 3.12: Multi-coil system for powering wireless sensors [66]

The investigation in [67] deals with a multi-coil inductive system, in which the sending side consists of an array of concentric air-core coils (see Fig. 3.13). In fact, building a system with three concentric sending coils increases the magnetic field density and orient it to the receiving coil. Thus, the mutual inductance between the two sides increases leading to the improvement of the transmitted power.

For demonstration, the diameters of the three concentric coils equal to 80 mm, 65 mm and 46 mm, respectively, and the diameter of the receiving coil equals to 80 mm. The sending and the receiving coils have 9 turns.

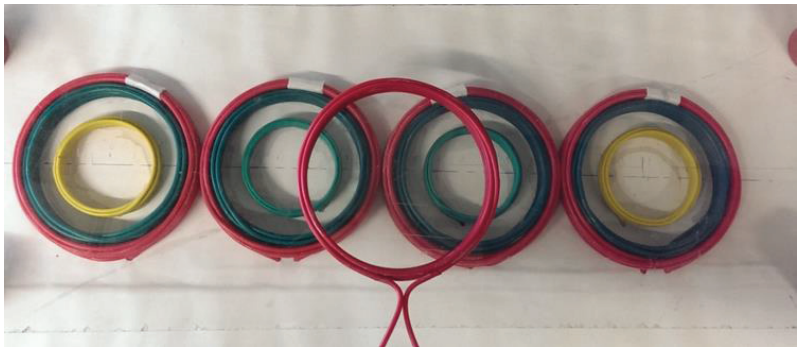

Fig. 3.13: Inductive system consisting of an array of concentric coils

Fig.3.14 shows the simulation results of the mutual inductance. The obtained results prove, that by adopting an array of concentric coils, the mutual inductance is increased more than 3.5 and 2 times at a distance of 10 mm and 50 mm between the sending and receiving coils, respectively.

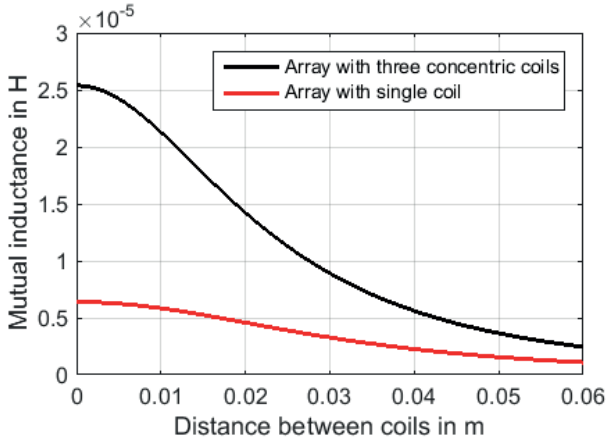

Fig. 3.14: Mutual inductance comparison

The proposed multi-coil inductive system in [68, 69] consists of a matrix of printed sending coils having a spiral hexagonal shape, two layers and 12.5 mm radius. The receiving coil is also a printed sending coil with the same shape but it has only one layer and its radius equals 20 mm. The number of turns per layer equals 13 and 23 for the sending and receiving coils, respectively. As illustrated in Fig.3.15, this CET desktop is suitable for powering and recharging one or multiple small electronic devices at very close distance. The objective is to find the maximum mutual inductance between the primary and secondary windings increasing thereby power transmission efficiency. In addition to that, the authors proposed a receiver detection method that allows a free positioning of the receiver.

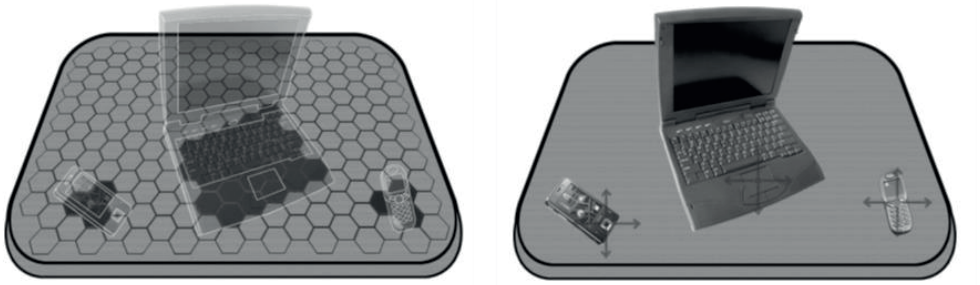

Fig. 3.15: Contactless energy transfer [68]

3.1.4 Evaluation

Different solutions have been proposed for inductive power transmission systems with large air gap, lateral misalignment and movable receivers. However, there is no recent investigation dealing with all these problems at the same time.

Three-coil systems [52-54] succeeded to improve the power transmission efficiency at large air gap and lateral misalignment. However, they are not suitable for systems dealing with movable receivers. They show not only a strong dependency on the position of the receiver and its orientation but also a high controlling complexity.

Four-coil systems present also an improved solution to extend the misalignment tolerance at a certain limit, while increasing the axial distance between the sending and receiving sides [55-57]. Like the three-coil systems, they are not suitable for systems with movable receiver and they show a high dependency on the position of the receiver. They present

also a high cost solution as the manufacturing process of coils with high quality factor is relatively expensive.

The majority of multi-coil systems presented in [61-62, 64-67] are suitable for the systems with movable receiver. They realize energy transfer at variable receiver position [61, 60, 63, 65, 68, 69] or a position detection of the receiver [68, 69].

Some investigations are dealing with large air gap using air-core coils, while others focus only on printed coils. By considering such properties, increasing both the complexity of the controllability and the manufacturing cost of the systems becomes possible.

Table 3.2 presents selected examples from the state of the art of multi-coil systems. In order to evaluate these systems, important criteria are proposed, such as the sensitivity to lateral misalignment, the capability to send power at large air gap, the dependency on the receiver, the design and control complexity, the cost, and the efficiency.

Table 3.2: Selected examples of SOA multi-coil inductive systems

Criteria		**References**													
		52	53	54	55	54	56	58	61/62	63	64	65	66	67	68/69
Large air-gap		x			x	x	x					x	x	x	
Misalignment tolerance		x	x	x				x	x	x		x			x
Movable receiver											x	x	x	x	
Dependency on receiver		x	x	x	x	x	x			x					
Free positioning								x	x		x	x	x	x	x
Receiver detection									x					x	x
Sending coils	Selection								x					x	x
	Activation strategy														
Design complexity		-	+	++	-	-	-	+	+	+	++	+	+	++	++
Control complexity		-	+	+	-	++	+	-	++	+	++	+	-	+	++
Cost		-	-	+	-	+	-	+	+	+	+	+	-	+	+
Efficiency		+	+	+	+	+	+	+	+	+	+	+	+	+	+

The performance comparison of SOA multi-coil-systems is shown in Table 3.3 with a focus on power transmission efficiency in dependence of the type, the size and the shape

of the coils. The inductive systems have different coils' size and different coil-to coil vertical distance (i.e. the gap between the sending side and the receiving side), making the comparison not evident. Therefore, in order to compare the system's efficiency of the different inductive systems, we propose to introduce a normalized parameter τ defined as the factor of the sending coil's diameter over the coil-to-coil vertical distance:

$$\tau = \frac{Sending\ coil\ diameter}{coil - to - coil\ vertical\ distance} \tag{3.1}$$

For example, investigations in [72] and [77] have both a system efficiency of 22%. On the other hand, τ equal to 8.62 and 3.46 respectively. The system described in [77] outperforms the second system presented in [72] because it has lower value of τ.

Table 3.3: Performance's comparison of selected inductive systems from the SOA

Coil Type	Coil shape	τ	Frequency	Load power	Efficiency	Reference
Ferrite core	Circular	0.6	< 150 kHz	90 mW	20%	[70]
Air core	Circular	0.3	9.9 MHz	60 W	40%	[71]
Air core	Circular	1	6 MHz	95 W	-	[79]
Printed	Square	8.62	1 MHz	10 mW	22%	[72]
Printed	Circular	> 20	2 MHz	1 W	30% - 40%	[80]
Printed	Square	2	1 MHz	10 mW	18.85%	[73]
Printed	Circular	> 13.33	500 kHz	1.2 W	-	[74]
Air core	Circular	1.27	742 kHz	-	24%	[56]
Air core	Circular	2	700 kHz	24mW	72%	[55]
Air core	Circular	3	4.5 MHz	10 mW	54%	[75]
Air core	Circular	2	700 kHz	50 mW	36%	[76]
Planar	Spiral	3.46	6.78 MHz	50 mW	22%	[77]
Air core	Circular	2	2 MHz	-	40%	[78]

Investigations dealing with large coil-to-coil distance have smaller values of $0 < \tau \leq 1$. Under this condition, low power transmission efficiency, low mutual inductance, and very weak coupling coefficient are expected. For higher value of τ, higher values of the parameters are expected.

These studies prove that the inductive systems with circular coils have better efficiency than the inductive systems with spiral or square coils. Besides, the inductive system with air core or ferrite core coils have better efficiency compared to the inductive systems with

printed or planar coils. Based on that, circular air core coils are suitable for inductive systems dealing with large distance between the sending and receiving sides.

3.2 State of the art of detection techniques

There are two different types of detection techniques. The first is the static detection, where the receiver is in a fixed position during the energy transmission phase. This technique is generally used for charging systems that offer a free positioning for the receiver. The second type is the dynamic detection, where the receiver is in movement during the energy transmission phase. Through literature, different types of detection techniques can be found [21, 80, 107-108].

3.2.1 Detection techniques

The proposed method in [21] is based on the detection of small frequency deviations from the nominal resonance frequency, which happen when the receiver position is under the charging station. The control of the nominal resonance frequency is performed by Self-tuning controllers. The proposed circuit has not been experimentally implemented and only a finite element analysis is presented.

A method is used when the receiver coil is covered by soft-magnetic material (ferrite) to provide shielding and flux guiding [80]. The circuit consists of sensor inductor located in each transmitter coils as shown in Fig. 3.16.

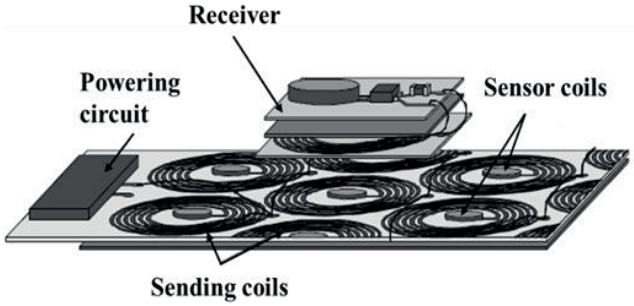

Fig. 3.16: Inductive system incorporating a sensor coil in every sending coil [80]

Its principle is based on the detection of soft-magnetic material causing changes of the inductance of the sensor inductor due to the soft-magnetic shielding in the receiver. The

resonant circuit is connected to a current source having a fixed operation frequency below the idle resonant frequency. If the resonance frequency of the circuit changes to lower frequencies, the output voltage of the sensor circuit increases. If it rises above a certain trigger level known as “Detection limit”, the sensor resonant circuit detects a receiver device and the related transmitter coil is activated. In case of a non-magnetic metallic device placed above the sending coils, the inductance of the sensor reduces and the resonance frequency change to higher frequencies. In this case, the output voltage decreases and does not set off the corresponding transmitter coil.

The sensor coil is considered as one part of a parallel resonant circuit. Due to the ferrite in the receiving coil, the inductivity of this sensor coil increases causing the redaction of the resonance frequency.

In [107] a load-detection method is proposed to reduce the power consumption of an inductive system by analysing the transmitting coil voltage and supply current space using a microcontroller with a built-in ADC. To extract the coil voltage, a high impedance half wave rectifier is used. A current sense resistor was used to extract the supply current. Their aim is to turn off the sending coils when no valid receiving devices are placed on the transmitting platform. If the supply current is below 0.3 A, the sending coil voltage must be in the range of 32 and 64 V. If it is above 0.3 A, the sending coil voltage must be in the range of 32 and 80 V. For these two conditions, the corresponding sending coil is activated and a valid receiving coil is present. For any other value of the supply current, which is higher as 0.85 A, it is considered that there is no valid receiving coil and the system would switch off the corresponding sending coil.

The method, explained in [108], uses the sending coil as sensor coils. It is named load detection method. The principal is to scan every sending coil, at the same time, measuring and evaluating their equivalent impedances. By using this method, it is also possible to identify the load type if it is conductive material or soft-magnetic material.

The load detection method takes place in three different stages defined as: calibration, load-position detection and load-type estimation. In the calibration stage, the equivalent winding impedances are estimated by measuring for every sending coil its current amplitude, relative current phase, voltage amplitude and voltage phase, when the sending

system doesn´t have any load devices. During the second stage, every sending coil is excited individually, for a short duration between 1 and 2 seconds. Simultaneously, its current amplitude, current phase, voltage amplitude and voltage phase are measured and stored. After the sending coils are scanned, measurements are the converted to impedance value and are compared against the calibrated values of the first stage.

The changes in impedance phases and amplitude can be calculated as

$$\Delta\phi = (\phi^S / \phi^C - 1)(100) \tag{3.2}$$

Where, ϕ^C and ϕ^S are the impedance phase measured in the calibration stage and stored in the second stage, respectively.

$$\Delta X = (|X^S| / |X^C| - 1)(100) \tag{3.3}$$

Where, X^C and X^S are the impedance amplitude measured in the calibration stage and stored in the second stage, respectively.

Any deviations outside ± 5% of the impedance phases and ± 10% of the amplitudes indicate that a load device is placed above the corresponding sending coil.

In the last stage, by analysing the change in the impedance amplitude and phases, the load type is estimated if it is a valid resonant load, conductive material or soft-magnetic material.

If the load is a valid resonant load, there is no extra shift between the current and the voltage. In this case, only the impedance amplitude is changed. In the case of a conductive material, the impedance phase is decreasing and becoming increasingly negative and its amplitude increases. In the case of a soft-magnetic material, both the impedance amplitude and phase increase.

3.2.2 Evaluation

A brief comparison between the proposed detection circuits is presented in Table 3.4. The detection method in [80] presents some advantages, such as its low-cost analogue devices and the safety mechanism, which prevents power delivery to the metallic objects. It has also some drawbacks such as the low detection height of only 2 mm and the difficulty to regulate the trigger level of each sending coil.

Table 3.4: Evaluation of detection circuits

Properties	**Detection technique**			
Reference	[21]	[80]	[107]	[108]
Movable receiver	no	Yes	yes	yes
Use of extra sensors	no	yes	no	no
Use of extra microcontroller	yes	no	yes	yes
Dependency on the receiver's material	yes	yes	no	no
Influence of external material	yes	yes	no	no
Detection height	high	very low	very low	very low
Design complexity	medium	medium	high	very high
Cost	medium	low	medium	medium
Power saving	no	no	yes	yes

Detection methods presented in [107, 108] are similar to each other's. The low detection height of these methods presents their major limitation. The first detection method has less complexity than the second one because it controls only the coil voltage and the supply current. On the other hand, the second detection method controls the phases of the coil's voltage and the coil's current in addition to their amplitudes.

3.3 Proposed approach

The efficiency of IPT systems depends on both the vertical (axial) and lateral distances between the sending and receiving coils. Placing the sending and the receiving coils in a perfect position is generally difficult. Thus, a lateral misalignment is unavoidable and leads to a sharp decrease of mutual inductance, coupling coefficient and transmitted power. Consequently, the efficiency of the IPT system drops dramatically. This is due to the high magnetic field losses occurred during the power transmission phase.

One of the proposed solutions to overcome these problems is the use of multi-coil systems. In this context, we suggest to improve the transmitted power, the mutual inductance, the power at the load, and consequently the power transmission efficiency of an inductive system in case of lateral misalignment between the sending side and the receiving side and at large coil-to-coil vertical distance. To reach this objective, a multi

input single output MISO coil system able to orientate the issued magnetic field to the receiving coil is designed. The orientation of the magnetic field is assured by the neighbouring coils of the active sending coils, which are powered with weak current and in the opposite direction (see Fig. 3.17).

For comparison matter, the sending coils are settled to occupy the same surface occupied by a bigger sending coil in a conventional two-coil system. For the investigation, we propose the use of circular air core sending coils in a hexagonal arrangement and having the half diameter of the receiving coil. Thus, an analytical model of the used coils and an accurate three-dimensional model of the system have been developed to predict the values of induced voltage, current and mutual inductance. For the experimental investigations, air core coils have been fabricated by copper wire and have been characterized using an impedance analyser. A multi-coil inductive system consisting of a matrix of 16 air core sending coils and a receiving coil has been designed.

In order to improve the transmitted power to the secondary side and consequently the total system efficiency at resonance, it is proposed the use of compensation capacitors in series or in parallel in the primary and/or in the secondary circuits. The selection of the adequate topology depends on the system requirement. Hence, four main compensation topologies are investigated, which are the series-series (SS), series-parallel (SP), parallel-series (PS) and parallel-parallel (PP) topologies.

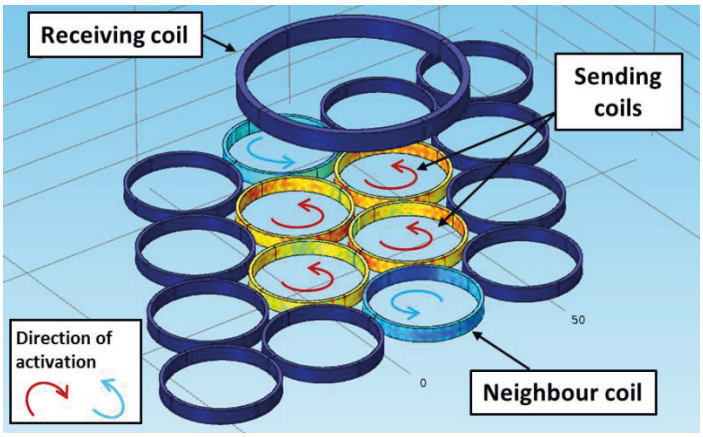

Fig. 3.17: Proposed multi-coil inductive system

In case of movable receiver, we propose to implement a detection method for the receiving coil without adding additional sensors to the circuit. Here, only the sending

coils, which are above the receiver, are activated and the others remain switched off. This novel solution uses the sending coils themselves as detector. The detection method is based on the measurement of the peak of the AC current of the sending coils, converts it to DC signal, and compares it with a detection threshold. The solution is easy to implement, inexpensive and it is composed of simple electrical components. It could be applied to all applications having movable receivers with different size and position.

After detecting the position of the receiver, some sending coils are activated and the others are turned off. Powering all the sending coils, which are under the receiver, by the same way lead to magnetic field leakage caused due to the mismatch between the surface of energy exchange of the receiver and the corresponding sending coils. As a solution, we propose a novel excitation strategy for the active sending coils in which we excite the perfectly aligned coils with the receiver more than the mismatched ones. This approach is followed for every lateral position of the receiving coil.

Chapter 4

Modelling of circular air-core coils

The aim of this section is to define an accurate and simple model for a circular coil. The simplicity and the accuracy of the analytical model of the coils are needed to provide guide lines in the choice of the design's parameters, system's performance indices as well as for the efficiency optimization of the inductive power transmission systems.

The first part of this chapter is addressed to the modelling of circular air-core coils in which the self-inductance, coil's resistance, self-capacitance and quality factor are estimated. In the second part, rules for the choice of coil's properties are provided in order to improve the induced voltage and the transmitted power and consequently the power transmission efficiency of the inductive systems.

4.1 Coil model

A coil is modelled as an inductance L with a series resistance R_{coil} and a capacitance C_L in parallel to them as shown in Fig.4.1.

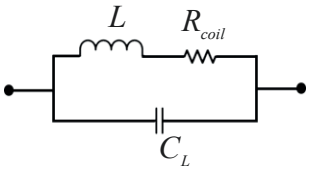

Fig. 4.1: Coil's model

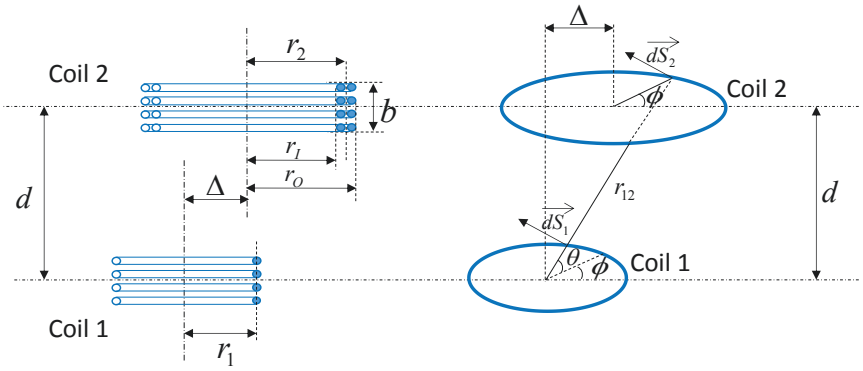

Fig. 4.2: Geometric parameters of the coils

For experimental investigation of the different coil models, we propose to use sending and receiving coils having the following parameters as presented in Table 4.1.

Table 4.1: Coils' parameters

Parameters	**Definition**	**Sending coil**	**Receiving coil**	**Extra coil**
r	Coil mean radius	15 mm	30 mm	40 mm
r_o	Coil outer radius	16 mm	32 mm	41.52 mm
r_I	Coil inner radius	14 mm	28 mm	38.47 mm
D	Coil diameter	30 mm	60 mm	80 mm
N	Number of turns	4	8	9
b	Coil length	8 mm	8.5 mm	10 mm
a	Winding's wire radius	0.5 mm	0.5 mm	0.5 mm
m	Number of layer	1 layer	2 layers	2 layers

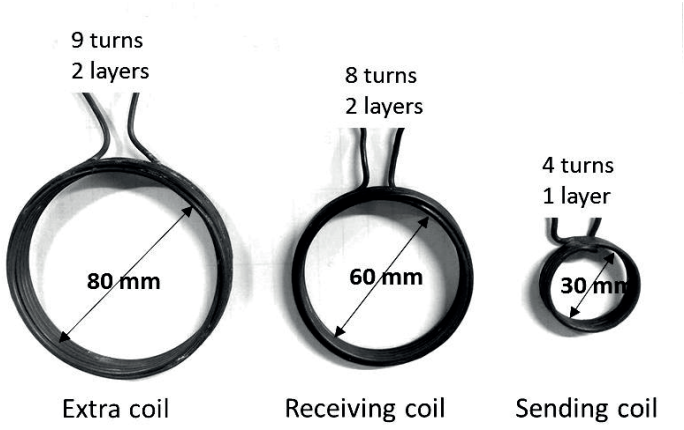

Fig. 4.3: Coils used in experimental investigations

4.1.1 Self-inductance estimation

4.1.1.1 Models

Kirchhoff and Maxwell first developed formulas for the calculation of the self-inductance [48, 81]. The self-inductance of a coil is defined as the rates of change of the magnetic flux ϕ through the coil with respect to the current *I*.

$$L = \frac{\Phi}{I} \tag{4.1}$$

The flux through the coil with N turns, a radius r and a length b is equal to:

$$\Phi = \frac{4\pi\, r^2 N^2 I}{b} \tag{4.2}$$

Substituting Eq.4.2 in Eq.4.1, we got:

$$L = \frac{4\pi\, r^2 N^2}{b} \tag{4.3}$$

This formula is accurate only for coils with extremely long length b.

Other models have been developed in [82, 83]. One of the important models for the calculation of the self-inductance for circular coil with circular section has been proposed by Rayleigh and Niven [84]

$$L = 4\pi N^2 r\left\{\left(1+\frac{a^2}{8r^2}\right)\log\frac{8r}{a}+\frac{a^2}{24r^2}-1.75\right\} \tag{4.4}$$

For a single layer coil, the model becomes

$$L = 4\pi N^2 r\left\{\log\frac{8r}{b}-\frac{1}{2}+\frac{b^2}{32r^2}\left(\log\frac{8r}{b}+\frac{1}{4}\right)\right\} \tag{4.5}$$

Another model has been proposed by Wheeler [85, 86]. In case of a single layer air core coil, the self-inductance of the coil is given by Eq. 4.5 and for the case of multi-layer air core coil the self inductance is given by Eq.4.6 as follows

$$L = \frac{N^2 r^2}{9r+10b}\ \mu H \tag{4.6}$$

Note that in this equation, *r* and *b* are in inches.

$$L = \frac{31.6\, N^2 r_I^{\,2}}{6r_I + 9b + 10(r_O - r_I)}\ \mu H \tag{4.7}$$

Note that in this equation, r_I, r_o and *b* are in meters.

Another inductance's model is presented in [87, 88] by B. B. Babani as follows

$$L = \frac{N^2 (r_I + r_O)^2}{127(13r_O + 9b - 7r_I)}\ \mu H \tag{4.8}$$

Note that in this equation, r_I, r_o and *b* are in millimetres.

4.1.1.2 Evaluation

The proposed models for the self-inductance are simulated in MATLAB software and then compared to the experimental values measured at a frequency of 1.2 MHz. For the experimental investigation, an Agilent impedance analyser has been used as shown in Fig.4.4. The obtained results are explored in Table 4.2.

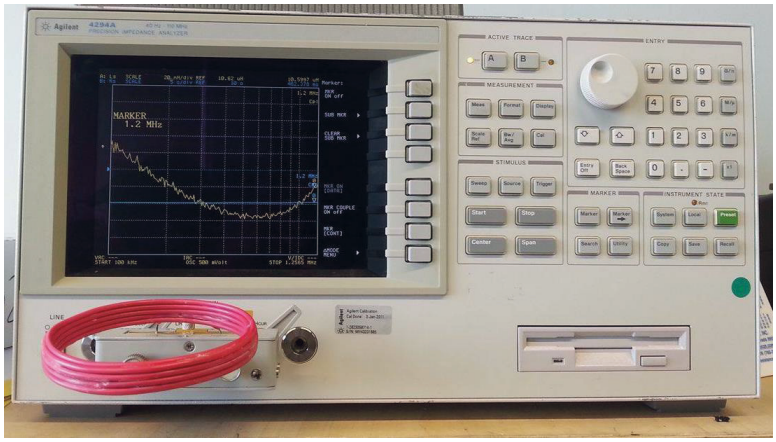

Fig. 4.4: Measurement set up for experimental investigations

Table 4.2: Simulation and experimental results of coils' self-inductance

Formula	**Self-inductance in µH**		
	Sending coil	Receiving coil	Extra coil
Maxwell (eq. 4.3)	0.64	9.09	16.28
Rayleigh and Niven (eq. 4.4)	1.12	10.67	19.18
Rayleigh and Niven (eq. 4.5)	0.69	-	-
Wheeler (eq. 4.7)	0.66	6.31	10.39
Babani (eq. 4.8)	0.68	6.66	11.06
Experiment	0.73	6.30	10.56

Based on the results shown in Table 4.2, we conclude that the coil self-inductance expression proposed by Wheeler is more accurate than the other ones. The error between the experimental and the analytical values is less than 3%. So, this expression is sufficiently to model the sending and receiving coils' inductance.

4.1.2 Resistance estimation

The prediction of the coils' resistance is important for designing inductive power transmission applications, as it is one of the influencing factors that limit the capability of power transfer and the efficiency of inductive systems.

4.1.2.1 Models

Based on the literature, several methods for estimating the resistance of coils are proposed. One of the most important expressions was proposed by Butterworth [89]:

$$R_{coil} = R_{DC}\left(\alpha(1+F)+(\beta u_1+\gamma u_2)\frac{d^2}{D^2}G\right) \tag{4.9}$$

Where: d is the wire diameter in centimetres, R_{DC} is the DC resistance of the coil and all the other parameters are functions of coil's diameter, coil's length, distance between adjacent turns, wire's diameter, operation frequency, and the resistivity and the permeability of the conductive material. They are tabulated in [89].

Then, Butterworth modified Eq. 5.9 for shorter coils with different number of turns and layers [90, 91]:

$$R_{coil} = R_{DC}\left(1+F\left(1+\frac{1}{8}W_n\frac{d^4}{D^4}\right)+U_nG\frac{d^2}{D^2}\left(1+\frac{1}{2}V_n\Phi_1\frac{d^2}{D^2}\right)\right) \tag{4.10}$$

Where U_n, V_n, and W_n are functions of number of turns and Φ_1 is function of wire diameter, operation frequency, coil's diameter, and the resistivity and the permeability of the conductive material as tabulated in [89-91].

Afterwards, Jackson [92] proved experimentally the validity of these formulas indicating at the same time that they are not suitable for coils of intermediate lengths.

Since Butterworth's expressions are very complicated, other simplified expressions for coil resistance, based on Butterworth's model, are proposed. In [79], Pinuela et al. proposed the following expression:

$$R_{coil} = R_{rad} + R_{skin} \tag{4.11}$$

Where: R_{rad} is the radiation resistance [93], and R_{Skin} is the skin-effect resistance, which also considers the proximity effects. They are equal to the following expressions:

$$R_{rad} = N^2 \eta_0 \left(\frac{\pi}{6}\right)\left(\frac{2\pi}{\lambda_d}\right)^4 \tag{4.12}$$

$$R_{skin} = \frac{N r}{2a}\sqrt{\frac{\omega \mu_0}{2\sigma}} \tag{4.13}$$

Where: ω is the angular frequency, N and r are the number of turns and the radius of the coil, respectively, a and σ are the radius and the conductivity of the copper wire, respectively, η_0 and μ_0 are the impedance and the permeability of free space, respectively, and λ_d is the free space wavelength at the corresponding operation frequency.

In [70], two simplified models for the coil resistance have been proposed. These models are dependent on the operation frequency f and on the value of the skin depth δ, which equals to:

$$\delta = \frac{1}{\sqrt{\pi \sigma \mu f}} \tag{4.14}$$

where σ and μ are the conductivity and permeability of the copper wire respectively. Based on [94] and [95], the two models for the coil resistance are equal:

If $\delta > r/2$:

$$R_{coil} = R_{DC}\left[1 + \frac{1}{3}\left(\frac{r}{2\delta}\right)^4\right] \tag{4.15}$$

If $\delta < r/2$:

$$R_{coil} = R_{DC}\left[\frac{r}{2\delta} + \frac{1}{4} + \frac{3}{64}\left(\frac{2\delta}{r}\right)\right] \tag{4.16}$$

Where, r is the radius of the coil and R_{DC} is its DC resistance, which is estimated as in [96]:

$$R_{DC} = \frac{4\rho b\left(r_0^2 - r_I^2\right)}{(2a)^4} \tag{4.17}$$

Here, r_O is the outer radius of the coil, r_I is the inner radius of the coil, b is the coil length and a is the wire radius.

In case of high frequencies, that means $\frac{a}{2\delta} >> 1$, the resistance could be estimated as in [97] and [98]:

$$R_{coil} = R_{DC} \frac{a}{2} \sqrt{\pi \sigma \mu f} \tag{4.18}$$

4.1.2.2 Evaluation

Experimentally, the resistances of the coils are measured by the Agilent impedance analyser. The simulations and experimental results are shown in Fig.4.5. (a), (b) and (c).

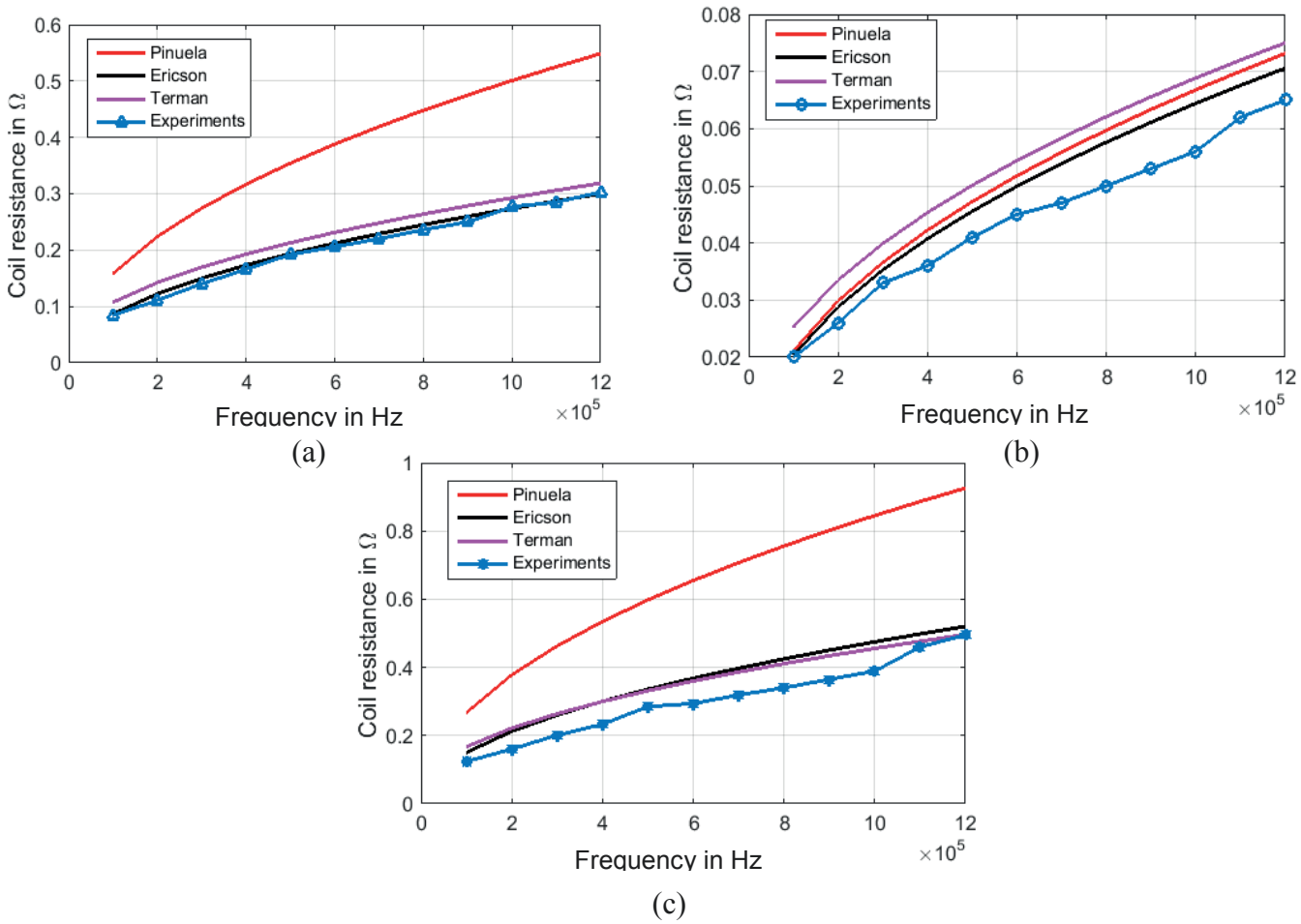

Fig. 4.5: Simulation and experimental results of the resistance of (a) receiving coil with 60 mm diameter (b) sending coil with 30 mm diameter and (c) extra coil with 80 mm diameter

Three different coil sizes are chosen for the verification. The Pinuela's model is presented by the red curve, Ericson's model is presented by the black curve and Terman's model is

presented by the pink curve. The experimental values are presented by the blue curve with small triangles.

Based on the obtained results, the model of coil's resistance, which is proposed by Ericson in [97, 98] is more accurate than the other ones. Deviation between the measured values of the resistance and Ericson's analytical model is less than 2%. Consequently, for the rest of the work we will use Ericson's model for the estimation of the coil's resistance.

4.1.3 Self-capacitance estimation

In addition to the self-inductance and the series resistance, the coil also has a parasitic capacitance corresponding to the inter-winding capacitance, which exists between coil's turns.

The parasitic capacitance in general occurs in parallel to the coil's inductance provoking a parasitic resonance known as self-resonance, which limits the operation frequency of the coil. In practice, it is recommended to operate the coil at a much lower frequency then its self-resonance frequency. In this case, we have more current flowing through the coil turns and the parasitic capacitance could be neglected. At frequencies, higher than the self-resonating frequency, the coil acts as a capacitor and no longer as an inductor.

4.1.3.1 Models

Based on the literature, many researches are concentrated on the measurement of the coil's capacitance. The most important expressions are proposed by Palermo [99], Medhurst [100] and Grandi et al. [101].

The corrected version of Palermo's [99] is given as follows:

$$C_L = \frac{\varepsilon_0 \pi^2 D(N-1)}{N \operatorname{arccosh}\left(\frac{b}{N.2a}\right)} \tag{4.19}$$

Where, "*D*" and "*b*" are respectively the diameter and the length of the coil, "N" is the number of turns and "a" is the wire radius.

Medhurst's refitted formula [100] is given by Eq.4.20

$$C_L = \frac{4\varepsilon_0 b}{\pi}\left[1 + 0.8249\,\frac{D}{b} + 2.395\left(\frac{D}{b}\right)^{3/2}\right] \text{[Fahrad]} \tag{4.20}$$

Grandi, Kazimierczuk, Massarini and Reggiani"GKMR" [101] formula is given as follows:

$$C_L = \frac{\varepsilon_0 \pi^2 D}{(N-1)\ln\left(\frac{b}{N.2a} + \sqrt{\left(\frac{b}{N.2a}\right)^2 - 1}\right)} \tag{4.21}$$

4.1.3.2 Evaluation

The analytical value of the parasitic capacitance of the coils used in experiments is given by equations (4.19), (4.20) and (4.21). In practice, the aforementioned parameter is measured by Agilent Impedance Analyser. Table 4.3 depicts the obtained results. Based on the obtained results, we conclude that Palermo's model [99] is the more accurate model among the proposed ones to determine the coil's self-capacitance. The use of the extra coil for the verification is decisive.

Table 4.3: Simulation and experimental results of coils parasitic capacitance

Formula	**Parasitic capacitance in F**		
	Sending coil	Receiving coil	Extra coil
Palermo (eq. 4.19)	1.6e-10	1.4e-9	1.3e-9
Medhurst (eq. 4.20)	2.1e-10	5.2e-10	7e-10
GKMR (eq. 4.21)	8.5e-11	6.6e-10	4.4e-10
Experiments	2e-10	2.8e-9	1.7e-9

4.1.4 Coil quality factor estimation

As definition, the quality factor of a coil is the ratio of apparent power to the power losses. Based on this definition, the quality factor results to:

$$Q = \frac{\omega L}{R_{coil}} \tag{4.22}$$

Where, $\omega = 2\pi f$ is the angular frequency and f is the operation frequency.

In general, the quality factor Q of coils has a value between 0 and infinity. In practice, it is difficult to get values higher than 1000 due to the self-resonating frequency and the resistance limitations of coils. On the other hand, a very low value (for example lower than 10) is not very useful. There are other parameters that the quality factor depends on such as the shape, the size and the material of the coil.

Figure 4.6 shows the quality factor of the sending and receiving coils in both simulations and experiments.

In simulations, Ericson's model of coil's resistance [97, 98] and Wheeler's model of coil's self-inductance [85, 86] have been used. Experimental investigations are carried out by an Agilent impedance analyser.

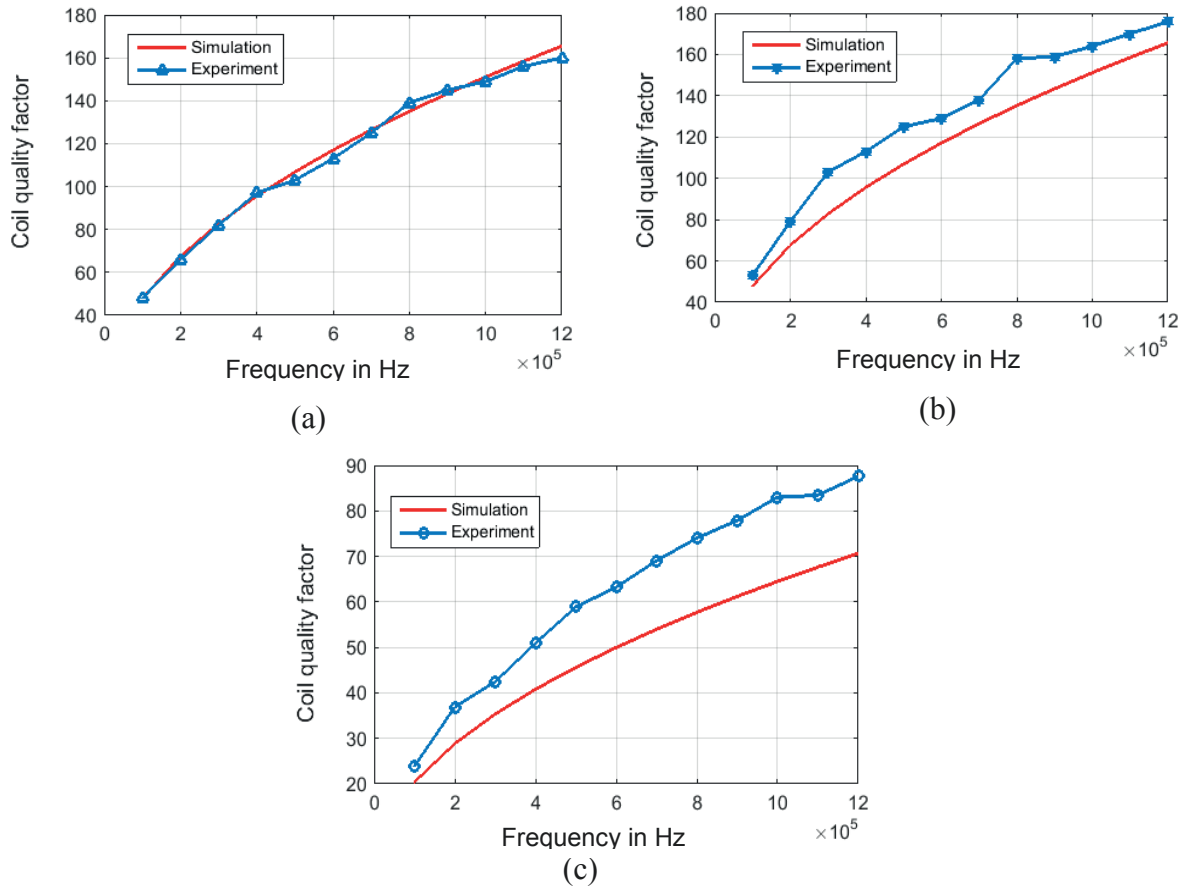

Fig. 4.6: Simulation and experimental results of the quality factor of (a) receiving coil with 60 mm diameter (b) extra coil with 80 mm diameter and (c) sending coil with 30 mm diameter

4.2 Effect of coil parameters on the efficiency of inductive link

The geometry and properties of the sending and receiving coils have a decisive effect on the efficiency of the inductive power transmission systems. In this section, we study in details the effect of coil parameters such as the coil's diameter, the number of turns, the winding's wire diameter, and the coil's shape on the induced voltage and the transmitted power to the load. An open circuit test is performed to investigate the induced voltage and a closed-circuit test is performed to investigate the induced current and thereby the transmitted power.

4.2.1 Number of turns

In order to investigate the induced voltage in the receiving side, an open circuit test is performed. Using Eq. 2.1, the induced voltage in the receiving coil is given as follows:

$$V = -\frac{d\phi}{dt} = -A\frac{d\vec{B}}{dt} \tag{4.23}$$

In case of a receiving coil with "N" turns, Eq. 4.23 becomes:

$$V = -NA\frac{d\vec{B}}{dt} \tag{4.24}$$

Referring to Eq.4.24, we conclude that by increasing the number of turns of the receiving coil, the induced voltage increases linearly. Figure 4.7 depicts the simulation and experimental results of the influence of the number of turns N_2 of the receiving coil. For the experimental investigation, the distance between the primary and secondary sides is adjusted to 1 cm.

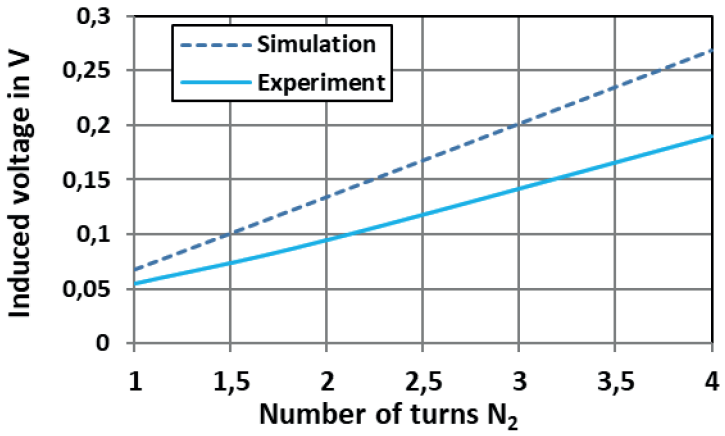

Fig. 4.7: Influence of the number of turns N_2 of the receiving coil on the induced voltage

At this short coil separation, a small deviation between simulation and experimental results is due to the fact that the close coil filaments respond more to the mutual inductance.

Equation 4.24 could be written also in terms of the number of turns of the sending and the receiving coils N_1 and N_2 respectively. The resulting equation is given as follows:

$$V = k_{12} L_1 \frac{N_2}{N_1} \frac{dI_1}{dt} \tag{4.25}$$

Where, k_{12} is the coupling factor between the sending and receiving coils and L_1 and I_1 are, respectively, the self-inductance and the current of the sending coil.

Referring to Eq. 4.25, we conclude that by increasing the number of turns N_1 of the sending coil, the induced voltage V decreases linearly.

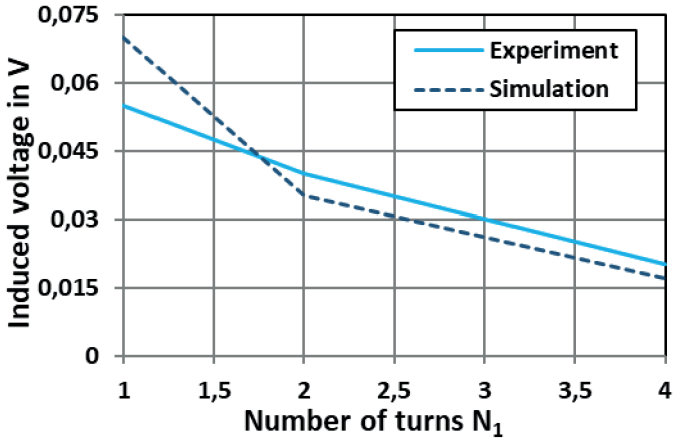

Fig. 4.8: Influence of the number of turns N_1 of the sending coil on the induced voltage

In order to investigate the transmitted power to the receiving side, a closed loop circuit test was performed. For that, a load of 1 Ω was added in series to the receiving coil.

In the first test, some parameters of the sending coil are fixed to the following values: the diameter D_1 equals to 7.5 cm and the number of turns N_1 equals to1 turn. Then, it is proposed to change the number of turns N_2 of the receiving coil. The diameter D_2 of the receiving coil equals to 6.5 cm and the axial distance d between the sending and receiving coils equals to 6 cm. Table 4.4 depicts the obtained experimental and simulation results by changing the number of turns N_2 of the receiving coil from 2 to 4 turns while maintaining the number of turns N_1 of the sending coil fixed to one turn.

Table 4.4: Influence of the number of turns N_2 of the receiving coil on the transmitted power

Number of turns N_2 of the receiving coil	**Transmitted power in mW**	
	Simulation	Experiment
2	6.9	6.8
4	22.9	18.2

Based on the obtained results, it is better work with a receiving coil having a number of turns N_2 greater than that of the sending coil. In this case, as the number of turns increase, the transmitted power is also increased.

In the second test, some parameters of the receiving coil are fixed to the following values: the diameter D_2 equals 6.5 cm and the number of turns N_2 equal 2 turns. Then, it is proposed to change the number of turns N_1 of the sending coil. The diameter D_1 of the sending coil equals 7.5 cm and the axial distance d between coils equals 5 cm.

Table 4.5: Influence of the number of turns N_1 of the sending coil on the transmitted power

Number of turns N_1 of the sending coil	**Transmitted power in mW**	
	Simulation	Experiment
1	75	74.2
2	19.8	19.2

Table 4.5 shows the obtained experimental and simulation results by changing the number of turns of the sending coil from 1 to 2 turns while maintaining the number of turns N_2 of the receiving coil fixed to 2 turns.

In accordance to the first test, the obtained results show that if the number of turns N_1 of the sending coil increases, the transmitted power decreases.

Referring to the first and the second tests, in both open and closed circuits, and in order to increase the transmitted power, the number of turns N_1 of the sending coils used for the multi-coil system should be inferior or equal to the number of turns N_2 of the receiving coil.

4.2.2 Diameter

In this section, it is proposed to investigate the effect of the diameter of both the sending and the receiving coils, first, on the induced voltage and, secondly, on the transmitted power.

In the first test, the parameters of the sending coil are kept fixed to the following values: the diameter D_1 equals 6.5 cm and the number of turns N_1 equals 9 turn. Then, it is proposed to change the diameter of the receiving coil D_2 from 4 cm to 10 cm. The number of turns N_2 of the receiving coil equals 9 turns and the axial distance d between the sending and receiving coils equals 6 cm. Figure 4.9 presents the obtained results.

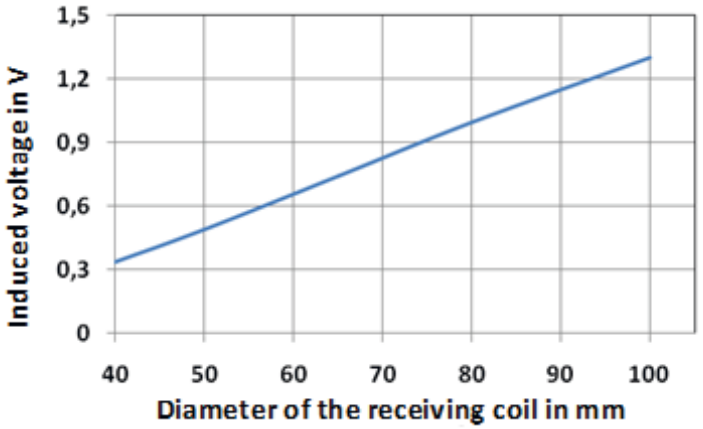

Fig. 4.9: Influence of the receiving coil's diameter D_2 on the induced voltage

Results show that the induced voltage increases by increasing the diameter of the receiving coil. This also justified by Eq. 4.33. By increasing the surface area A, the induced voltage V increases.

In the second test, the parameters of the receiving coil are kept fixed to the following values: the diameter D_2 equals 6 cm and the number of turns N_2 equals 9 turns. Then, it is proposed to vary the diameter D_1 of the sending coil from 4 cm to 10 cm. The number of turns N_1 of the sending coil equals 9 turns and the axial distance d between the sending and receiving coils equals 6 cm. Figure 4.10 depicts the obtained results.

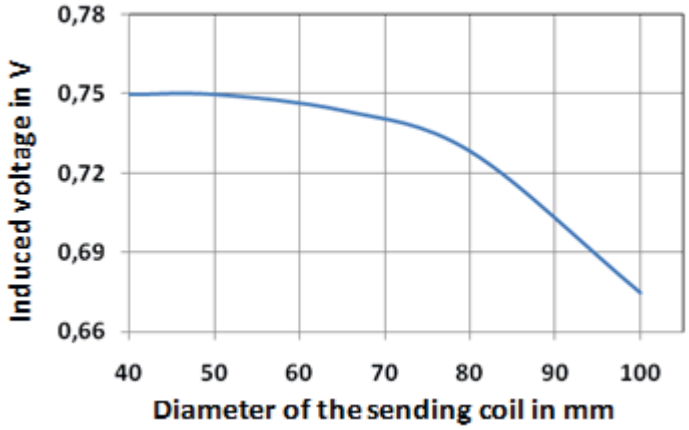

Fig. 4.10: Influence of the sending coil's diameter D_1 on the induced voltage

Results show that the induced voltage V starts to decrease when the diameter D_1 of the sending coil becomes greater than the diameter D_2 of the receiving coil.

Based on the open circuit test, it is better to work with sending coils having a diameter inferior or equal to the receiving one.

In order to investigate the transmitted power to the receiving side, a closed loop circuit test is performed. For that, a load of 1 Ω is added in series to the receiving coil.

As for the open circuit test, the first closed circuit test is performed by keeping some parameters of the sending coil fixed to the following values: the diameter D_1 equals 7.5 cm and the number of turns N_1 equals 1 turn. The number of turns N_2 of the receiving coil equals 4 turns and the axial distance d between coils equals 5 cm.

Table 4.6 depicts the experimental and simulation results by changing the diameter D_2 of the receiving coil from 6.5 cm to 9.5 cm while maintaining the diameter D_1 of the sending coil fixed to 7.5 cm.

Table 4.6: Influence of the receiving coil's diameter D_2 on the transmitted power

Diameter D_2 of the receiving coil	**Transmitted power in mW**	
	Simulation	**Experiment**
6,5 cm	21.4	19.3
9,5 cm	44.7	42

Based on the obtained results, we conclude that by increasing the diameter D_2 of the receiving coil, the transmitted power is also increased because the surface area A of exchanged power is increased.

In the second test, the diameter D_2 and the number of turns N_2 of the receiving coil are kept fixed to 6 cm and 4 turns, respectively. Then, it is proposed to vary the diameter D_1 of the sending coil from 6 cm to 9.5 cm. The number of turns N_2 of the receiving coil equals to 2 turns and the axial distance d between the sending and the receiving coils 5 cm.

Table 4.7: Influence of sending coil's diameter D_1 on the transmitted power

Diameter D_1 of the sending coil	**Transmitted power in mW**	
	Simulation	**Experiment**
6	7.8	7.2
9,5	13	11.6

Table 4.7 shows that by increasing the diameter of the sending coil, the transmitted power increases, because the generated magnetic field is augmented by using bigger coils.

Referring to the first and the second tests in both open and closed circuits, and in order to increase the transmitted power, it is better to deal with sending coils having a diameter D_1 inferior or equal to the diameter D_2 of the receiving coil.

4.2.3 Wire diameter

The winding's wire diameter of the coils has a great impact on the efficiency of the inductive power transmission systems. In order to study its effect, it is proposed to make two tests. The first one is to keep the parameters of the sending coil fixed to certain values while varying the winding's wire diameter of the receiving coil. In the second test, we make the opposite. That means we fix the parameters of the receiving coil while changing

the winding's wire diameter of the sending coil. Table 4.8 shows the parameters used in both tests.

Table 4.8: Parameters for the first and the second tests

Test	**First test**		**Second test**	
Axial distance	5 cm		5 cm	
Parameters	Sending coil	Receiving coil	Sending coil	Receiving coil
Diameter	7.5 cm	6.5 cm	7.5 cm	6.5 cm
Number of turns	1 turn	1 turn	1 turn	2 turns
Winding's wire diameter	1 mm	variable	variable	1 mm

Table 4.9 depicts the experimental results of varying the winding's wire diameter of the sending and the receiving coils. Refereeing to the obtained results and in order to have more transmitted power, it is better to deal with sending coils having a winding's wire diameter superior or equal to that of the receiving coil. This is justified by the fact that when the thickness of the wire increases, the skin effect, which limits the performance of the coil has a lower effect at higher frequency

Table 4.9: Influence of the winding's wire diameter of the receiving coil

First test		**Second test**	
Wire's diameter of the receiving coil	Transmitted power in mW	Wire's diameter of the sending coil	Transmitted power in mW
1 mm	27.4	1 mm	70.5
2 mm	9.5	2 mm	75.5

4.2.4 Shape

The choice of the shape of the sending and receiving coils is very important for the optimization of the efficiency of the inductive links. In this section, it is proposed the study of four combinations of coil's shape as shown in Fig. 4.11: a) circular-circular b) circular-square c) square-square and d) square-circular. The objective behind that is to find the best combination that offers the highest transmitted power. For the simulation study, the sending coils have the following parameters: the diameter D_1 equals to 4 cm and the

number of turns N_1 equal to 3 turns. On the other side, the diameter D_2 and the number of turns N_2 of the receiving coils equal to 4 cm and 5 turns, respectively. The axial distance d between the sending and receiving coils equals 2 cm.

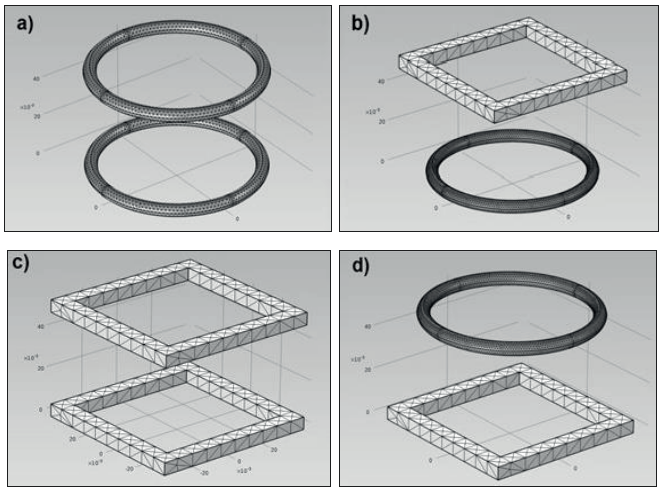

Fig. 4.11: Different combination of coil's shape: (a) circular-circular (b) circular-square (c) square-square and (d) square-circular

A three-dimensional simulation is performed by finite element simulation software and the obtained results are illustrated in Table 4.10.

Table 4.10: Simulation results for coil's shape combination

Coil's shape combination	**Transmitted power in mW**	**Efficiency in %**
circular-circular	143	21
circular - square	112	17
square - square	87	13
square - circular	54	8

Based on these results, we conclude that a better transmitted power is achieved by using both sending and receiving coils with circular shape. This configuration gives a symmetric distribution of the magnetic field and a uniform current circulation along the coils' windings as shown in Fig 4.12.

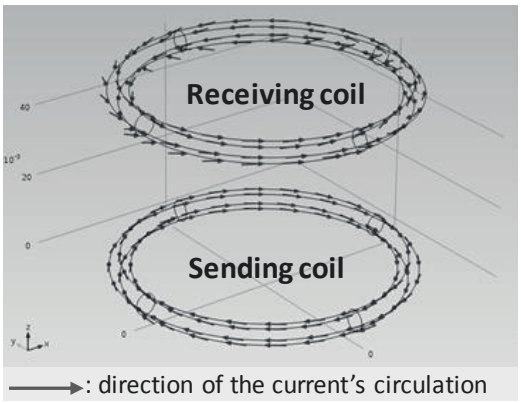

Fig. 4.12: Current's circulation in the sending and the receiving coils with circular shape

4.3 Discussion of the modelling results

In this chapter, expressions for self-inductance, coil's resistance, self-capacitance, and quality factor are estimated analytically and verified by experiments. An accurate and simple model of these coil's parameters are proposed. The resulting model is a combination of Wheeler's model [85] for the self-inductance, Ericson's model [97] for the coil's resistance and Palermo's model [99] for the self-capacitance. The circular air core coils are modelled in order to provide guide lines in the choice of design parameters, system performance indices as well as for the efficiency optimization of the inductive power transmission systems.

In the second part, we proposed rules for the choice of coil's diameter, coil's number of turns, winding's wire diameter and coil's shape in order to improve the induced voltage and the transmitted power and consequently the power transmission efficiency of the inductive systems.

Chapter 5

Large air-gap multi-coil inductive system

The typical concept of an inductive system is presented in Fig.5.1. It is composed by the power supply, the interface power supply/coil system, the coil system, the interface coil system/load, and the load. The aspects that influence an IPT system are: The operation frequency *f*, separation distance *d*, lateral misalignment Δ, coils' properties and geometries (e.g. printed, air-cored, ferrite-cored, circular, square), compensation capacitors that form system topologies, system configuration (i.e. two-coil system or multi-coil system), source impedance, the interface between power source and coil system (e.g. ADC converter, amplifier), the interface between the coil system and the load (e.g. rectifier, voltage regulator) and finally the load.

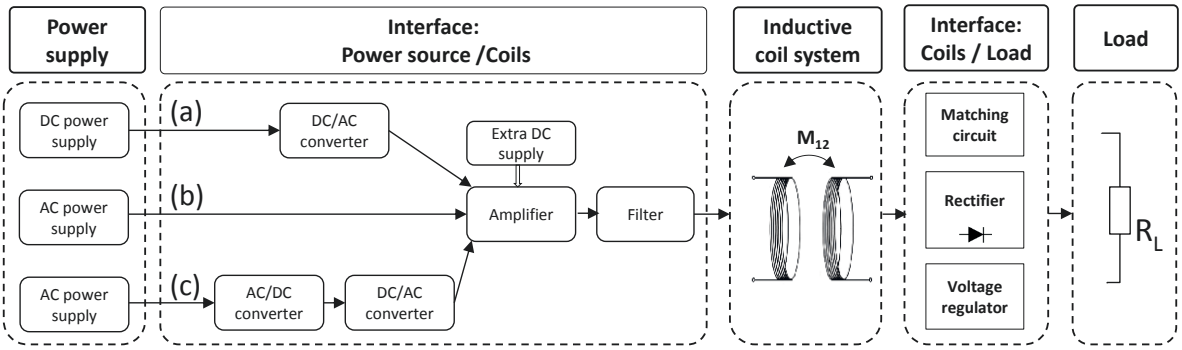

Fig. 5.1: Typical concept of inductive power transmission (IPT) system

In the first part of this chapter, the investigation of effects of both axial and lateral distances on the transmitted power is proposed. On the second part, a novel multi-coil system, which solves the problem of a large air-gap misalignment between the sending and receiving sides is designed. This problem occurs, generally, in most of inductive systems. Therefore, an analytical model of the multi-coil system is proposed in order to extract the important parameters of the system, which are the equivalent mutual inductance M_{eq}, the induced voltage V_{ind}, the induced current I_{ind}, the coupling factor k, the transmitted power P_t and the system efficiency η.

Simulations and experiments are performed, first, to validate the proposed analytical and three-dimensional models of the multi-coil system and, secondly, to determine the transmitted power and the power transmission efficiency of the system. The last part is devoted to the investigation of different compensation topologies for the studied multi-coil system to realize the resonance and increase, thereby, the transmitted power to the load and, consequently, the power transmission efficiency.

5.1 Effect of vertical and lateral distances on system performance

Power transmission efficiency of inductive systems is highly dependent on the lateral distance 'Δ' and the vertical distance '*d*' separating the sending side and the receiving side. Fig.5.2 depicts lateral misaligned coils at large air gap '*d'* in case of single input single output SISO coil system. It shows a magnetic flux leakage caused by the increase of the axial and lateral distances. In this case, some parameters are affected negatively such as the coupling factor and the mutual inductance between the sending and receiving coils.

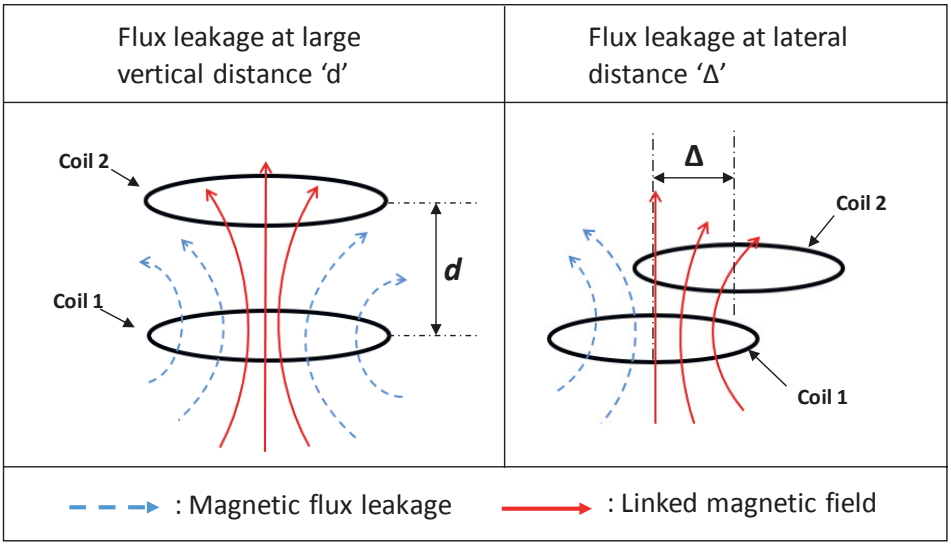

Fig. 5.2: Flux leakage in case of lateral misaligned coils at large air gap '*d*' in SISO system

Curves in Fig.5.3 (a) and Fig.5.3 (b) present, respectively, the coupling factor and the mutual inductance between two coils having a variable vertical distance from 1 cm to 5 cm and variable lateral distance from 0 cm to 2.5 cm. The diameter of the sending coil D_1 and the receiving coil D_2 are equal, respectively, to 3 cm and 6 cm and their number of turns N_1 and N_2 are equal, respectively, to 4 turns and 8 turns.

At 1 cm coil to coil vertical distance '*d*', the coupling coefficient '*k'* drops from 0.18 at 0 cm lateral deviation to 0.06 at 2.5 cm lateral deviation corresponding to 83.33% of the sending coil diameter. At large air gap, corresponding to more than 1.6 times of the diameter of the sending coil, the coupling factor decreases with a low slope (i.e. it drops with 8% of its initial value from 0 cm to 2.5 cm misalignment) comparing to a nearby distance in which the coupling coefficient drops with more than 66% of its initial value.

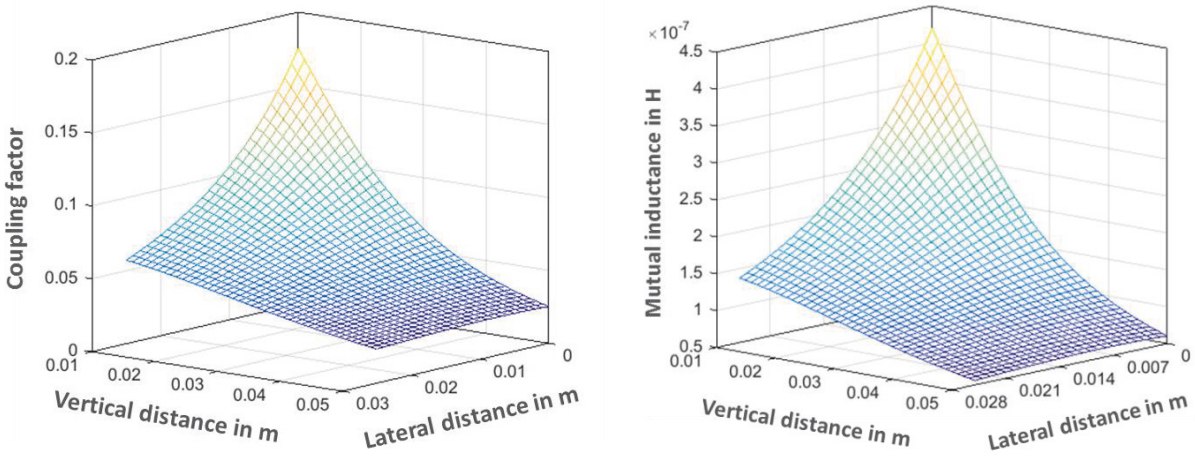

(a) (b)

Fig. 5.3: Coupling factor (a) and mutual inductance (b) for different lateral and vertical distances

Similar to the coupling factor, the mutual inductance is affected by both vertical and lateral distances. At perfect alignment, the mutual inductance drops significantly by more than 85% of its initial value from 1 cm vertical distance to 5 cm vertical distance. At a lateral misalignment of 2.5 cm, the mutual inductance is decreased by 59% of its initial value from 0.137µH at 1 cm vertical distance to 0.056 µH at 5 cm vertical distance.

Additionally, in case of a large air gap lateral misalignment, not all magnetic field lines produced by the sending coils go through the receiving coil. As result, the induced current

I_{ind} and the induced voltage V_{ind} decrease. Consequently, the transmitted energy decreases. This is justified by Faraday's law [42], which shows a proportional relation between the magnetic field $\vec{B}$ and the induced circulating electric field $\vec{E}$

$$\text{Faraday's law: } \oint_C \vec{E}\, d\vec{l} = -\frac{d}{dt}\int_S \vec{B}\, d\vec{A} \tag{5.1}$$

The transmitted power has been also evaluated, first, in case of variable vertical distance '*d*' and, secondly, in case of variable lateral distance 'Δ'. The resulting curves of the transmitted power with respect to vertical and lateral distance are plotted in Fig.5.4 (a) and Fig.5.4 (b), respectively.

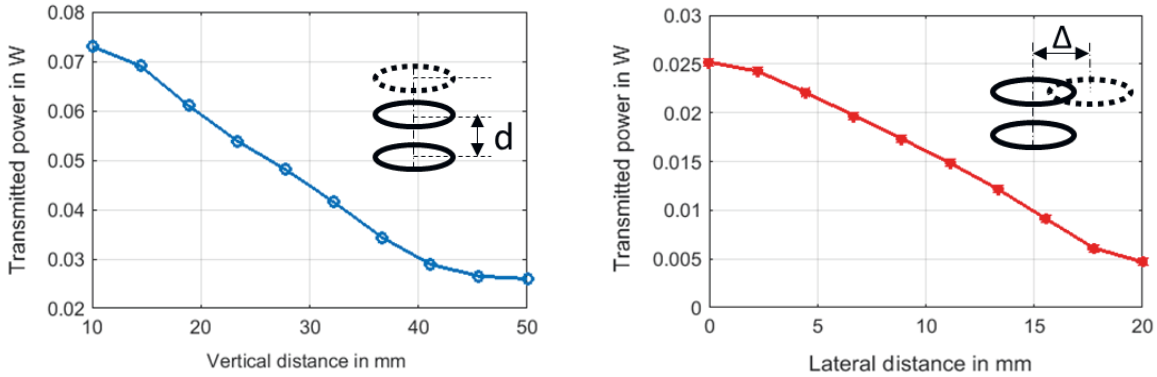

(a) (b)

Fig. 5.4: Transmitted power with respect to vertical (a) and lateral (b) distances

By increasing the vertical distance '*d*' from 10 mm to 50 mm corresponding to 166% of the sending coil diameter, the transmitted power decreases by more than 64% of its initial value. It also shows a very high drop of 80% of its initial value in case of lateral misalignment that varies from 0 mm to 20 mm, which corresponds to 66% of the sending coil diameter.

Based on the results shown in Fig. 5.3 and Fig. 5.4, we conclude that IPT systems are highly dependent on both lateral and vertical distances. They show a sharp decrease of mutual inductance, coupling coefficient and transmitted power. Consequently, the efficiency of the IPT system drops dramatically. This is justified by the high magnetic field losses occurred during the power transmission phase.

One of the proposed solutions to overcome the problem of large air gap misaligned coils, is the use of multi-coil systems in place of the conventional two-coil system. In this

context, a Multi Input Single Output MISO coil system is proposed in which the sending side is composed by multiple sending coils occupying the same surface of a bigger coil.

5.2 Design of the MISO coil system

5.2.1 Introduction

As shown in section 5.1, inductive power transmission systems show a sharp decrease of more than 60% in their performance in case of large air gap misalignment between the sending and the receiving coils. The proposed multi-coil inductive system overcomes this influencing effect while the receiver is in fixed position and/or in movement during the power transmission phase.

Firstly, guidelines for the appropriate choice of the number of sending coils, their diameter and their arrangement are presented.

The second part is devoted to the analytical model and the three-dimensional model of the multi-coil system. Having a simplified and appropriate model of the inductive power transmission systems is highly needed in developing and optimizing any application in which they are used.

5.2.2 Coil configuration

5.2.2.1 Arrangement

The sending side of the multi-coil inductive system consists of a matrix of circular air-cored coils. Therefore, the magnetic field distribution is not uniform and it has a distribution of peaks and valleys, corresponding to the coil's centres and edges, respectively. To improve the coupling between the sending and receiving coils and their mutual inductance, these valleys of low magnetic fields should be reduced. This is achievable by removing the gap between the neighbouring coils.

First, a hexagonal and square coils' arrangement, is implemented in square surface that corresponds to the surface area of the receiving side (see Fig. 5.5).

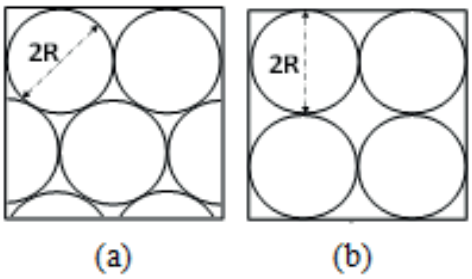

Fig. 5.5: Hexagonal (a) and square (b) coils' arrangement

For the hexagonal arrangement (Fig. 5.5 (a)), the area ratio between the sending side and the receiving side can be expressed as follows:

$$\frac{A_{Coils}}{A_{Square}} = \frac{4.5 \times \pi R^2}{4R \times 4R} = \frac{4.5\pi R^2}{16R^2} = \frac{4.5\pi}{16} \approx 0.883 \tag{5.2}$$

For the square arrangement (Fig. 5.5 (b)), the area ration between the sending and receiving sides is equal to the following expression:

$$\frac{A_{Coils}}{A_{Square}} = \frac{4 \times \pi R^2}{4R \times 4R} = \frac{4\pi R^2}{16R^2} = \frac{\pi}{4} \approx 0.785 \tag{5.3}$$

The area ratio between the receiving side and the sending side using circular air core coils with the hexagonal arrangement is higher than that of square arrangement. Therefore, the use of a matrix of circular air-core sending coils with a hexagonal arrangement encloses more power transmission area and therefore less magnetic flux leakage.

5.2.2.2 Diameter

For the investigation the influence of lateral misalignment with different coil numbers, the surface area for power transmission of the sending side are set equal to that of the receiving one, in order to treat all cases in a standardized manner. For the demonstration, the receiving coil was chosen with a diameter 'D_2' equal to 6 cm.

To consider the MISO coil-system configuration, sending coils should have a diameter smaller than the receiving one. That means, for the same area occupied by a bigger coil of 6 cm diameter, the biggest diameter of the sending coil equals to D/2 = 3 cm if we use at least 2 sending coils. Based on this approach, different configurations are illustrated in Table 5.1 and shown in Fig. 5.6. The choice of coils is based on the highest value of

mutual inductance between one sending coil and a receiving one. The expression of mutual inductance is explored in the next section.

Table 5.1: Parameters of different coil configurations

Diameter of the sending coil in cm	**Maximal possible number of coils**	**Maximal possible number of turns**
$D_2/2 = 3$	4.5	3.5
$D_2/2.4 = 2.5$	6.5	2.9
$D_2/3 = 2$	10.25	2.3
$D_2/4 = 1.5$	18	1.7

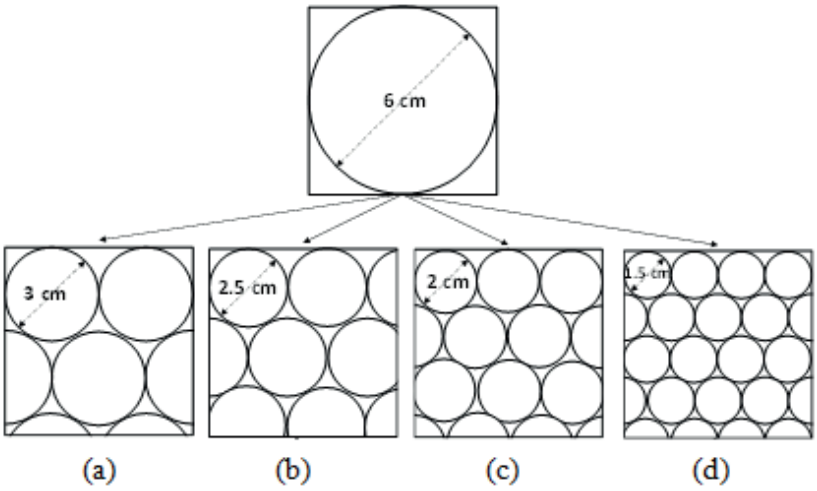

Fig. 5.6: Possible coil configurations

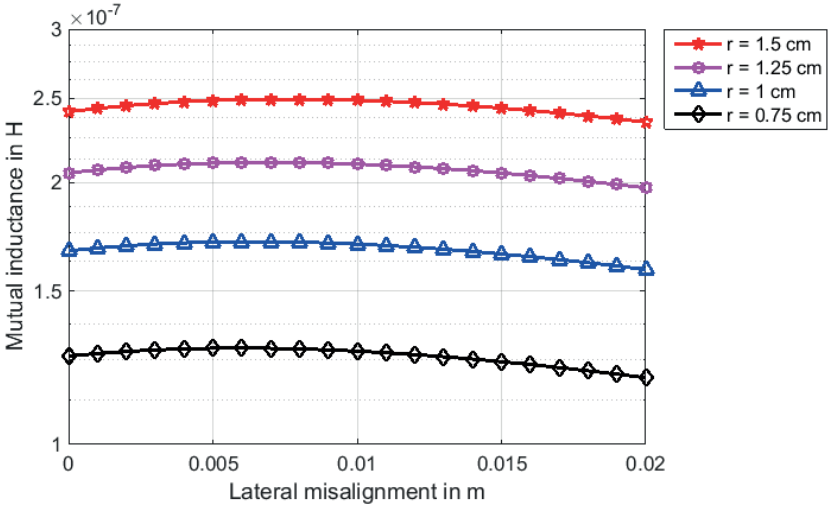

Fig. 5.7: Mutual inductance for different coil's diameters

Considering the numerical simulation results shown in Fig. 5.7, the highest mutual inductance is achieved by using a sending coil having a diameter of 3 cm. Therefore, based on Table 5.1 and on the obtained results, the design of an inductive system is highly required. The sending side of the investigated system consists of four sending coils with a diameter of 3 cm and each coil has 4 turns.

5.2.3 Analytical model

A 3D view of the designed multi-coil inductive system is shown in Fig. 5.8. The sending side consists of a matrix of circular air core coils, where no magnetic or soft-magnetic materials are present in or around them. The receiving side consists of a receiving coil, which can move in a parallel plane to the sending side. A large air gap is considered between the two sides in which a high loss of magnetic field is expected. This scenario has frequently happened especially in medical applications, wireless sensors, conveyor systems and other industrial applications. It becomes critical for low power applications.

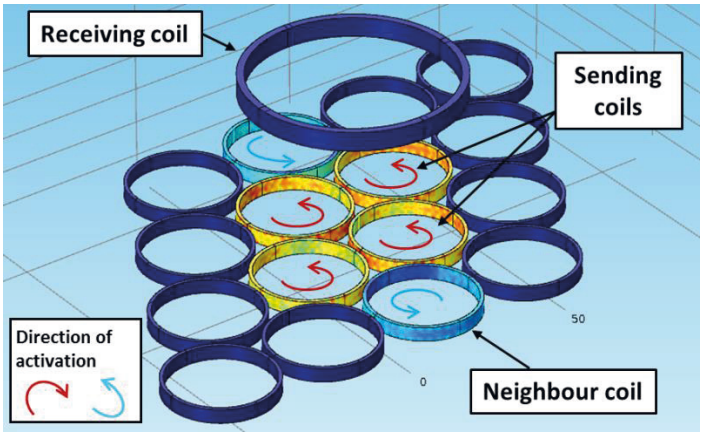

Fig. 5.8: Proposed multi-coil inductive system

The analytical model of the system is needed to extract the important parameters of the system, which are the mutual inductance, the coupling factor, the transmitted power, the induced voltage, and the induced current. Moreover, this model is able to optimize the power transmission efficiency.

Based on the literature, previous investigations have concentrated on the modelling of stationary inductive systems considering the terms mutual inductance [72, 73], the

coupling factor [74], resonant capacitor circuits [75, 76] and other critical parameters. These investigations are not suitable either for the multi-coil systems or the systems with movable receivers.

The equivalent circuit of the proposed multi-coil system is presented in Fig. 5.9. L_1, L_2 and R_{L1}, R_{L2} refer to the self-inductance and the resistance of the sending and the receiving coil, respectively. C_{SP}, C_{SS}, C_{RS}, and C_{RP} refer to the added capacitance to the sending and the receiving circuits to realize the resonance. M_{ij} refers to the mutual inductance between the send coil 'i' and the other sending coil 'j'. M_{ir} refers to the mutual inductance between the sending coil 'i' and the receiving coil 'r'.

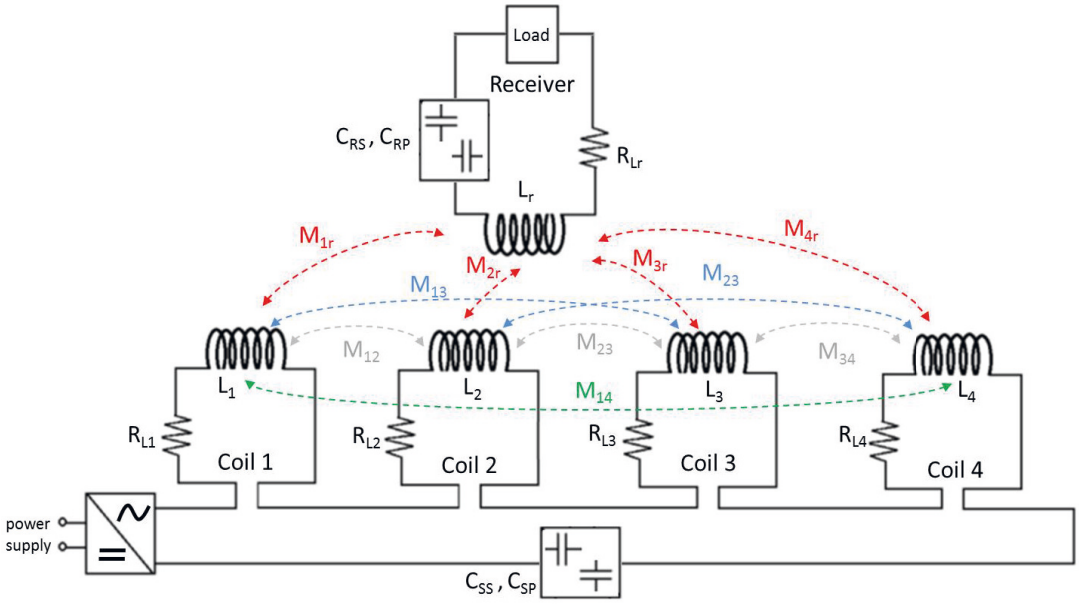

Fig. 5.9: Equivalent circuit of the proposed multi-coil inductive system

5.2.3.1 Equivalent inductance

At every position of the receiving coil, four sending coils, which are excited in the same direction, are responsible for power transmission and two neighbouring coils are responsible for the orientation of the magnetic field and are excited in opposite direction with respect to the sending ones. For that the equivalent inductance 'L_{eq}' of the sending coils, which are connected in series and the same direction is given as follows:

$$L_{eq} = \sum_{i} L_i + \sum_{i \neq j} M_{ij} \tag{5.4}$$

Where: L_i is the self-inductance of the coil 'i' and M_{ij} is the mutual inductance between coil 'i' and coil 'j'. Expending the Eq. 5.4, we obtain the equivalent inductance:

$$L_{eq} = L_1 + L_2 + L_3 + L_4 + 2(M_{12} + M_{13} + M_{14} + M_{23} + M_{24} + M_{34}) \tag{5.5}$$

In case of coils that are connected in series but in opposite direction the expression of equivalent inductance becomes as follows:

$$L_{eq} = \sum_{i} L_i - \sum_{i \neq j} M_{ij} \tag{5.6}$$

Expending the Eq. 5.6, we obtain:

$$L_{eq} = L_1 + L_2 + L_3 + L_4 - 2(M_{12} + M_{13} + M_{14} + M_{23} + M_{24} + M_{34}) \tag{5.7}$$

By exciting the sending coils in parallel in the same direction, the equivalent inductance expression equals to

$$L_{eq} = \frac{\sum_{i \neq j} \frac{1}{2}\left(L_i L_j - M_{ij}^{\,2}\right)}{\sum_{i} L_i - \sum_{i \neq j} M_{ij}} \tag{5.8}$$

In case of coils that are connected in parallel but in opposite direction the equivalent inductance expression becomes as follows:

$$L_{eq} = \frac{\sum_{i \neq j} \frac{1}{2}\left(L_i L_j - M_{ij}^{\,2}\right)}{\sum_{i} L_i + \sum_{i \neq j} M_{ij}} \tag{5.9}$$

Table 5.2 resumes the different expressions of the equivalent inductance in multi-coil inductive systems in which the sending coils can be connected in series or in parallel in the same or in opposite directions.

Table 5.2: Expressions of the equivalent inductance L_{eq}

	Coils connected in series	Coils connected in parallel
Same direction	$L_{eq} = \sum_{i} L_i + \sum_{i \neq j} M_{ij}$	$L_{eq} = \frac{\sum_{i \neq j} \frac{1}{2}\left(L_i L_j - M_{ij}^{\,2}\right)}{\sum_{i} L_i - \sum_{i \neq j} M_{ij}}$
Opposite direction	$L_{eq} = \sum_{i} L_i - \sum_{i \neq j} M_{ij}$	$L_{eq} = \frac{\sum_{i \neq j} \frac{1}{2}\left(L_i L_j - M_{ij}^{\,2}\right)}{\sum_{i} L_i + \sum_{i \neq j} M_{ij}}$

5.2.3.2 Equivalent mutual inductance

Geometrical parameters of the system are introduced in Fig. 5.10, where the position presents the origin of all mathematical calculations. x_1, x_2, x_3 and x_4 are defined as the initial position of the centres of the sending coils along x-axis. If the receiving coil has a rectilinear movement along x-axis and referring to the geometrical parameters on Fig. 5.10, the lateral misalignment Δ_i between the receiving coil and of the sending coil "i" is defined as follows:

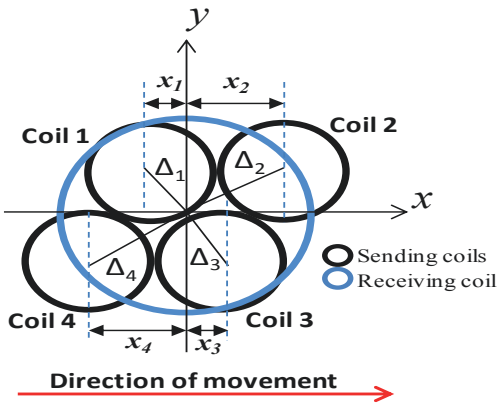

Fig. 5.10: Geometrical parameters of the designed multi-coil system

$$\Delta_1 = \frac{r_1}{\cos\left(\arctan\left(\frac{x_1 + x}{r_1}\right)\right)} \qquad \Delta_2 = \frac{r_2}{\cos\left(\arctan\left(\frac{|x_2 - x|}{r_2}\right)\right)} \qquad (5.10, 5.11)$$

$$\Delta_3 = \frac{r_3}{\cos\left(\arctan\left(\frac{|x - x_3|}{r_3}\right)\right)} \qquad \Delta_4 = \frac{r_4}{\cos\left(\arctan\left(\frac{x + x_4}{r_4}\right)\right)} \tag{5.12, 5.13}$$

Where, x is the variable relative position of the receiving coil along x-axis and r_i is the radius of the corresponding sending coil "i".

The equivalent mutual inductance 'M_{eq}' of the designed multi-coil inductive system can be derived from Eq. 2.26, Eq. 2.27 and Eq. 2.28. The resulting expression is given as follows:

$$M_{eq} = \sum_{i=1}^{n} M_{ir} \tag{5.14}$$

$$M_{eq} = \mu_0 N_r r_r \sum_{i=1}^{n} \frac{N_i r_i}{r_i (r_r - \Delta_i)} G(h_i) \tag{5.15}$$

Where,

$$G(h_i) = \left(\frac{2}{\sqrt{\frac{4 r_i (r_r + \Delta_i)}{(r_i + r_r + \Delta_i)^2 + d^2}}} - \sqrt{\frac{4 r_i (r_r + \Delta_i)}{(r_i + r_r + \Delta_i)^2 + d^2}} \right) K(h_i) - \frac{2}{\sqrt{\frac{4 r_i (r_r + \Delta_i)}{(r_i + r_r + \Delta_i)^2 + d^2}}} E(h_i) \tag{5.16}$$

N_i is the number of turns, r_i is the radius of the coil, d and Δ are, respectively, the vertical and lateral distances between the sending and the receiving coils. The sub-letters 'r' and 'i' refer, respectively, to the receiving coil and the sending coil number 'i'.

The equivalent mutual inductance of the proposed multi-coil system equals to

$$M_{eq} = \sum_{i=1}^{4} M_{ir} = M_{1r} + M_{2r} + M_{3r} + M_{4r} \tag{5.17}$$

Referring to Eq. 2.36, the analytical expression of the coupling factor is given as follows

$$k = \frac{M_{eq}}{\sqrt{L_{eq} L_r}} \tag{5.18}$$

Expending the expression of the equivalent mutual inductance 'M_{eq}', Eq. 5.17 becomes as follows:

$$k = \frac{\mu_0 N_r r_r \sum_{i=1}^{n} \frac{N_i r_i}{r_i (r_r - \Delta_i)} G(h_i)}{\sqrt{L_{eq}\, L_r}} \tag{5.19}$$

For example, in the case of four sending coils connected in series and in the same direction, the coupling factor k equals to:

$$k = \frac{\mu_0 N_r r_r \sum_{i=1}^{n} \frac{N_i r_i}{r_i (r_r - \Delta_i)} G(h_i)}{\sqrt{\left(\sum_i L_i + \sum_{i \neq j} \frac{\mu_0 N_1 N_2 r_1 r_2}{\sqrt{r_1 (r_2 + \Delta)}} G(h) \right) L_r}} \tag{5.20}$$

5.2.3.3 Induced voltage and current

The equation of the induced voltage can be derived from Faraday's law stating that a changing magnetic flux through a surface A induces a voltage V_{ind} in any boundary path of that surface.

In case of a multi-coil system, the induced voltage equals to

$$V_{ind} = -L_r \frac{dI_r}{dt} + \sum_i M_{ir} \frac{dI_i}{dt} \tag{5.21}$$

Where: M_{ir} is the mutual inductance between the receiving coil and the sending coil i (i varies from 1 to n, where n is the number of the sending coils.), I_i is the current circulating in each sending coil and L_r is the self-inductance of the receiving coil.

The induced voltage is measured by transforming Eq. 5.21 to the following expression:

$$V_{ind} = -j\omega L_r I_r + \mu_0 N_r r_r \sum_i \frac{N_i r_i}{r_i (r_r - \Delta_i)} G(h_i)\, j\omega I_i \tag{5.22}$$

Where: I_r is the current of the receiving coil, $\omega = 2\pi f$ is the angular frequency and f is the operation frequency in Hz.

The expression of the induced current is also derived from Faraday's law and given as follows

$$I_{ind} = \frac{j\omega \sum_i M_{ir} I_i}{Z_2} \tag{5.23}$$

M_{ir} refers to the mutual inductance between the sending coil '*i*' and the receiving coil '*r*', I_i is the current of the sending coil '*i*', $\omega=2\pi f$ is the angular frequency and f is the operation frequency in Hz. Z_2 is the impedance of the secondary side that depends on system's topology. This is studied in details in section 5.5.

5.3 Finite Element Analysis

Finite element method is a current and quite suitable method for modelling and extracting the important parameters from the used coils. This support the estimation of several parameters of inductive power transmission systems such as the magnetic field intensity, the mutual inductance, the induced voltage and the induced current by modelling these systems in a three-dimensional domain, e.g. in Comsol Multiphysics.

5.3.1 Three-dimensional model

A three-dimensional model of the multi-coil inductive system, as depicted in Fig. 5.8, is developed using COMSOL software. The system is simulated in the "frequency domain". The sending coils are modelled with circular shape and rectangular section as shown in Fig. 5.11. 'w' and 'b' represent the coil's width and the coil's length, respectively, which are dependent on the number of turns of the coil, and the winding's wire diameter.

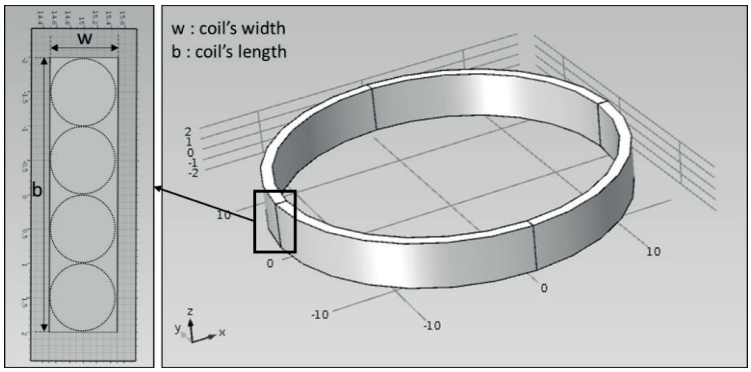

Fig. 5.11: Three-dimensional model of the sending coil

Firstly, the sending coils are defined as "multi-turn coil domain". Secondly, the coil's type is adjusted as "circular". Then, the "reference edge" for every coil is chosen. The

“reference edge” defines the path in which the current is flowing in the coil. It should be a closed loop as it is shown in Fig. 5.12.

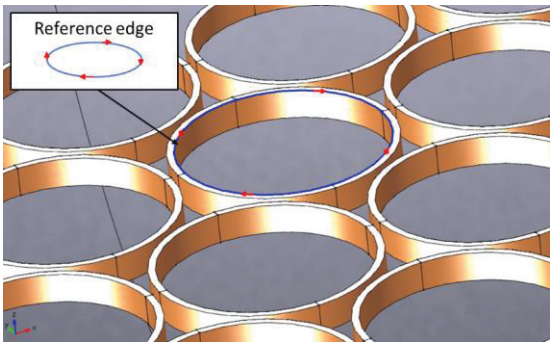

Fig. 5.12: Reference edge of one sending coil

The reference edge of the receiving coil is generated automatically by the developed model and is in the opposite direction of the sending coils. In order to excite the neighbouring coil of the active ones in the opposite direction, the orientation of the reference edge needs to be changed.

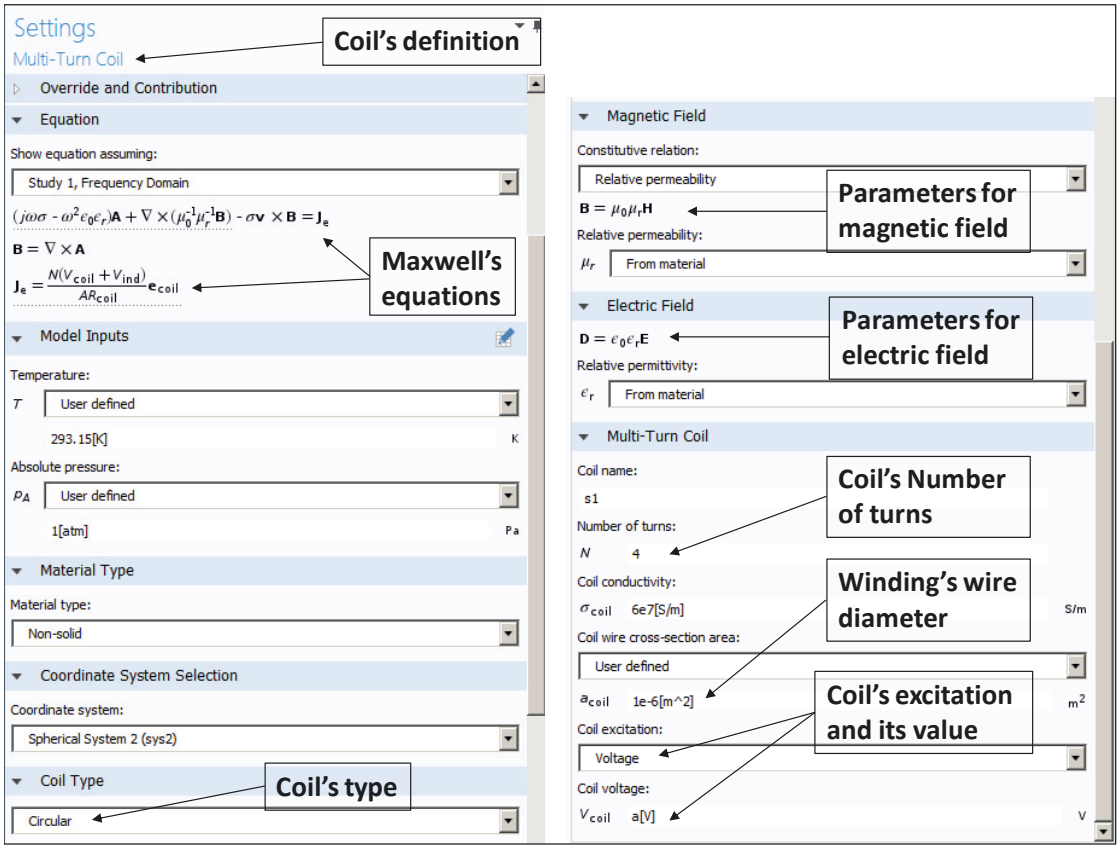

Fig. 5.13: Sending coil S1 definition in COMSOL

For the coil excitation, the “voltage” is selected and its value is settled. Afterward, the operation frequency, which is equal to 1.2 MHz is adjusted. This frequency is chosen because at this level the sending coils have the highest quality factor, which improves the transmitted power. In the same manner, the receiving coil is defined, but for the excitation the “current/voltage circuit” is selected, which means that the coil is excited by the induced current or voltage. Fig. 5.13 explains more how the coils are defined and excited.
After designing the coils, a boundary working space and a magnetic insulation area are settled in order to get converged values. For that, the air is defined as the working space and Maxwell's equations are included.
In order to obtain accurate results, a finer mesh element has been chosen for the whole model of the system as shown in Fig. 5.14. To change the position of the receiving coil, which represents in the system the misalignment Δ, an automatic parametric sweep is developped. Due to the requirement of a computer with very high computing performance and to reduce the calculation time, the parametric sweep was adjusted from the initial position to the final position of the receiving coil in 5 steps. The last step is to adjust the frequency at 1.2 MHz, run the simulations, then derive the results.

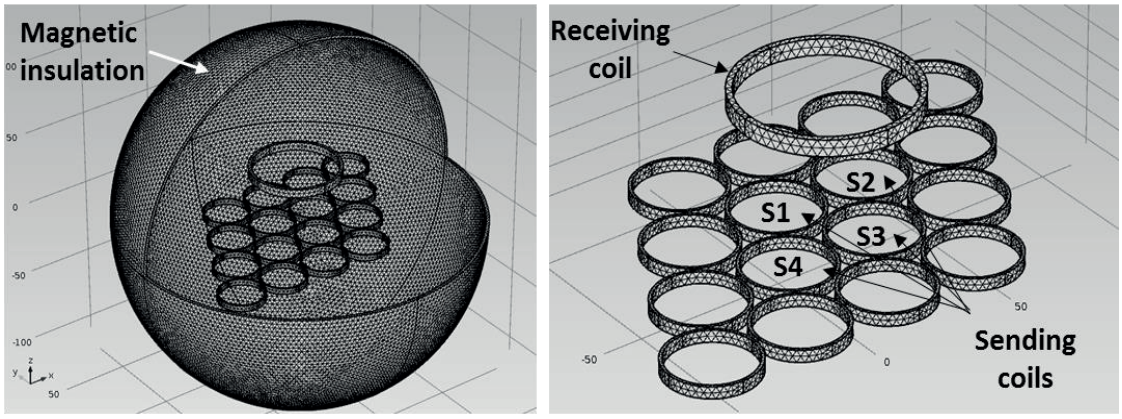

Fig. 5.14: 3D finer mesh element of the multi-coil inductive system

5.3.2 Simulation results

Different system parameters can be extracted by simulation. For example, the induced current, the induced voltage, coil’s power, coil’s inductance, coil’s resistance, the magnetic field intensity and the magnetic field distribution can be determined. All these

parameters can be found in the “Derived value” of the “Global evaluation” icon. On the other hand, there are some parameters that can be achieved by adjusting their expressions as input to the software. For example, in COMSOL, the mutual inductance between two coils is calculated as follows:

$$M = \frac{V_{coil}}{i\,\omega\,I_p} \tag{5.24}$$

Where V_{coil} is the total voltage of the receiving coil, ω is the angular frequency of excitation and I_p is the driving current in the primary coil. Thus, the equivalent mutual inductance M_{eq} is calculated using the following expression:

$$M_{eq} = \frac{V_{coil}}{i\,\omega\,I_{p1}} + \frac{V_{coil}}{i\,\omega\,I_{p2}} + \frac{V_{coil}}{i\,\omega\,I_{p3}} + \frac{V_{coil}}{i\,\omega\,I_{p4}} \tag{5.25}$$

$$M_{eq} = V_{coil}\left(\frac{1}{i\,\omega\,I_{p1}} + \frac{1}{i\,\omega\,I_{p2}} + \frac{1}{i\,\omega\,I_{p3}} + \frac{1}{i\,\omega\,I_{p4}}\right) \tag{5.26}$$

Where: I_{pi} is the driving current in the primary coil number ‘i’.

The first part of the simulations gives an idea about the behaviour of the system while increasing the vertical distance between the sending and the receiving coils. In the second part, the transmitted power with respect to lateral misalignment is simulated. To calculate the transmitted power of both two-coil and multi-coil inductive systems and at different position, we determine the induced voltage and the induced current in the receiving coil.

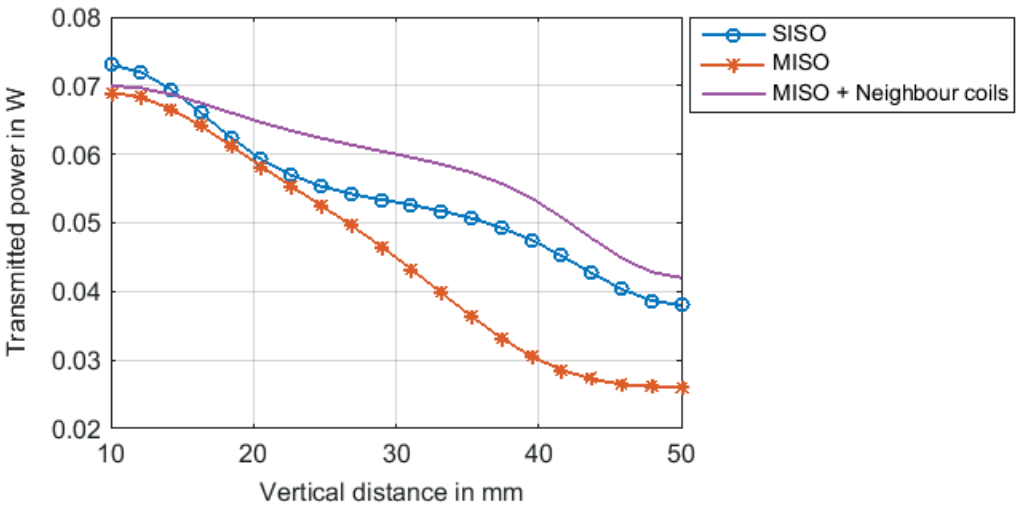

Fig. 5.15: Transmitted power with respect to the vertical distance d

Figure 5.15 shows the simulation results of the transmitted power with respect to the vertical distance '*d*'. As can be seen, at small vertical distance under 15 mm, corresponding to 25% of the diameter, two coil system "SISO" shows better transmitted power than multi-coil system "MISO" as most of the issued magnetic field passes through the receiving coil. However, it shows a dramatic drop of performance by increasing the vertical distance. For example, the transmitted power decreases about 2 times from 73 mW at 10 mm distance to 38 mW at 50 mm distance. The efficiency is also decreased from 52% to 27.1%, respectively.

Beginning with 15 mm coil-to-coil vertical distance, only MISO configuration with oriented magnetic field becomes better. At this distance, the system is able to transmit 68 mW with a transmission efficiency equals to 47%. The orientation of the magnetic field is influenced by the neighbouring coils of the four active ones. Figure 5.16 shows the magnetic field lines (in red colour) before and after orientation (guidance).

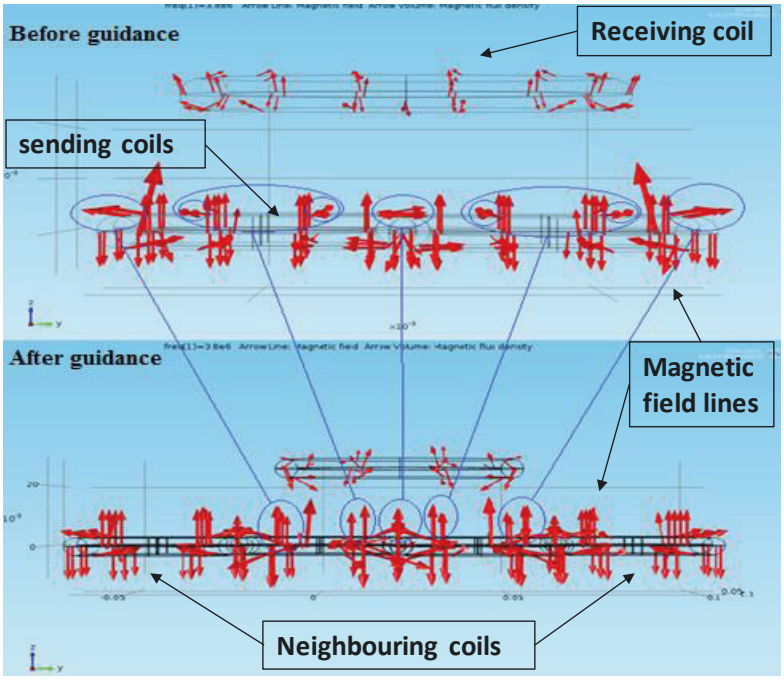

Fig. 5.16: Magnetic field lines before and after guidance

Before guidance, a lot of the magnetic field lines are not oriented to the receiving coil and the transmitted power equals to 23 mW. After orientation, the transmitted power is

improved by powering two neighbouring coils with les excitation and becomes equal to 43 mW.

Figure 5.17 depicts the transmitted power in case of the conventional two-coil system SISO (blue lines with circle), multi-coil system MISO (red lines with starts), and MISO coil system with oriented magnetic field (pink colour) with respect to the lateral misalignment Δ at 50 mm coil-to-coil vertical distance.

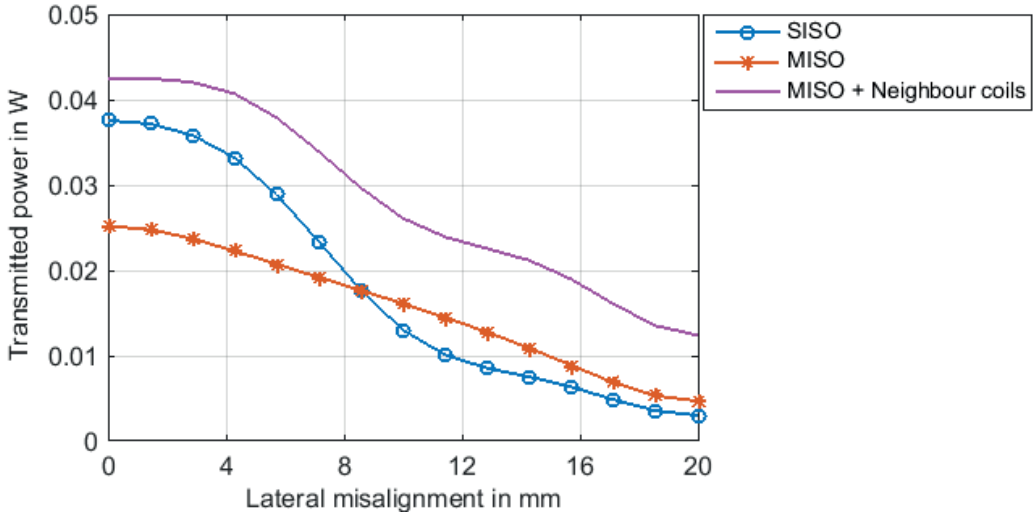

Fig. 5.17: Transmitted power with respect to the lateral misalignment Δ at 50 mm coil-to-coil vertical distance

Results show that at small lateral deviations less than 10 mm, SISO configuration has better performance compared to the MISO configuration by realizing about 27.1 % of power transmission efficiency. As expected, for larger misalignment, the multi-coil system becomes better. This is justified by the fact that the magnetic field in SISO configuration is concentrated only at the centre of the sending coil. However, in the case of MISO configuration, each sending coil has a concentrated magnetic field at its centre. Therefore, the resulting magnetic field is distributed along the whole surface of the sending coils. For example, at 10 mm misalignment, the MISO configuration is capable to send 17.5 mW realizing 12.5 % of efficiency instead of SISO configuration that can send only 13 mW realizing 9.2 % of efficiency. That means the MISO configuration offers 130 % transmitted power compared to that of SISO configuration. It can be also seen that the MISO configuration with oriented magnetic field has the highest transmitted power. At

perfect alignment, the system can transmit 43 mW, which correspond to the 110 % of the transmitted power reached by the SISO configuration. At 10 mm lateral misalignment, it gives the 200% of the transmitted power reached by SISO configuration. Table 5.3 gives an overview of the obtained simulation results.

Table 5.3: Transmitted power and efficiency of SISO, MISO, and MISO with oriented magnetic field coil systems [32, 110, 111]

Coil system	Vertical distance 'd' (mm)	Lateral misalignment 'Δ'(mm)	Transmitted power (mW)	Efficiency (%)
SISO	10	0	73	52
	50	0	38	27.1
		10	13	9.2
MISO	10	0	68	47
	50	0	26	18.5
		10	17.5	12.5
MISO + oriented magnetic field	10	0	70	49.6
	50	0	43	29.2
		10	26	17
		15	20	12.9

5.4 Experimental investigations

5.4.1 Experimental setup

An experimental setup for both the two-coil system "SISO" and the multi-coil system "MISO" are described in Fig. 5.18 and Fig. 5.19, respectively. Coils are made in the laboratory using copper coils and tested by an Agilent impedance analyser. An AC power source is used to feed the sending coils and an additional one is used to feed the neighbouring coils, which are mounted in the opposite direction.

The lateral position of the receiving coil, which represents in the proposed system the lateral misalignment, is adjusted manually from 0 mm to 20 mm in 5 mm steps.

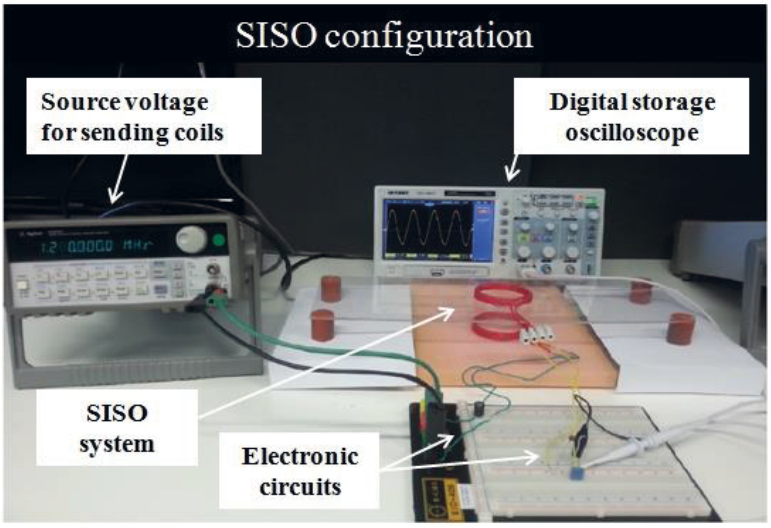

Fig. 5.18: Experimental setup of the two-coil inductive system “SISO”

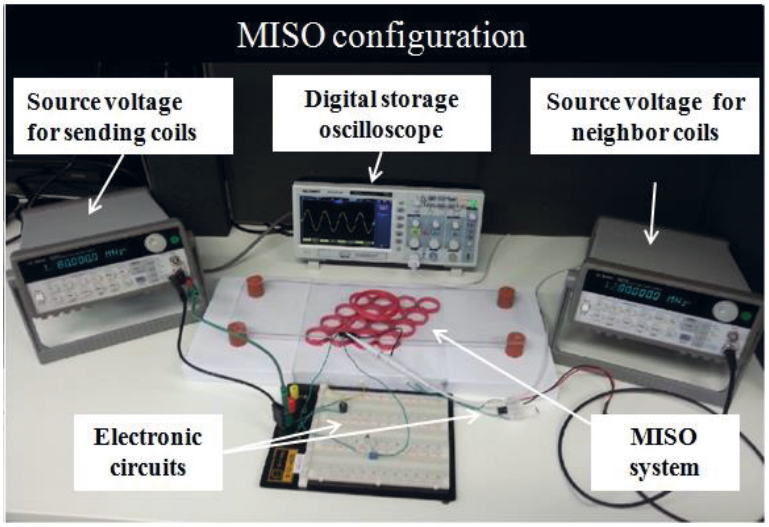

Fig. 5.19: Experimental setup of the multi-coil inductive system “MISO”

In case of the multi-coil system MISO, the initial position of the receiving coil as shown in Fig. 5.8 is adjusted. At this position, the four sending coils (S1, S2, S3, and S4) that are under the receiving coil are activated and the other coils are switched off. In addition, the two nearest neighbouring coils with less current and in the opposite direction are activated (see Fig. 5.8). To activate the two nearest neighbouring coils of the four active ones with weak current and in out-of-phase excitation, a second source voltage is needed (Fig. 5.19). To ensure that neighbouring coils are fed in out-of-phase, a simple and practical method is employed. As all sending coils are similar and have the same properties and number of

turns. The direction of the windings of the neighbouring coils is changed. That means the direction of current's circulation in the windings of the sending coils is in the opposite direction comparing to that of the neighbouring coils.

For both cases, SISO and MISO, a Series-Series topology for primary and secondary circuits is considered because the primary side compensation capacitor doesn't depend either on the coupling factor k or on the load R_L.

The receiving coil is connected to a pure resistive load. A resistor of 12 Ω is selected. As the components of the secondary side are connected in series, they have the same current. Consequently, the secondary side induced current 'I_r' can be determined by measuring the voltage across the resistor satisfying the following equation

$$V = R \,.\, I \tag{5.27}$$

Where R is the resistance and I is the current across the resistor.

By a simple mathematical calculation from Eq. 5.27, the induced current can be deduced. Then, the voltage across the receiving coil is determined, by using a digital oscilloscope, in order to obtain its received power that satisfies the following expression

$$P = V \,.\, I \tag{5.28}$$

Where P is the resulting power, I is the current across the coil and, V is the coil's voltage.

5.4.2 Experimental results

The source impedance *Rs*, the equivalent resistance of the sending coil *Req* and the receiving coil resistance are measured by Agilent impedance analyser. Their experimental values at a frequency of 1.2 MHz are equal to 50 Ω, 0.243 Ω and 0.31 Ω, respectively.

Experimental results are illustrated in Fig. 5.20 with solid lines, which show the received power as a function of the lateral misalignment at 5 cm coil-to-coil vertical distance.

Similar to the simulation results, at perfect alignment case, two-coil system "SISO" shows good results in which the received power equals to 32 mW and realizes 22.8% of efficiency whereas multi-coil system "MISO", which realizes only 16.7% of efficiency, as the received power is 23.5 mW.

Beginning with 9 mm of lateral misalignment, corresponding to 30% of the sending coil diameter, losses increase in SISO configuration due to the high magnetic flux leakage.

Consequently, the coupling between the sending and the receiving side becomes very weak. At this position, multi-coil system “MISO” becomes better. It offers more flexibility and it is less sensitive to the misalignment.

These results are improved more by adopting a MISO oriented system (Fig. 5.20, pink lines) where the two nearest neighbouring coils of the four active ones are excited by an opposite and lower current. It shows better performance, comparing to SISO and MISO without oriented magnetic field, at both ideal and lateral misalignment cases.

Even at high degree of misalignment, corresponding to 50% of the sending coil diameter, the received power equals 18 mW and achieves 14% of the efficiency. This meets the power consumption requirement of low-power application systems such as the sensor systems.

Deviation between simulation and experimental results equals 12.73%, 13.78% and 8.47% for SISO, MISO and MISO with oriented magnetic field configurations, respectively. This is caused by the presence of other type of losses in the inductive system such as coils’ interference, heat losses of used wires, and the influence of experiment’s environment on the distribution of the magnetic field

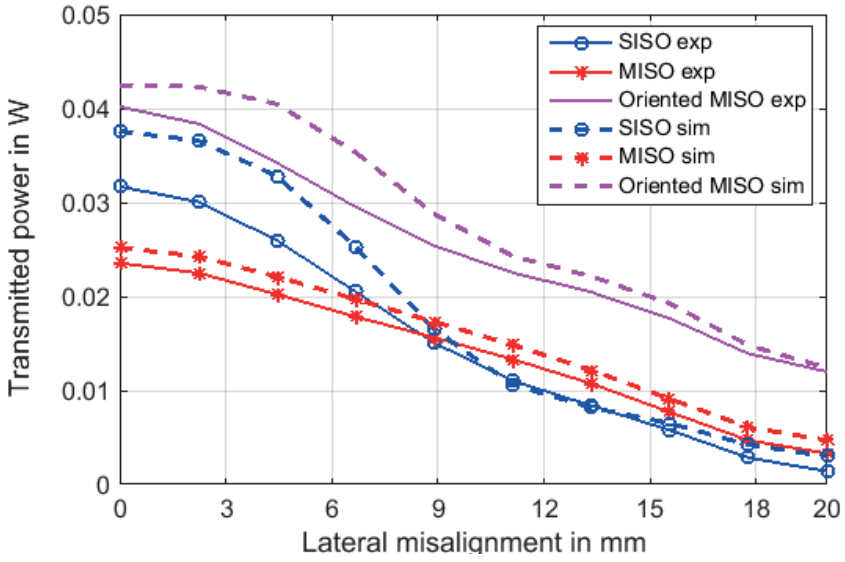

Fig. 5.20: Simulation and experimental results of the received power at the receiving coil for different coil system configurations at 50 mm vertical distance

The received power is optimized more by adjusting the appropriate circuit topology. For that, compensation capacitors are involved in series and/or in parallel to realise the resonance. This is studied in detail in the next section.

5.5 Investigation of compensation topologies

In order to improve the transmitted power to the secondary side and consequently the total system efficiency, the use of compensation capacitors in primary and/or in secondary circuits to work in resonance is proposed. The selection of the adequate topology depends on the system requirements. For that, four main topologies are suggested: Series-series (SS), series-parallel (SP), parallel-series (PS) and parallel-parallel (PP) topologies.
The equivalent circuit of magnetically coupled resonators is shown in Fig. 5.21.

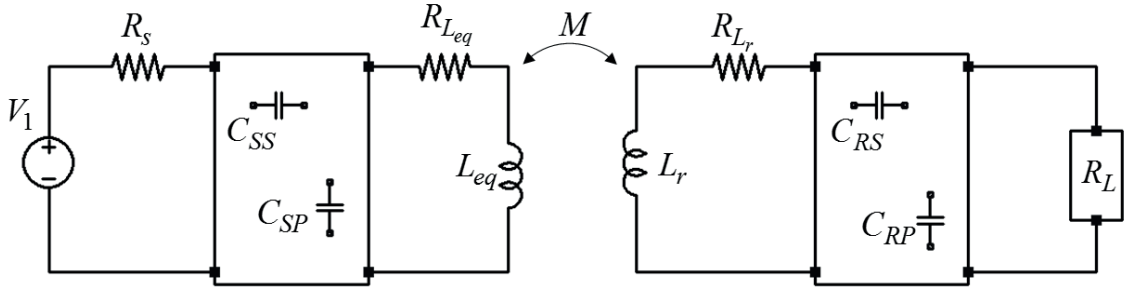

Fig. 5.21: Equivalent circuit of magnetically coupled resonators

L_{eq} and L_r represent, respectively, the equivalent inductance of the sending coils and the self-inductance of the receiving coil. R_{Leq} is the equivalent resistance of the sending coils and R_{Lr} is the receiving coil resistance. The capacitors C_s and C_r are added in series (C_{SS}, C_{RS}) or in parallel (C_{SP}, C_{RP}) to the primary and secondary circuits, respectively, to work in resonance. The load is modelled as a resistor R_L. V_1 and R_s represent the source voltage and its resistance, respectively. M is the mutual inductance between the sending side and the receiving side and $\omega=2\pi f$ is the angular frequency where f is the frequency of the inductive system.

5.5.1 Primary side compensation

5.5.1.1 Series compensation

The equivalent circuit of the primary side with series compensation with respect to the secondary side topology is shown in Fig. 5.22.

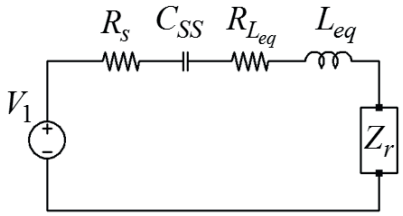

Fig. 5.22: Equivalent circuit of the primary side with series compensation C_{SS}

Where: Z_r is the secondary side impedance reflected to the primary side and it is given by

$$Z_r = \frac{(\omega M)^2}{Z_2} \tag{5.29}$$

Where: M is the mutual inductance between the primary and secondary sides and Z_2 is the total impedance of the secondary side that equals to:

$$Z_2 = R_L + R_{L_r} + j\omega L_r + \frac{1}{j\omega C_r}, \text{ in case of SS topology} \tag{5.30}$$

$$Z_2 = R_{L_r} + j\omega L_r + \frac{1}{j\omega C_r + \frac{1}{R_L}}, \text{ in case of SP topology} \tag{5.31}$$

The equivalent circuit of the primary side with series compensation in resonance is shown in Fig. 5.23. Based on that, the primary coil current I_S is expressed by:

$$I_S = \frac{V_1}{R_S + R_{L_{eq}} + R_r} \tag{5.32}$$

Where, R_r is the expression of Z_r at resonance that depends on the circuit topology.

By assuming that $R_1 = R_S + R_{L_{eq}}$ the primary coil current becomes

$$I_S = \frac{V_1}{R_1 + R_r} \tag{5.33}$$

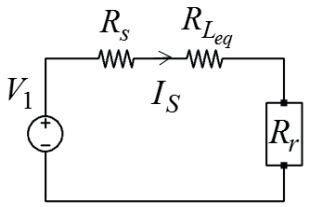

Fig. 5.23: Equivalent circuit of the primary side with series compensation in resonance

The expressions of the source power and the transmitted power from the sending side to the receiving one are given in Table 5.4.

Table 5.4: Source power and transmitted power for primary series compensation circuit

Parameter	Expression	Equation number
Source power	$P_S = V_1 I_S$	Eq. 5.34
	$P_S = \frac{V_1^2}{R_1 + R_r}$	Eq. 5.35
Transmitted power	$P_t = I_S^2 R_r$	Eq. 5.36
	$P_t = \left(\frac{V_1}{R_1 + R_r} \right)^2 R_r$	Eq. 5.37

5.5.1.2 Parallel compensation

The equivalent circuit of the primary side with parallel compensation with respect to the secondary side topology is shown in Fig. 5.24.

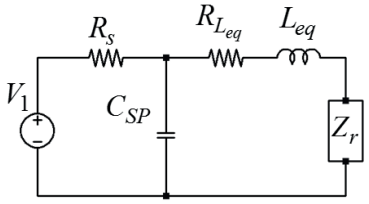

Fig. 5.24: Equivalent circuit of the primary side with parallel compensation C_{SP}

Where: Z_r is the secondary side impedance reflected to the primary side and its expression is given by Eq. 5.29. The equivalent circuit of the primary side with series compensation in resonance is shown in Fig. 5.26, where Z_1 is expressed as follows

$$Z_1 = R_S + \left\{ \frac{1}{jC_{SP}\omega} // \left(Z_r + R_{L_{eq}} + jL_{eq}\omega \right) \right\} \tag{5.38}$$

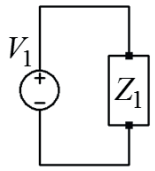

Fig. 5.25: Equivalent circuit of the primary side with parallel compensation in resonance

By assuming $R_0 = R_r + R_{L_{eq}}$, $A = 1 - C_{SP}L_{eq}\omega^2$ and $B = C_{SP}R_0\omega$, the expression of Z_1 Z_1becomes equal to:

$$Z_1 = R_S + \frac{R_r + R_{L_{eq}}}{A^2 + B^2} + j\frac{AL_{eq}\omega - BR_0}{A^2 + B^2} \tag{5.39}$$

At resonance, from the equation 5.39 of Z_1, the expression of the equivalent resistance of the primary side noted R_1 can be easily determined by:

$$R_1 = R_S + \frac{R_r + R_{L_{eq}}}{A^2 + B^2} \tag{5.40}$$

Thus, the primary current I_s of the sending coil equals

$$I_S = \frac{V_1}{R_1} = \frac{(A^2 + B)V_1}{R_S(A^2 + B^2) + R_r + R_{L_{eq}}} \tag{5.41}$$

The selection of the value of the primary capacitorC_{sp} C_{SP} in order to nullify the reactance of Z_{eq} is determined by solving $Im(Z_{eq}) = 0$ $Im(Z_{eq})$ = 0. The resulting expression is given by

$$C_{SP} = \frac{L_{eq}}{(L_{eq}\omega)^2 + {R_0}^2} \tag{5.42}$$

The source power of the primary side with parallel compensation can be defined as

$$P_S = V_1 I_S \tag{5.43}$$

Subsisting I_S by its expression; the source power becomes equal to:

$$P_S = \frac{V_1^2}{R_1} = \frac{(A^2 + B)V_1^2}{R_S(A^2 + B^2) + R_r + R_{L_{eq}}} \tag{5.44}$$

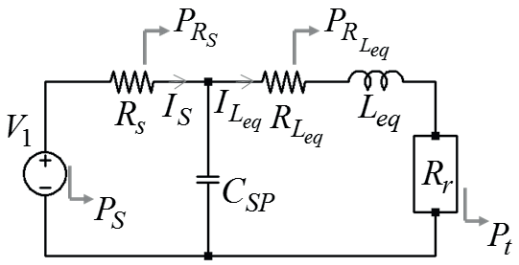

Fig. 5.26: Power distribution at primary side

At resonance, the power is consumed by the resistive load. Fig. 5.27 shows the different types of power in the primary circuit that are:

i. The source power P_s that equals to:

$$P_S = P_{R_S} + P_{R_{L_S}} + P_t \tag{5.45}$$

ii. The transmitter power P_t from the sending side to the receiving side that equals to:

$$P_t = I_{L_{eq}}{}^2 R_r \tag{5.46}$$

iii. The power dissipated by source impedance P_{R_s} that equals to:

$$P_{R_S} = I_S{}^2 R_S = \frac{P_S}{R_1} R_S \tag{5.47}$$

iv. The power consumed by the resistance of the sending coil $P_{R_{L_S}}$ that equals to:

$$P_{R_{L_{eq}}} = I_{L_{eq}}{}^2 R_{L_{eq}} = \frac{P_t}{R_r} R_{L_{eq}} \tag{5.48}$$

Referring to the equations mentioned above, the expression of the source power can be expressed as:

$$P_S = P_t + \frac{P_t}{R_r} R_{L_{eq}} + \frac{P_S}{R_1} R_S \tag{5.49}$$

That gives:

$$P_S\left(1-\frac{R_S}{R_1}\right)=P_t\left(1+\frac{R_{L_{eq}}}{R_r}\right) \tag{5.50}$$

Substituting the expression of P_S $P_s$from Eq. 5.50 to Eq. 5.49, the expression of the transmitted power from the primary side with parallel compensation to the receiving side becomes as follows:

$$P_t=\frac{V_1^2 R_r}{R_1+(R_r+R_{L_{eq}})}\left(1-\frac{R_S}{R_1}\right) \tag{5.51}$$

5.5.2 Secondary side compensation

5.5.2.1 Series compensation

The equivalent circuit of the secondary side with series compensation with respect to the primary side topology is shown in Fig. 5.27.

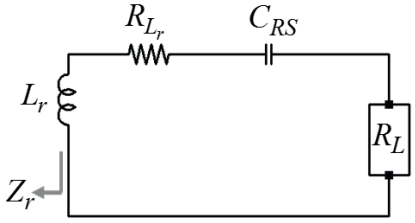

Fig. 5.27: Equivalent circuit of the secondary side with series compensation C_{RS}

Where: Z_r is the secondary side impedance reflected to the primary side. Its expression is given by Eq. (5.29). In this case Z_2 is given as follows:

$$Z_2=R_L+R_{L_r}+j\omega L_r+\frac{1}{j\omega C_{RS}} \tag{5.52}$$

The equivalent circuit of the primary side with series compensation in resonance is shown in Fig. 5.28. At resonance, we have the imaginary part of Z_2 equals to zero (i.e. $\mathrm{Im}\{Z_2\}=0$). This leads to the following equations:

$$Z_2=R_2=R_L+R_{L_r} \tag{5.53}$$

$$Z_r=R_r=\frac{(\omega M)^2}{R_2} \tag{5.54}$$

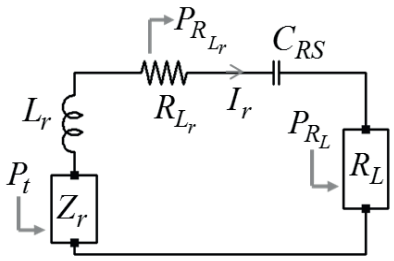

Fig. 5.28: Equivalent circuit of the secondary side with series compensation C_{RS}

At resonance frequency, the transmitter power P_t from the sending side to the receiving side is only consumed by the load R_L and the resistance of the receiving coil R_{L_r}. Its expression is given as follows

$$P_t = P_{R_{L_r}} + P_{R_L} = \left(R_{L_r} + R_L\right) {I_r}^2 \tag{5.55}$$

Where: P_{R_L} the power at the load and its expression is equals to

$$P_{R_L} = R_L {I_L}^2 = R_L {I_r}^2 \tag{5.56}$$

From Eq. 5.55, the expression of the secondary side current I_r equals to

$${I_r}^2 = \frac{P_t}{R_{L_r} + R_L} \tag{5.57}$$

Substituting the expression of I_r of Eq. 5.57 into Eq. 5.56, the expression of the power at the load becomes as follows:

$$P_{R_L} = \frac{R_L}{R_2} P_t \tag{5.58}$$

5.5.2.2 Parallel compensation

The equivalent circuit of the secondary side with parallel compensation with respect to the primary side topology is shown in Fig. 5.29.

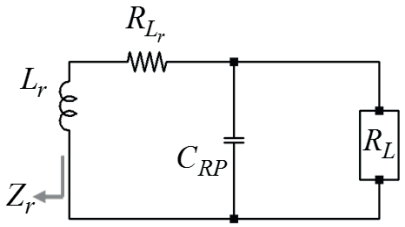

Fig. 5.29: Equivalent circuit of the secondary side with parallel compensation C_{RP}

Where: Z_r is the secondary side impedance reflected to the primary side and its expression is given by Eq. (5.29). In this case Z_2 is given by

$$Z_2 = jL_r\omega + R_{L_r} + \left\{ \frac{1}{jC_{RP}\omega} // R_L \right\} \tag{5.59}$$

The equivalent circuit of the secondary side with series compensation in resonance is shown in Fig. 5.30. We define Z_{eq} as the equivalent impedance of the receiving side

$$Z_{eq} = R_{L_r} + \frac{R_L}{1+(R_L C_{RP}\omega)^2} + j\left(L_S\omega - \frac{C_{RP}{R_L}^2\omega}{1+(R_L C_{RP}\omega)^2} \right) \tag{5.60}$$

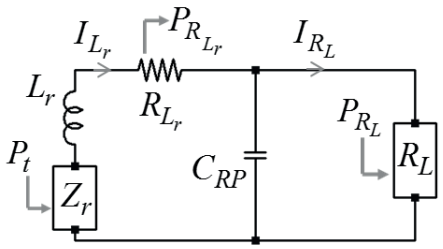

Fig. 5.30: Equivalent circuit of the secondary side with parallel compensation in resonance

A maximum power is delivered to the load can be reached by adjusting the value of the compensation capacitor C_{RP} is in order to nullify the reactance of the equivalent impedance of the secondary side. That means C_{RP} is determined by solving the equation $Im\{Z_{eq}\} = 0$. This leads to $L_S\omega - \frac{C_{RP}{R_L}^2\omega}{1+(R_L C_{RP}\omega)^2} = 0$ and consequently to

$${C_{RP}}^2{R_L}^2{L_S}\omega^2 - C_{RP}\,{R_L}^2 + L_S = 0 \tag{5.61}$$

By solving the equation 5.61 of second degree we obtain

$$C_{RP} = \frac{{R_L}^2 \pm \sqrt{{R_L}^4 - (2\omega R_L L_r)^2}}{2L_r\omega^2{R_L}^2} \tag{5.62}$$

It can be remarked that for a real value of C_{RP}, a particular range of load R_L is required that should fulfil the following condition

$${R_L}^4 - (2\omega R_L L_r)^2 > 0 \tag{5.63}$$

Hence,

$$R_L > 2\,\omega\,L_r \tag{5.64}$$

To have a maximum power at the load, at resonance, the compensation capacitor C_{RP} and the load R_L should fulfil conditions 5.61 and 5.64 respectively. Therefore, the total impedance of the secondary side Z_2 and the reflected impedance to the primary side Z_r equal respectively

$$Z_2 = R_2 = R_{L_r} + \frac{R_L}{1+(R_L C_r \omega)^2} \tag{5.65}$$

$$Z_r = R_r = \frac{(\omega M)^2}{R_2} \tag{5.66}$$

At resonance, the received power from the primary is dissipated by the load and the resistance of the receiving coil. Thus, the expression of the received power from the primary side P_t is given as follows:

$$P_t = P_{R_{L_r}} + P_{R_L} \tag{5.67}$$

Where: $P_{R_{L_r}}$ is the power dissipated by the receiving coil resistance and its expression is given as follows:

$$P_{R_{L_r}} = \frac{R_{L_r}}{R_2} P_t \tag{5.68}$$

5.6 Concluding remarks

In this chapter, a multi-coil inductive system overcoming the problem of misalignment between the sending and receiving sides and at large air gap is proposed, which offers more flexibility by increasing the interval of misalignment tolerance till 50% of the sending coil diameters. This system can orientate the issued magnetic field to the receiving coil by exciting the nearest neighbour coils of the active ones with less current and in the opposite direction. The investigation is confirmed in simulation and by experiments.

In the second part, different circuit topologies are studied in order to realise resonance conditions and enhance thereby the transmitted power and consequently the power transmission efficiency.

Chapter 6

Activation strategy

Inductive power transmission has an important use especially in applications where the receivers are in movement, having different positions during the power transmission phase or are not in the right position with respect to the transmitters. The independence from a stationary power supply enables more flexibility to these inductive systems. In fact, a detection of the receiver is required not only to guarantee the good operation of the system but also to save power by switching off the coils which are not under the receiver increasing thereby the system efficiency.

In the first part of this chapter, different receiver detection techniques are proposed. Some of them use additional sensors and others use the sending coils themselves as detectors. A detection of the receiver coil based on the measurement of their influences on the sending coil are proposed. In the second part, an excitation strategy has been proposed to supply the active sending coils S1, S2, S3 and S4 (see Fig. 6.1) aiming to limit the magnetic field losses and improve thereby the power transmission efficiency by increasing of the mutual coupling between the sending and the receiving coils.

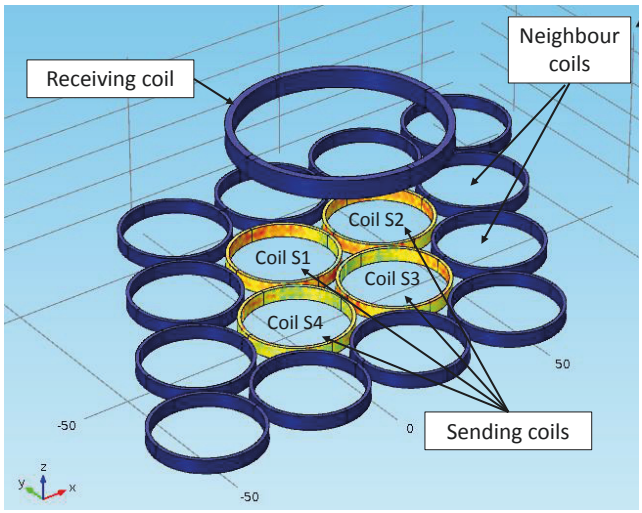

Fig. 6. 1: Studied multi-coil inductive system

6.1 Receiving coil detection

In order to reach a high system performance, a suitable detection circuit is selected based on the application requirements. For that, three different techniques to detect the receiver coil are presented and described in the diagram presented in Fig. 6.2. The first detection method is suitable for the systems with movable receivers and having both constant speed and linear path. The second detection method is applied for the systems with movable receivers and having variable speed and linear path. The third proposed detection method is used for systems with movable receiver independently from their position and speed.

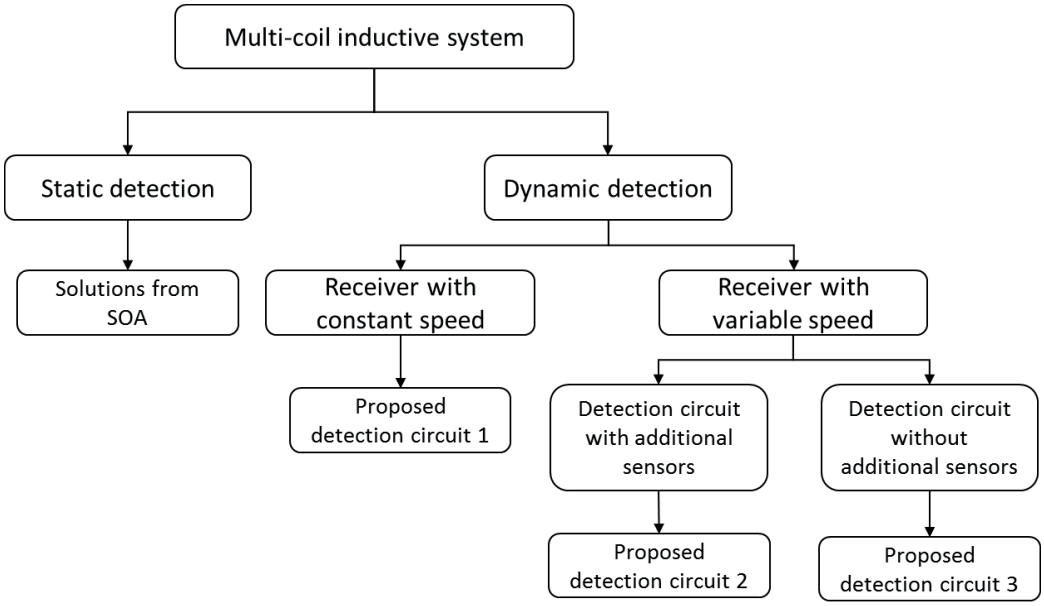

Fig. 6.2: Summary of the proposed detection methods

6.1.1 Constant speed

When the receiving coil has a constant speed and a linear path, their reached positions are known during the energy transmission phase. In fact, the receiver comes above the powering coils at a fixed time interval. Here, the sending coils are switched on and off at the same time sequence matched with that of the receiving coil speed. In the proposed circuit, this time sequence operation is achieved by an IC timer circuit, such as the NE555.

Figure 6.3. depicts the proposed detection circuit with the three important times intervals for a sending coil A which defined by:

-Time 1: It represents the time that the receiving coil takes to reach all the sending coils separately. It represents also the delay needed in the circuit for the first switch on of the corresponding sending coil.

-Time 2: It represents the time that the receiving coil takes to pass over the respective sending coil. It represents also the activation time of the corresponding sending coil.

-Time 3: It represents the time during which the sending coil is kept switched off.

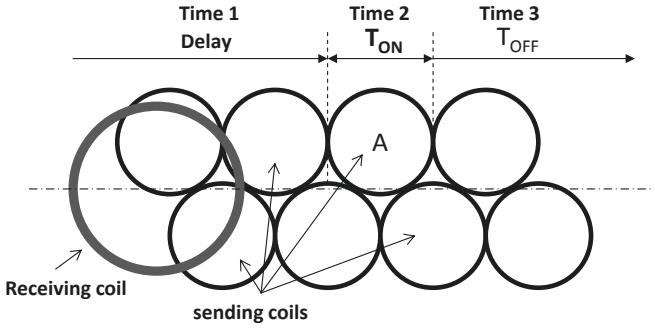

Fig. 6.3: Detection method for a receiver with constant speed

To implement the proposed detection method, every sending coil needs a time delay circuit followed by a square wave circuit connected with a relay to activate the valid sending coil. The "Time 1" is presented by the "Delay". It is implemented using NE555 integrated circuit (Figure. 6.4) and it can be designed by the proper choice of the capacitor C_1 and the resistor R_1. Its expression is given as follows:

$$\text{Delay (s)} = 1.1\ R_1\ (\Omega)\ C_1\ (\text{F}) \tag{6.3}$$

The square wave generator circuit is responsible to present the "Time 2" and "Time 3". It uses a NE555 integrated circuit to generate highly accurate free running waveforms in which the output frequency can be adjusted by introducing an externally connected RC tank circuit consisting of two resistors R_2 and R_3 and a capacitor C_3 (Figure. 6.4). The "Time 2" presented by the ON time "T_{ON}" and the "Time 3" presented by the OFF time "T_{OFF}" of the oscillator can be determined by the proper design of R_2, R_3 and C_3. They are given as follows:

$$T_{ON} = 0.693(R_2 + R_3)\,C_3 \tag{6.4}$$

$$T_{OFF} = 0.693 R_3 C_3 \quad (6.5)$$

By using this method, every sending coil should be connected with the respective control circuit and with a proper time sequence design which increase the complexity of the circuit. If the receiving coil is changed by another one having different size or speed, all the parameters of the control circuit which are the delay, the T_{ON} and the T_{OFF} should be adjusted from the beginning and this presents the main disadvantage of this method.

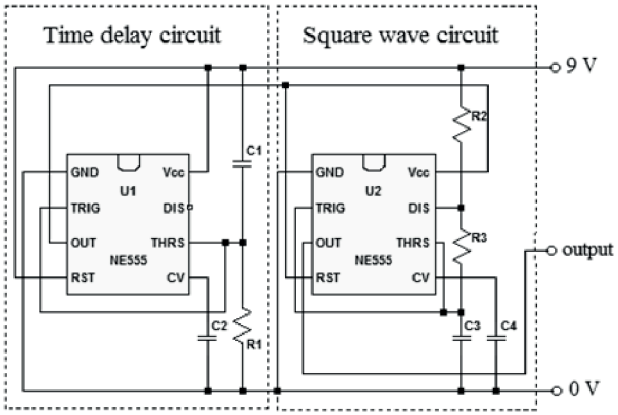

Fig. 6.4: Control circuit for a multi-coil system with constant speed

6.1.2 Variable speed and rectilinear path

The scenario of a receiver with variable speed and linear path can be found in conveyor systems, transportation systems, and special case of electric trains. A detection method using additional sensors is applied to a multi-coil system consisting of an array of sending coils is shown in Figure. 6.5.

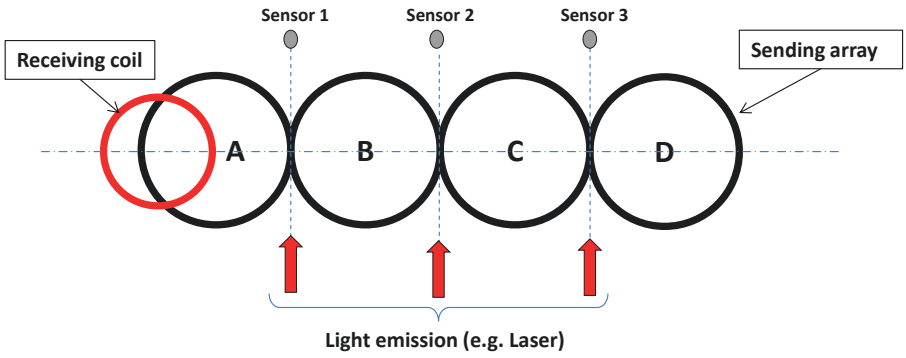

Fig. 6.5: Detection method of a receiver having a rectilinear path

The objective is to switch on one sending coil when the receiving coil is moving above it. The following sending coils' names are: coil A, coil B, coil C and coil D.

The control circuit of the sending coils is realized as shown in Figure. 6.6 (a). The coils are switched separately and each one is connected with a relay. The relay is controlled by a sensing circuit based on photo-resistor sensor called also a light dependent resistor "LDR" as shown in Figure. 6.6 (b). Depending on the position of the receiving coil, the respective relay turns on to activate the corresponding sending coil.

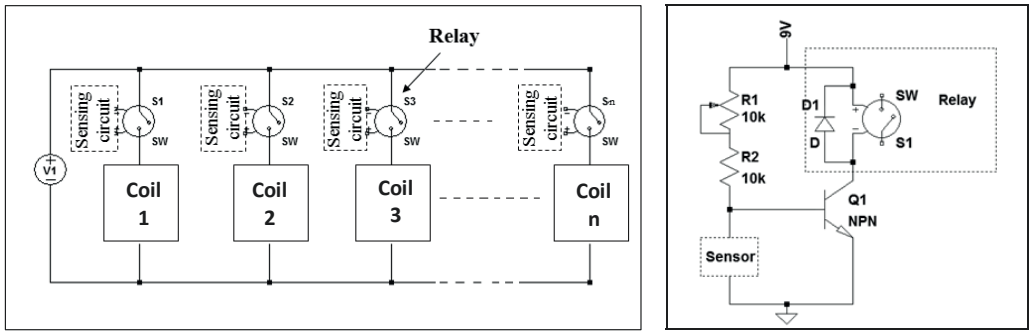

(a) (b)

Fig. 6.6: Control circuits: (a) of the sending coils, (b) of the relay

The detection principle is as follows; When the laser light is falling on the photo-resistor due to the absence of a receiver, so that no base current flows through the transistor. The relay keeps off and the corresponding sending coil is disactivated.

When the receiving coil comes in the way, the light path is blocked and the photo-resistor sensor gets triggered. Consequently, a base current flows through the transistor and switch on the respective sending coil. The diode across the relay is connected to prevent the flow of current in the opposite direction through the relay and in turn it holds on the mechanical switch. Figure 6.7 shows the realized sensing circuit, which should be connected to each sending coil. This detection method is simple, easy to implement, inexpensive and it is composed of simple electronic components. In case of the size of the receiving coil is bigger than the sending coil, the transmitted power decreases because the power source feeds more than one sending coil in parallel. Another disadvantage of the proposed method is that the receiving coil should move in a rectilinear path during the energy transmission phase

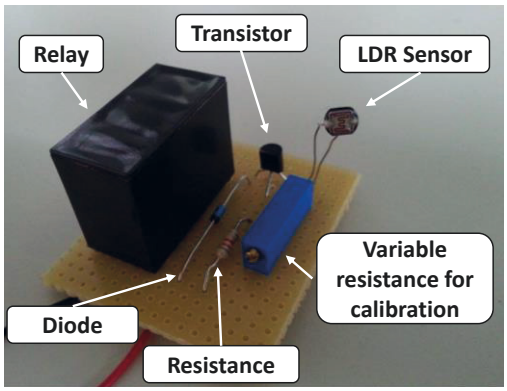

Fig. 6.7: Realized sensing circuit

6.1.3Variable speed and arbitrary path

A detection method for inductive systems with movable receiver, independently from its position and speed has been proposed. The solution overcomes the use of any additional sensors or coils, which can be realized by introducing only simple circuits and using the sending coils themselves as detectors. The proposed solution is applied to the designed multi-coil inductive system shown in Figure. 6.1.

6.1.3.1 Detection principle

The detection method is based on the measurement of the peak of the AC current of the sending coils, which shows a significant difference between invalid receiver (metallic targets or no targets) and valid receiver (the receiving coil), and then compare it to a detection threshold.

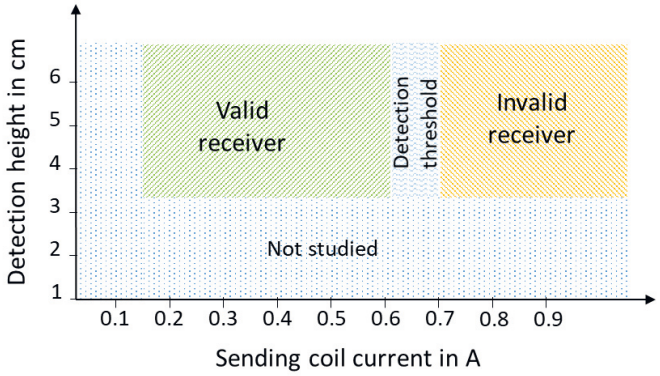

Fig. 6.8: Detection principle

As presented in Figure. 6.8, the threshold voltage limit is dependent on the receiver positions and distances and on the sending coil current

In order to define the detection threshold, three-dimensional finite element simulations of the multi-coil system are performed to predict the variation of the current value of every sending coil. The coils are excited by sinewave signal with an amplitude of 5 $V_{p\text{-}p}$ and a frequency of 1.2 MHz. During simulations, the distance between sending and receiving coil is kept constant to 50 mm with variable lateral misalignments. The obtained simulation results of the current of the sending coils S1, S2, S3 and S4 are presented in Figure. 6.9 and Figure. 6.10.

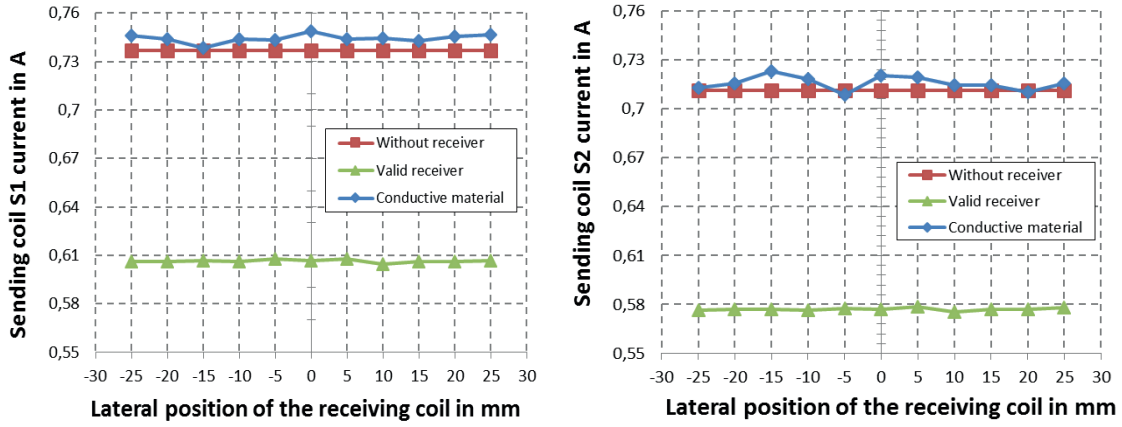

(a) (b)

Fig. 6.9: Current of the sending coil S1 (a) and the sending coil S2 (b)

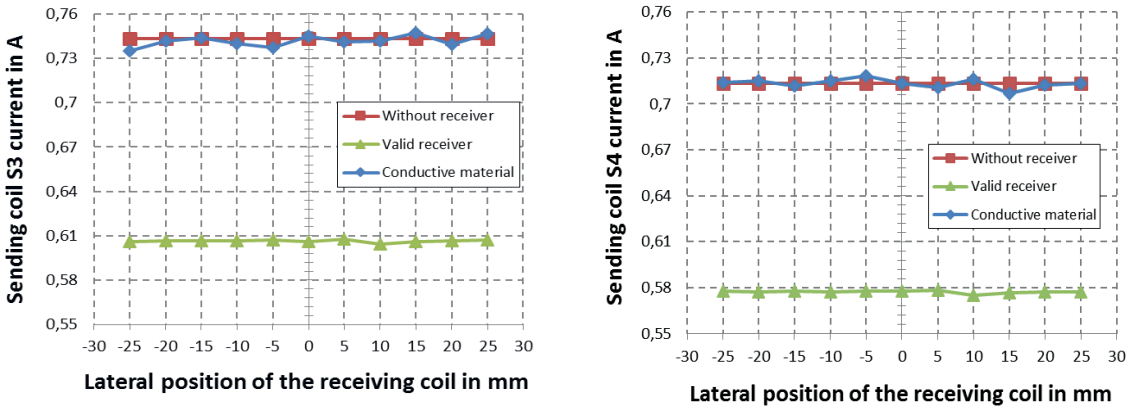

(a) (b)

Fig. 6.10: Current of the sending coil S3 (a) and the sending coil S4 (b)

Results show that the current amplitude of the sending coils decreases only in case of the presence of the receiving coil in their proximity. Based on that, a detection threshold can be chosen between 0.61 A and 0.7 A at every lateral position of the receiver. It is better to choose a value in the middle of this range to avoid circuit's ripples. Hence, a threshold current of 0.65 A was chosen.

The designed detection circuit design is presented in Figure. 6.11. Its connected in series to each sending coil. Their principle is as follows: Via a toroidal transformer, the sending coil current is transferred to a galvanically separated circuit. The measured AC current in the secondary side of the toroidal transformer is converted to DC voltage noted V_{coil} by a simple peak detector based on diode rectifier circuit and then compared to the detection voltage threshold noted V_{ref}. In order to periodically test for valid loading conditions (presence of the receiving coil) when the sending coils is switched off, a timer and flip-flop memory circuit are added. The time interval for detection is controlled by the capacitor C2 and the resistances R3 and R4.

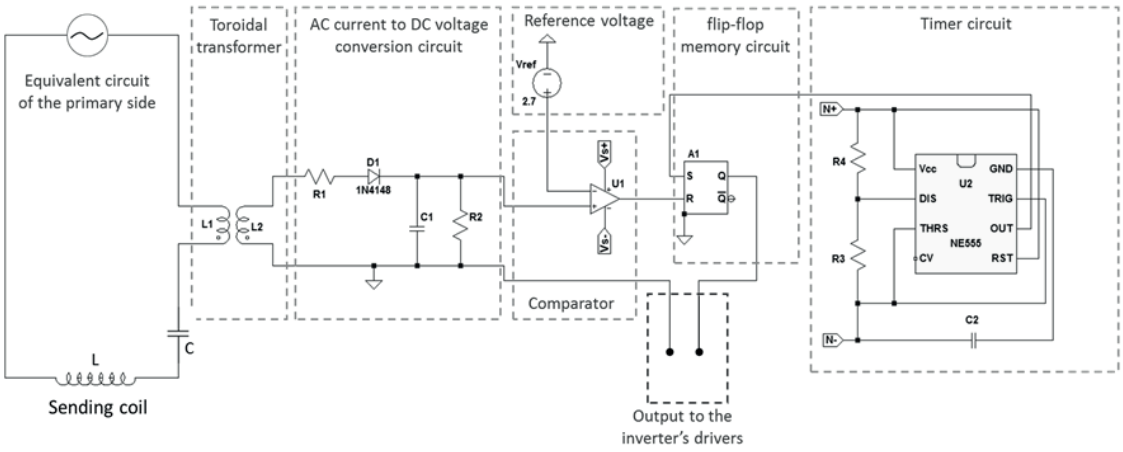

Fig. 6.11: Proposed detection circuit for movable receiver [109]

6.1.3.2 Practical implementation and evaluation

A laboratory set-up for the detection method is shown in Fig. 6.12. A ferrite ring (Ferrox cube TN23/14/7-3C90) is used for the toroidal transformer. Two integrated circuits NE555 are used for the timer and flip-flop memory circuit, respectively. An LM311P is used as a comparator.

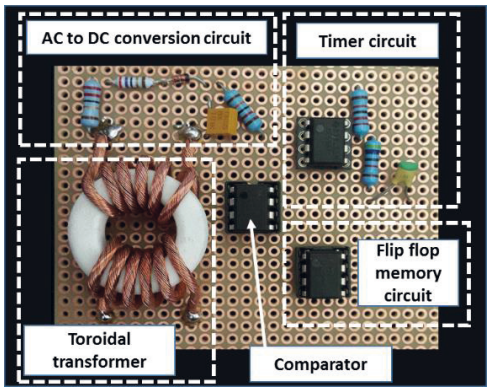

Fig. 6.12: Detection circuit [109]

In order to evaluate the detection method, two currents values corresponding to the sending coil current are generated. After the toroidal transformer and the AC/DC conversion, two voltage values are obtained: 1.5 V present the valid load and 3.4 V present the either no load or invalid load (see Figure. 6.13, black curve).

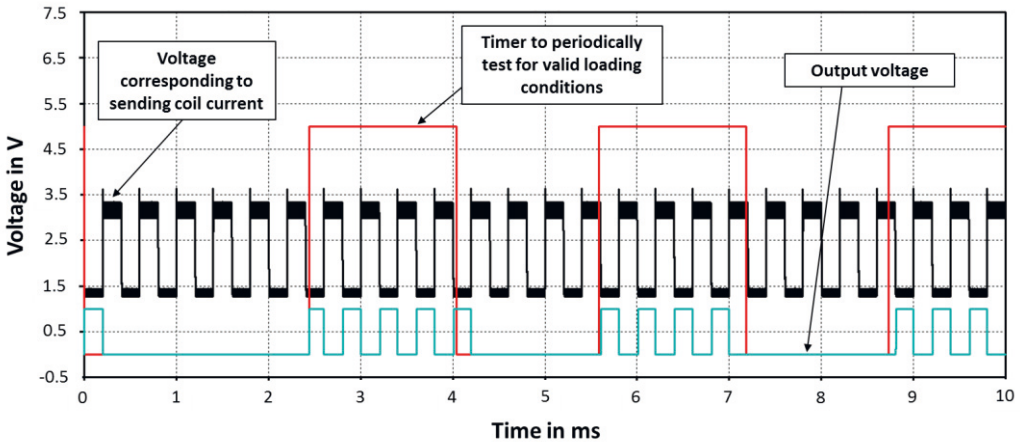

Fig. 6.13: Simulation results of the implemented detection method [109]

A short time interval was chosen for the evaluation of the circuit to clearly identify these two operation modes. The timer and flip-flop are also programmed to test at each time interval for valid loading conditions (the presence of the receiving coil). As mentioned before, the interval time can be adjusted to the receiving coil speed. The green lines in Figure. 6.13 represents the output signal of the proposed detection method which present the input signal to the driver of the signal generator inverter.

When Vcoil>V_{ref}, the output voltage is equal to zero (V_{out} = 0 V), which means no receiver or other conductive material is present in the coils. When V_{coil}<V_{ref}, the output voltage V_{out} = 1 V which indicate the presence of a valid receiving coil.

6.1.3.3 Influence of the receiver position

During power transmission, some obstacles can be present in the top of the sending coils which impose a vertical distance 'd' between the sending side and the receiving side changes or a small angular misalignment (Figure. 6.14 (a)). This may affect the detection threshold. Figure 6.14 depicts the different possible deviations of the receiver that can be happen during its movement.

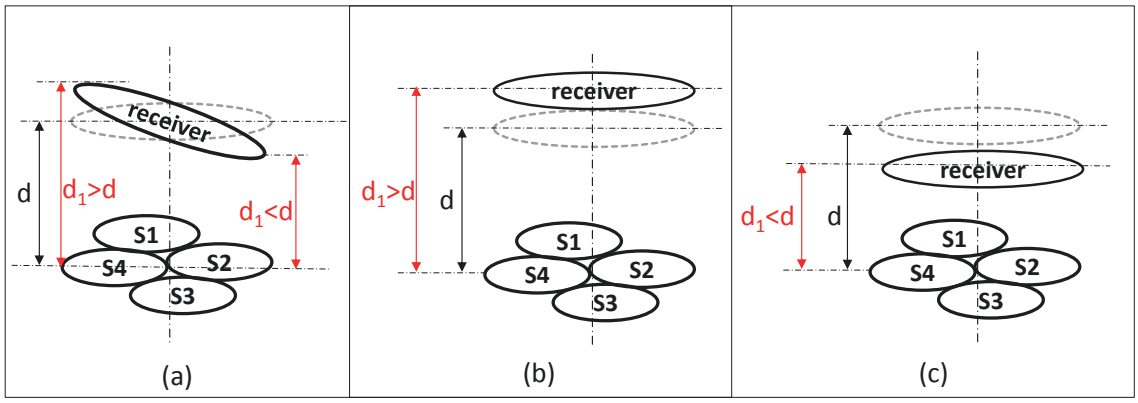

Fig. 6.14: Position deviations of the receiver

In order to investigate the behavior of the proposed detection method into vertical receiving coil deviation, three-dimensional finite element simulations in COMSOL software are performed with an excitation signal characterized by 1.2 MHz of frequency and 5 V_{p-p} of amplitude. The aim is to determine the current level at every sending coil while varying the lateral and vertical positions of the receiver. The receiver can be the valid receiving coil or an invalid receiver such as a metallic plate. Figures 6.15 and 6.16 show the simulation results of the sending coils' current at different vertical distances (40 mm, 50 mm, and 60 mm) of a conductive material and a valid receiving coil, respectively.

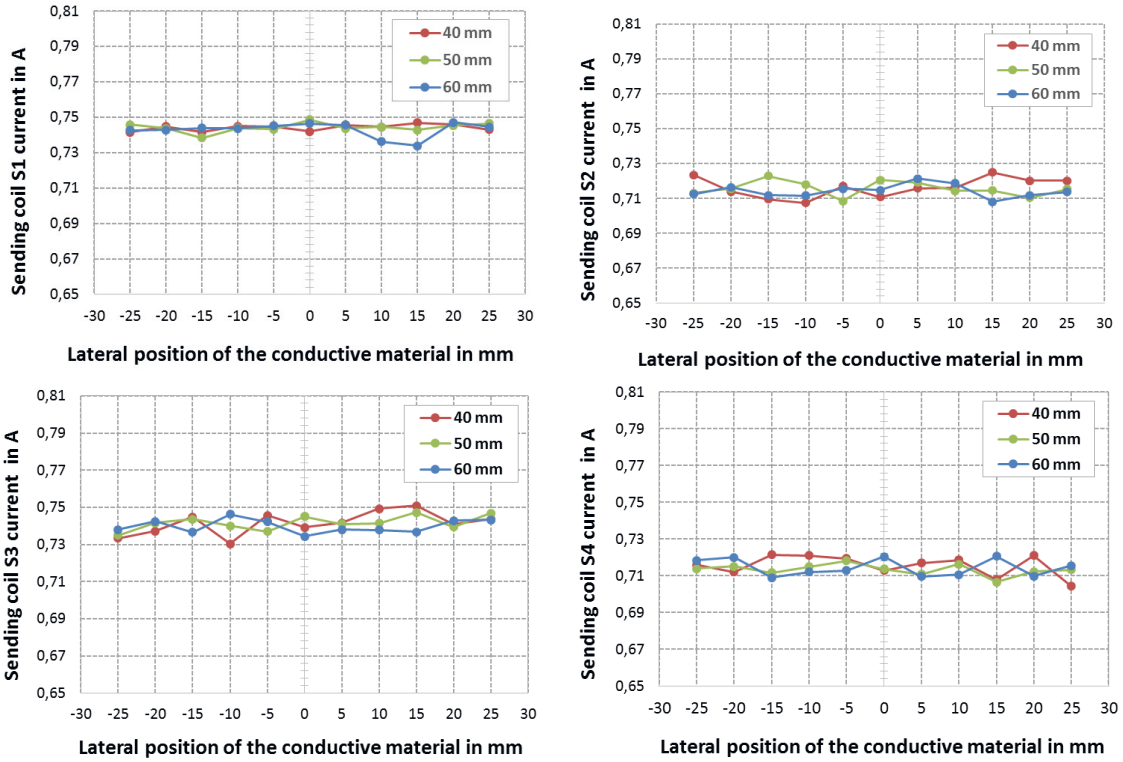

Fig. 6.15: Sending coils current for different vertical distances in case of conductive material in the proximity

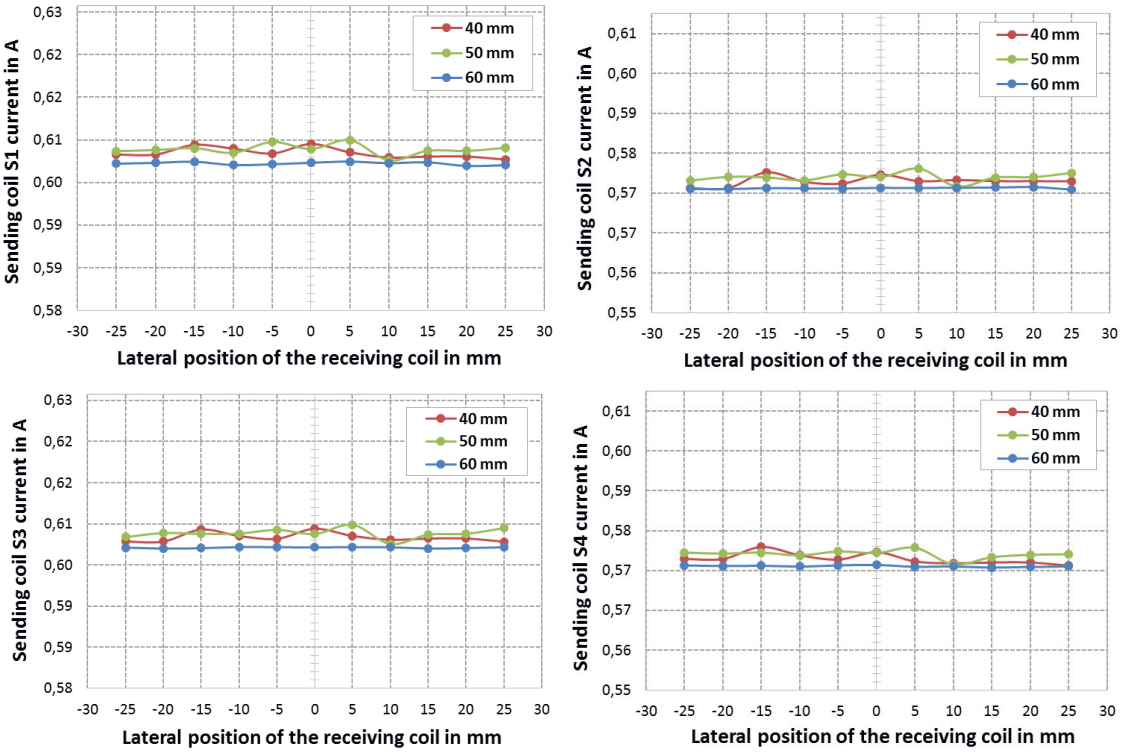

Fig. 6.16: Sending coils current for different vertical distances in case of valid receiving coil in the proximity

Results shows that there is no significant change of the sending coils current, first, at different vertical distance of the receiver between 40 mm and 60 mm and, secondly, along its lateral misalignment. Therefore, a detection threshold between 0.611 A and 0.697 A can be chosen. As conclusion, the detection current threshold of 0.65 A is not affected by the change of the vertical distance of the receiver (valid or invalid one) from 40 mm to 60 mm and it can be maintained along the receiver's displacement.

6.1.4Evaluation of the detection methods

In this section, we proposed three different detection methods. Method 1 is limited to movable receivers having constant speed and rectilinear path. Method 2 is limited to systems

Table 6.1: Evaluation of the proposed detection methods

Properties		**Detection method**		
		Method 1	Method 2	Method 3
Movable receiver		x	x	x
Receiver movement	Rectilinear	x	x	
	Arbitrary			x
Use of extra sensors			x	
Influence of external obstacles			x	
Receiver speed	Constant	x		
	Variable		x	x
Detection height		+	-	+
Design complexity		-	+	+
Detection response (rapidity)		+	+	+
Cost		-	+ +	+

With movable receivers having variable speed and rectilinear path and method 3 is used for systems with movable receiver independently from their position and speed. A brief comparison between the proposed circuits is presented in Table 6.1. Referring to that, we conclude that the circuit 3 is the suitable detection method applied to the designed multi-coil inductive system. By introducing this detection method, the receiver has more freedom to move and change its position, path and height.

6.2 Sending coils activation

The emission of electromagnetic field within an uncoupled region should be avoided, not only to eliminate unsafe exposure but also to increase the induced voltage and the equivalent mutual inductance between the coupled regions increasing thereby the energy transmission efficiency. In this context, a primary coils excitation strategy is proposed.

6.2.1 Principle

As demonstrated in the section 5.3.2, a good system configuration is to work with multiple sending coils having a hexagonal arrangement and occupying the same surface area occupied by a bigger sending coil. Figure 6.17 depicts both 2D and 3D view of the studied multi-coil inductive system. The position of the receiving coil shown in Fig. 6.17 is assumed as its initial position for all next calculations.

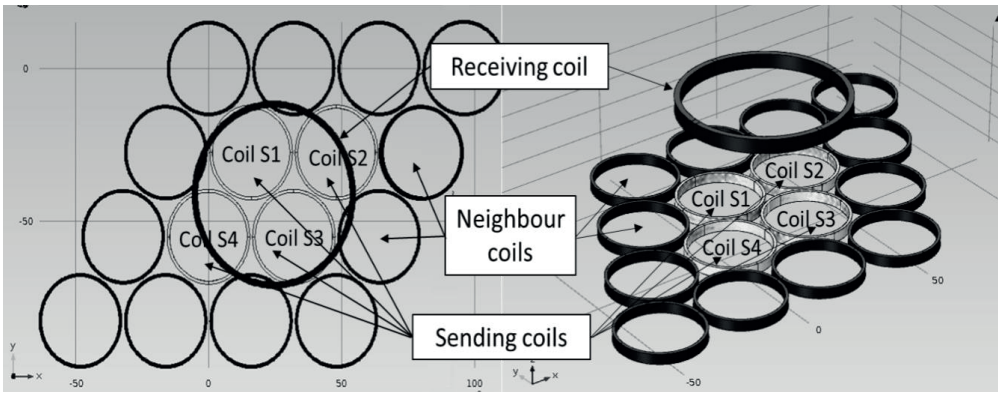

(a) (b)

Fig. 6.17: 2D (a) and 3D (b) views of the proposed multi-coil inductive system

Initially, the four sending coils S1, S2, S3 and S4 are powered equally as they are connected in series and they have the same properties. That means every coil are excited by 25% of the total system excitation independently from the lateral position of the receiving coil. In this case, the region above coils S2 and S4 is not be completely coupled (see Fig. 6.17). This leads to magnetic field leakage caused by coil S2 and S4. As solution, we propose to reduce the excitation power of these two coils and power more the coils S1

and S3. This approach which reduces the excitation power for the less covered coils will be followed for every lateral position of the receiving coil.

For example, at 10 mm of lateral misalignment, a high magnetic flux leakage between the receiving coil and the sending coil S4 is expected. Therefore, the excitation is concentrated on coils S1, S2 and S3 rather than S4. In order to realise the optimal coil-activation strategy, different possibilities are suggested in Table 6.2 and simulated in COMSOL software.

Table 6.2: Distribution of excitation power on sending coils

Lateral distance of the receiving coil	**Excitation in %**			
	Coil S1	**Coil S2**	**Coil S3**	**Coil S4**
0 mm	25	25	25	25
	30	20	30	20
	35	15	35	15
	40	10	40	10
	45	5	45	5
5 mm	25	25	25	25
	25	25	30	20
	25	25	35	15
	25	25	40	10
	30	20	45	5
10 mm	25	25	25	25
	25	30	35	10
	20	30	40	10
15 mm	25	25	25	25
	15	40	40	5
	9	45	45	1

6.2.2 Excitation circuit

To excite the sending coils by a certain percentage of the total system excitation, as shown in Table 6.2, intermediate components should be introduced between the power supply and the coils. For that, variable resistances (P1, P2, P3, and P4) are added in parallel to each resonant sending coil as shown in Fig. 6.18. As can be seen, the sending coils are connected in series. If they are connected in parallel, a different excitation circuit should be designed. In order to evaluate the output of the proposed excitation circuit, simulations in LTspice software are performed with a full bridge inverter to generate a voltage of 10 $V_{p\text{-}p}$, at a system frequency of 1.2 MHz.

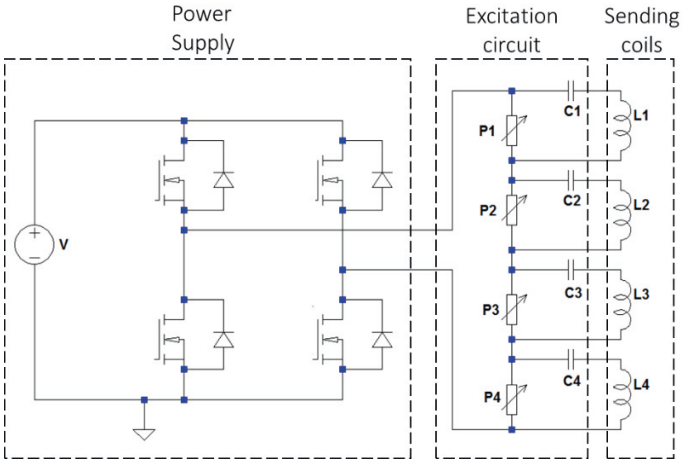

Fig. 6.18: Excitation circuit for the proposed system

Figure 6.19 depicts the simulation results of the excitation circuit for the sending coils at the initial position of the receiving coil. The case presented in Fig.19 has the following configurations: the first primary coil S1 is excited by 40%, the coil S2 is excited by 30%, the coil S3 is excited by 10% and the coil S4 is excited by 20% of the total system excitation.

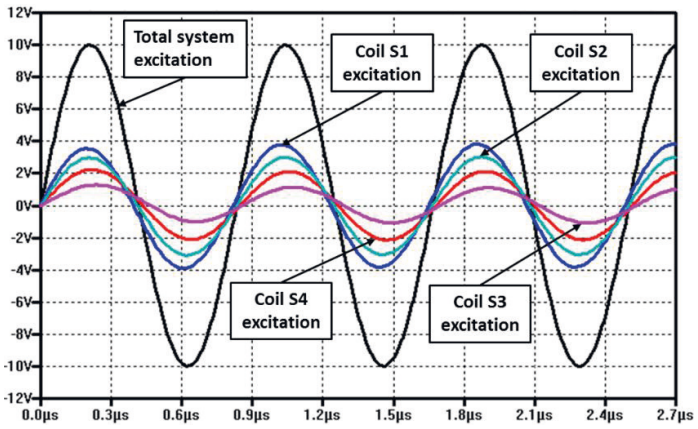

Fig. 6.19: Simulation results for the proposed excitation circuit

6.2.3 Model based evaluation

A three-dimensional model of the studied multi-coil inductive system is presented in Fig.6. 20. Neighbouring coils are also included in the model but they are not powered. This is to consider their influencing effect and to keep the simulations as close as possible to the real case. The two sides are separated by 50 mm vertical distance. The sending and

receiving coils are modelled in 3D space. In order to obtain accurate results, a finer mesh element was chosen. The sending coils are modelled as multi-turn coil domains excited by the proposed excitation-strategy as discussed in section 6.1.3. The receiver coil is modelled also as a multi-turn coil domain excited by the induced current and voltage. To change the lateral position of the receiving coil a "parametric sweep" was programmed from 0 mm to 15 mm in 4 steps. Other important parameters of the simulations are presented in Table 6.3.

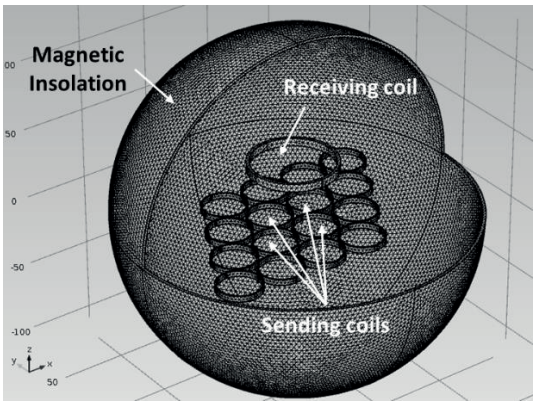

Fig. 6.20: 3D COMSOL model of the multi-coil inductive system

Table 6.3: Design of the sending and the receiving coils in COMSOL

Coil	**Receiving**	**Sending**
Number	1	4
Coil's material	Copper	
Core	Air-core	
Coil's type	Circular	
Radius	30 mm	15 mm
Coil's domain	Multi-turn coil domain	
Number of turns	8	4
Winding's wire diameter	1 mm	1 mm
Coil's excitation	Induced current, Induced voltage	Proposed strategy

The sending coils are excited differently, as shown in Table 6.4, in order to find the optimal excitation of every coil at every lateral position of the receiving coil and consequently to increase the equivalent mutual inductance and the coupling between the primary and the secondary sides. Simulation results of the equivalent mutual inductance and the induced voltage are presented in Table 6.4.

Based on the obtained results, we conclude that the equivalent mutual inductance between the sending and the receiving coils and the induced voltage are strongly dependent on the lateral position of the receiving coil. Additionally, at every lateral position of the receiving coil, there is a specific coil-excitation strategy that gives much more induced voltage and mutual coupling between the coils.

For example, at 0 mm displacement of the receiving coil, if we excite the coil S1 and the coil S3 each by 45% of the total system excitation and the coil S2 and the coil S4 each by only 5% of the total system excitation, the induced voltage and the equivalent mutual inductance equals 0.981 V and 1.208 µH, respectively. On the other hand, they are equal to 0.868 V and 0.65 µH, respectively, if we excite the coils each by 25% of the total excitation. Thus, an improvement of more than 13% and 85% of the induced voltage and the equivalent mutual inductance, respectively, is achieved

Table 6.4: Simulation results of the mutual inductance and the induced voltage for different coil excitations

Lateral position of the receiving coil	**Excitation in %**				**Simulation results**	
	Coil S1	**Coil S2**	**Coil S3**	**Coil S4**	**Equivalent mutual inductance (µH)**	**Induced voltage (V)**
0 mm	25	25	25	25	0.650	0.868
	30	20	30	20	0.690	0.897
	35	15	35	15	0.770	0.925
	40	10	40	10	0.919	0.953
	45	**5**	**45**	**5**	**1.208**	**0.981**
5 mm	25	25	25	25	0.639	0.857
	25	25	30	20	0.666	0.879
	25	25	35	15	0.800	0.925
	25	25	40	10	0.714	0.902
	30	**20**	**45**	**5**	**0.989**	**0.945**
10 mm	25	25	25	25	0.616	0.826
	25	30	35	10	0.779	0.906
	20	**30**	**40**	**10**	**0.805**	**0.917**
15 mm	25	25	25	25	0.581	0.778
	15	**40**	**40**	**5**	**1.777**	**0.982**
	9	45	45	1	0.533	0.716

Figure 6.21 and Fig. 6.22 depict the magnetic field density at each lateral position of the receiving coil without and with adjusting the coil-excitation strategy, respectively.

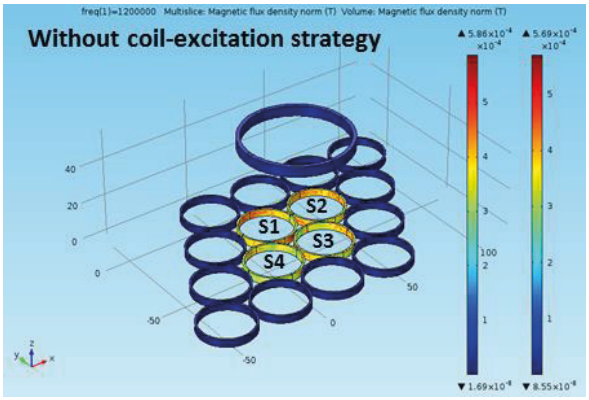

Fig. 6.21: Magnetic field density without coil-excitation strategy at different lateral positions of the receiver

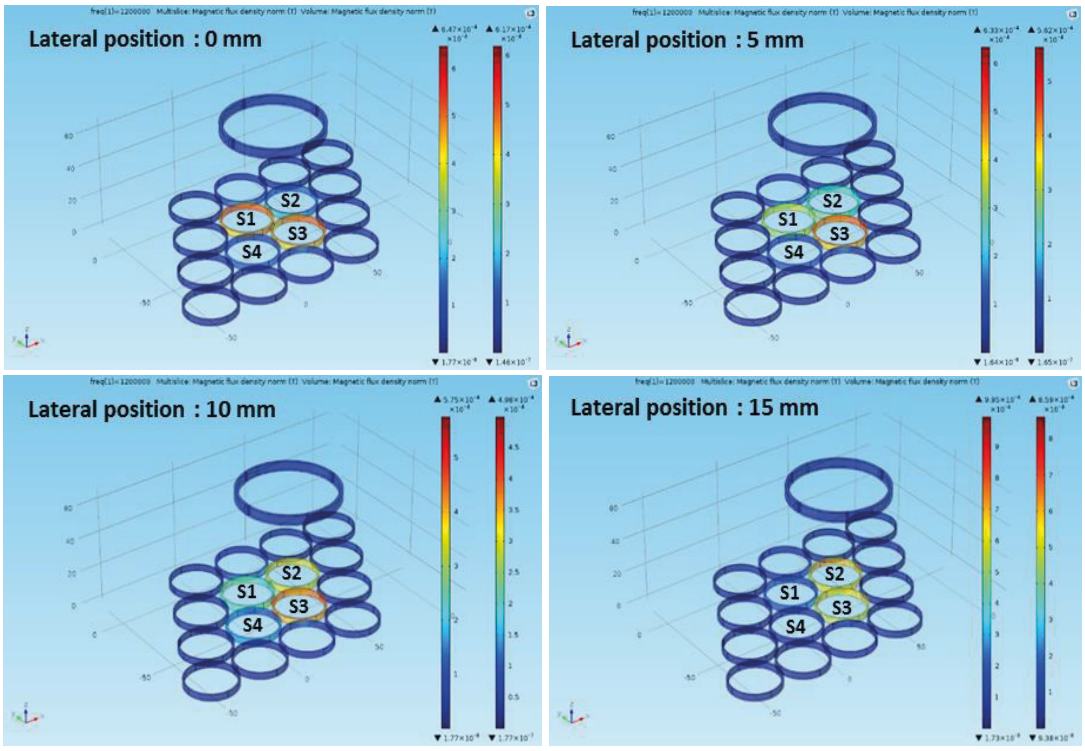

Fig. 6.22: Magnetic field density with coil-excitation strategy at different lateral positions of the receiver

The coloured scale from dark blue to dark red indicates a very low magnetic field density (1.69×10^{-8} T) and a very high magnetic field density (5.86×10^{-8} T), respectively.

Referring to Fig. 6.21, without coil-excitation strategy, the yellow colour indicates that the magnetic field is distributed evenly above the four sending coils. However, with coil excitation strategy at 0 mm lateral position (Fig. 6.22), the orange/red colour of the sending coils S1 and S3 indicates that the magnetic field is concentrated above them while the light blue colour indicates less magnetic field density above the sending coils S2 and S4.

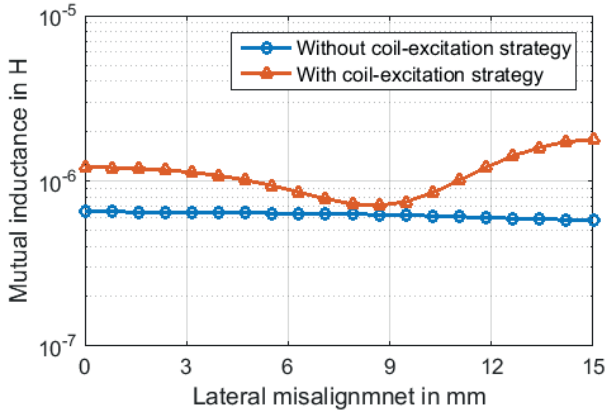

Fig. 6.23: Equivalent mutual inductance with and without the proposed excitation strategy

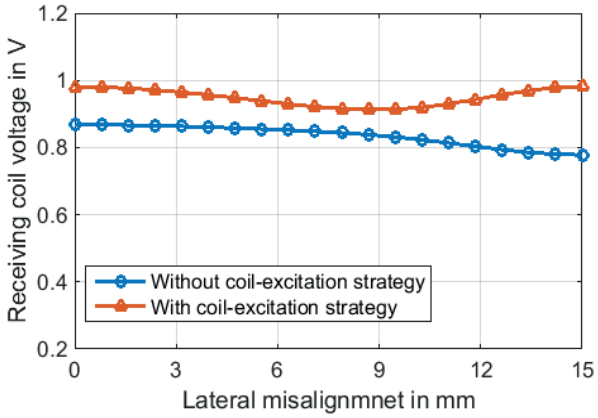

Fig. 6.24: Receiving coil voltage with and without the proposed excitation strategy

Figures 6.23 and Fig. 6.24 show the equivalent mutual inductance and the receiving coil voltage with and without the proposed coil-excitation strategy, respectively. Referring to obtained results, a great improvement of the equivalent mutual inductance and the receiving coil voltage is achieved. At perfect alignment, the equivalent mutual inductance

and the induced voltage increase by 85% and 13%, respectively, comparing to their initial value without implementing the excitation strategy. They are improved by 30.58% and 10.98% at 10 mm misalignment, respectively.

Table 6.5 presents the percentage of enhancement of the induced voltage and the equivalent mutual inductance between the primary and secondary sides at different lateral positions of the receiving coil.

Table 6.5: Percentage of the improvements at different lateral position of receiving coil

Lateral position of the receiving coil	% of the improvement of the equivalent mutual inductance	% of the improvement of the induced voltage
0 mm	85.72%	13.07%
5 mm	54.67%	10.34%
10 mm	30.58%	10.98%
15 mm	205.66%	26.21%
Mean value	94.15%	15.15%

A remarkable increase is detected at 15 mm of the lateral misalignment (lateral position of the receiving coil with respect to its initial position shown in Fig. 6.17). It shows an enhancement of 205.66% of the equivalent mutual inductance and 26.21% of the induced voltage. At this specific position, three sending coils contribute to energy transmission with 99% of the total system excitation. That means, at this lateral position of the receiving coil, the sending coil in the neighbourhood of the coil S3 noted N, should be activated to contribute to the energy transmission as shown in Fig. 6.25.

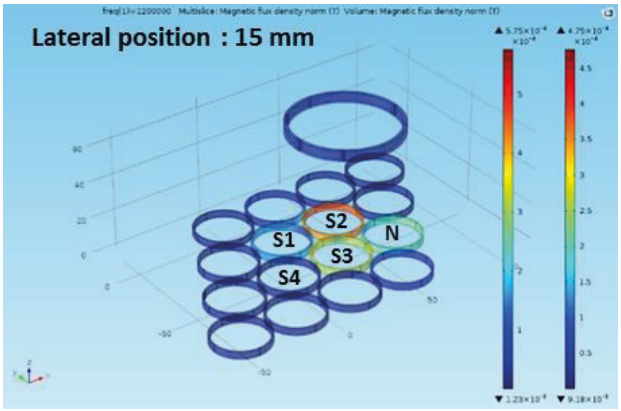

Fig. 6.25: Magnetic field density in case of the activation of the neighbouring coil N

6.2.4 Adaptation of the detection threshold

In this part, we propose the study of the effect of the sending coils excitation strategy on the detection threshold of the detection method, which is dependent on the sending coils currents. For that, three-dimensional simulations of the optimal excitation strategy are carried out in COMSOL software in order to extract the current value of each sending coil. Figure 6.26 depicts the obtained results.

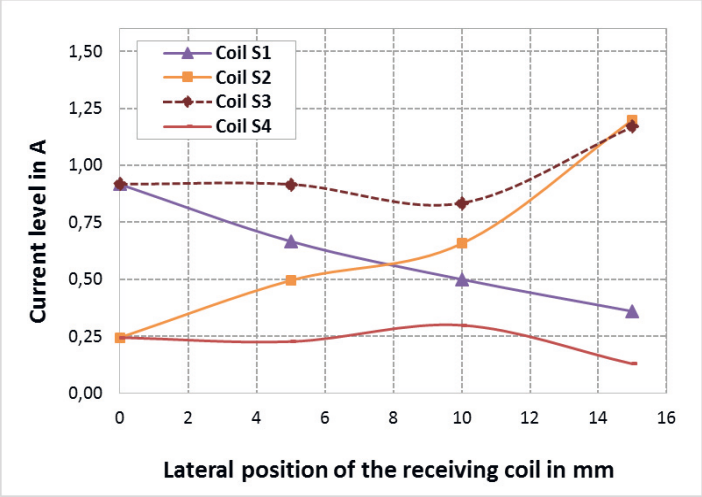

Fig. 6.26: Sending coils current in case of the selected coil-excitation strategy

We conclude that by applying the selected coil-excitation strategy along the lateral displacement of the receiving coil, the sending coils current becomes variable. For example, the current of the sending coil S1 varies from 0.85 A at the initial position of the receiver to 0.23 A at 15 mm lateral displacement of the receiver. On the other hand, the detection threshold of the detection method is equal to 0.65 A. That means, when the sending coil current exceeds this value, the detection method switches off automatically the corresponding sending coil. In this case, a programmable detection threshold must be implemented with respect to every lateral position of the receiver.

In order to implement the excitation circuit together with the detection method, extra sensor and components must be incorporated in the circuit. For that, a solution is proposed but we didn't implement it experimentally. The solution is based on incorporating a voltage sensor via a microcontroller for each sending coil and a DAC converter. The microcontroller controls the variable analogue voltage of the sending coils and decides

which threshold limit should be given to the comparator and the DAC converter converts the digital output voltage of the micro controller (which represents the detection threshold) to analogue one. The new detection principle is described in Fig. 6.27. The analogue input pins of the micro controller read the analogue voltage of each sending coils. Depending on the read value, the microcontroller adjusts the detection threshold and its output digital voltage is converted to the comparator through a DAC converter. The rest of the circuit remains the same as shown in Fig. 6.11.

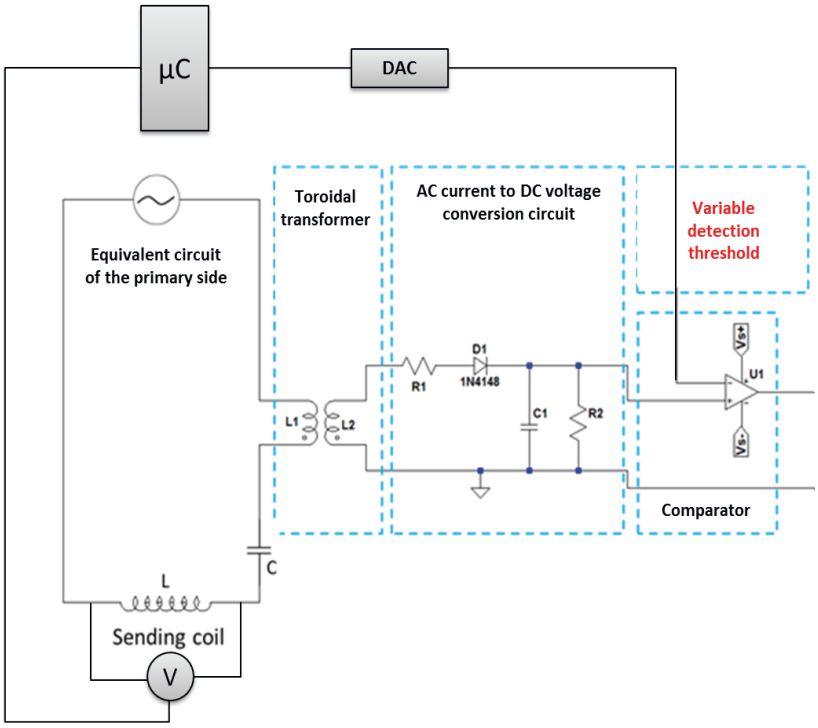

Fig. 6.27: Detection circuit in case of variable detection threshold

6.3 Concluding remarks

In this chapter, a detection method for the receiving coil is implemented independently from its position and speed. The detection method is based on the measurement of the peak of the AC current of every sending coil and compares it to a detection threshold. The detection method is able to differ between valid receivers (the receiving coil) and invalid ones (no receiver or any other conductive material) and it is not affected by small angular and/or vertical deviations of the receiver.

In the second part, we proposed a novel excitation strategy of the active sending coils in order to improve the induced voltage and the equivalent mutual inductance between the sending and the receiving coils. Results show an improvement of more than 13% and 85% of the induced voltage and the equivalent mutual inductance, respectively, comparing to their value without using the excitation strategy.

In order to implement the excitation circuit together with the detection method, a control circuit for the variable detection threshold using microcontroller is proposed.

Chapter 7

Energy management

Energy management is important for increasing the transmitted power of the proposed inductive multi-coil system. In the first part of this chapter, a concept for energy management is proposed by setting up different resonant topologies. Analytical and experimental investigations of the impact of these resonant topologies, which are the series-series (SS), the series-parallel (SP), the parallel-series (PS), and the parallel-parallel (PP) topologies, are carried out. In the second part of this chapter, the effect of the load impedance values on the transmitted power for different system topologies is studied. The last part addresses the quantitative evaluation of improvement to the state of the art.

7.1 Investigation of system topology

One of the proposed solutions to increase the transmitted power is to realize the resonance compensation topologies [112-117]. For that, series or parallel capacitors are added to the primary side and/or secondary side to realise the resonance by nullify the reflected impedance from the secondary side to the primary side. Different types of topologies can be applied, such as series-series (SS), series-parallel (SP), parallel-series (PS), and parallel-parallel (PP) topologies. The different configurations of the compensation topologies are shown in Fig.7.1.

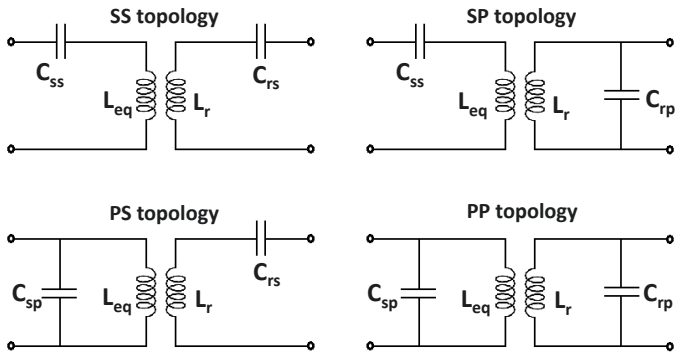

Fig. 7.1: Compensation topologies of the multi-coil inductive system

The selection of the adequate topology depends on the system requirement. In [112], a comparison between SS and SP topologies is carried out for a two-coil system at a 1 MHz frequency. Results show that the SP topology leads to a better transmission efficiency. Similar results have been reported in [113]. Here, the authors have presented the design considerations of compensation capacitors in SP topology to have a maximum delivered power. However, Campi et al. have demonstrated in [114] that the selection of compensation topologies should be done dependently on the frequency. They demonstrated that the appropriate topologies are the SP configuration at a frequency of 300 kHz and the SS configuration at a frequency of 13.56 MHz. A comparison between both one-side and two-sides compensation topologies was carried out in [116]. Investigation shows that the parallel compensation of both primary and secondary sides has much better performance than compensating only in one-side. The practical evaluation of the different compensation topologies shows that the PP topology has better performance than the other studied topologies.

In this context, we propose to study the different compensation topologies on both primary side and secondary side to improve the transmitted power. The proposed compensation topologies are: The series-series (SS), the series-parallel (SP), the parallel-series (PS), and the parallel-parallel (PP) topologies. For the verification and the comparison, a resistive load at the secondary side at a system frequency of 1.2 MHz is chosen.

7.1.1 Analytical study

In this section, an analytical study of the resonant topologies is carried out in order to parametrize the compensation capacitors and to calculate the impedances in resonance in both sending and receiving sides, the power at the load, the transmitted power and the system efficiency for the studied topologies.

Figure 7.2 depicts the equivalent circuit of the studied multi-coil inductive system. V_1 is the source voltage, L_i represents the self-inductance of the coil i, R_{eq} is the equivalent resistance of the four in series connected sending coils, R_L is the resistive load, and C_{ij} represents the compensation capacitor where the sub-letter (i) refers to the sending (s) or

the receiving (r) side and the sub-letter (*j*) refers to the series (s) or the parallel (p) connection of the capacitor on the circuit. From here, four possible compensation topologies could be defined: SS, SP, PS and PP topologies.

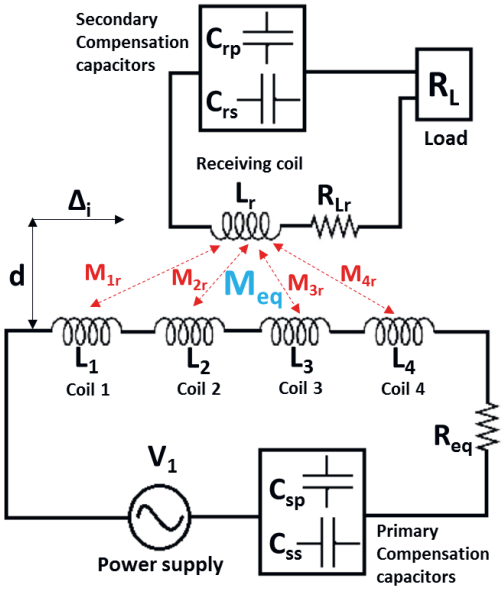

Fig. 7.2: Equivalent circuit of the studied multi-coil inductive system

Table 7.1 presents the different expressions of the compensation capacitors C_{ss}, C_{sp}, C_{rs} and C_{rp}, of both the sending side and the receiving side at the resonance frequency.

Table 7.1: Values of compensation capacitors at resonance

Topologies	**Compensation capacitor**	**Value of R_2**
Series compensation on the sending side	$C_{ss} = \dfrac{1}{\omega^2 L_{eq}}$	-
Parallel compensation on the sending side	$C_{sp} = \dfrac{L_{eq}}{(L_{eq}\omega)^2 + (R_r + R_{eq})^2}$ Where $R_r = (M_{eq}\omega)^2$	-
Series compensation on the receiving side	$C_{rs} = \dfrac{1}{\omega^2 L_r}$	$R_2 = R_{L_r} + R_L$
Parallel compensation on the receiving side	$C_{rp} = \dfrac{R_L^2 + \sqrt{\mathrm{Re}\left(R_L^4 - (2\omega R_L L_r)^2\right)}}{2L_r(\omega R_L)^2}$	$R_2 = R_{L_r} + \dfrac{R_L}{1 + (R_L C_{rp}\omega)^2}$

Table 7.1 shows that the selection of the value of compensation capacitor should be done in dependence on the selected topology. For example, if the SP topology is chosen, the capacitors values of series compensation on the sending side and parallel compensation on the receiving side should be selected. That means C_{ss} and C_{rp} should be chosen. The same way is applied to select capacitors of the other topologies.

For series compensation, the choice of capacitors doesn't depend either on the load or on the coupling factor, which is dependent on the mutual inductance (M_{eq}). However, the values of compensation capacitors show a dependency on both the load and coupling factor in case of parallel compensation. In order to evaluate the multi-coil system, the load R_L is kept fixed to 330 Ω. This value was chosen to fulfil the condition (5.64): $R_L \geq 2\omega L_r$.

The expressions of the equivalent resistances R_1 and R_2 on the sending side and the receiving side, respectively, the transmitted power, the power at the load and the system efficiency are given in Table 7.2.

Table 7.2: Analytical expressions of transmitted power, power at the load and system efficiency

Topologies	**Transmitted power P_t Power at the load P_L**	**System efficiency η**	**Value of R_1 and R_2**
Series compensation on the sending side	$P_{t_1} = \frac{V_1^2 R_r}{(R_r + R_1)^2}$	Depending on the receiving side compensation	$R_1 = R_s + R_{eq}$
Parallel compensation on the sending side	$P_{t_2} = \frac{V_1^2 R_r}{R_1 (R_r + R_{eq})^2}$	Depending on the receiving side compensation	$R_1 = R_s + \frac{R_r + R_{eq}}{A^2 + ((R_r + R_{eq})C_{sp}\omega)^2}$ Where, $A = 1 - L_{eq} C_{sp} \omega^2$
Series compensation on the receiving side	$P_{L_1} = \frac{R_L}{R_2} P_t$	$\eta_1 = \frac{R_L}{R_2} \frac{R_r}{R_r + R_1}$	$R_2 = R_{L_r} + R_L$
Parallel compensation on the receiving side	$P_{L_2} = P_t \left(1 - \frac{R_{L_r}}{R_2}\right)$	$\eta_2 = (1 - \frac{R_{L_r}}{R_2}) \frac{R_r}{R_r + R_1}$	$R_2 = R_{L_r} + \frac{R_L}{1 + (R_L C_{rp} \omega)^2}$

The results in Fig. 7.3 show the simulation results of the power at the load for a multi-coil system with a 50 mm of distance between the sending side and the receiving side. The y-axis is represented in logarithmic scale in order to have a clear presentation and

comparison between the different topologies. During the simulation, the used self-inductances and mutual inductances values for different misalignments values are defined from the results of the FEM simulations.

Based on the obtained results, the highest level of power at the load is achieved by using the PP compensation topology along the lateral misalignment from 0 mm to 25 mm. The second best performance was reached by the SP topology.

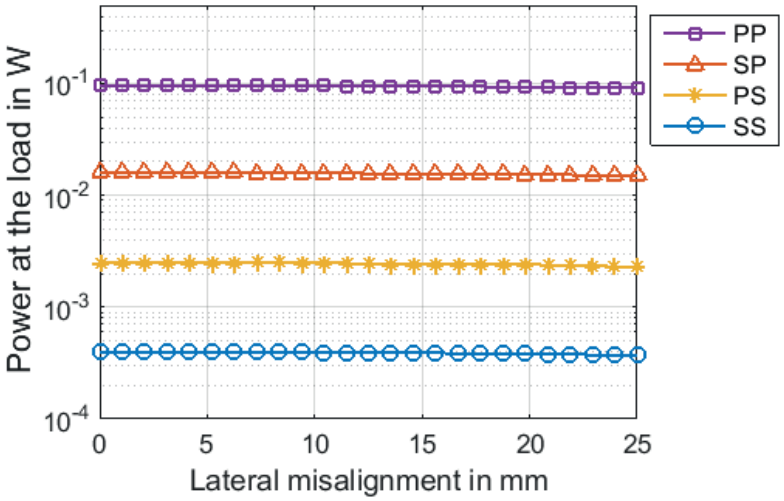

Fig. 7.3: Simulation results of the power at the load for different topologies

7.1.2 Experimental verification

The power at the load for the different compensation topologies is evaluated experimentally. Fig. 7.4 depicts the experimental setup of the studied multi-coil inductive system. The operation frequency is adjusted to 1.2 MHz by an AC power source and a resistance of 330 Ω has been chosen for the load verifying condition (6.64). The signal wave generator has a series impedance of 50 Ω and generates a voltage with a peak-to-peak amplitude of 10 Vp-p .

The sending and receiving coils are made of copper wire of 1 mm diameter. The distance separating the two sides equals to 5 cm using a plastic holder. Misalignment was adjusted manually from 0 cm to 25 mm in 6 steps. The load voltage across the load is controlled with a digital oscilloscope in order to measure the received power.

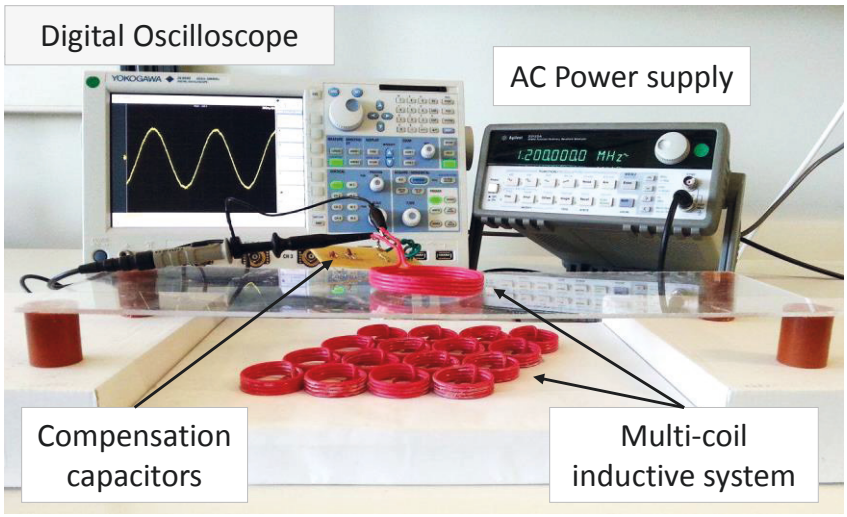

Fig. 7.4: Experimental set up for topologies investigation

The analytical and experimental values of the compensation capacitors are given in Table 7.3. Because of the unavailability of standard commercial values of capacitors that equal the analytical ones, near values are used in experiments.

Table 7.3: Analytical and experimental values of the used compensation capacitors

Topologies	**Analytical value**	**Experimental value**
Series compensation on the sending side	C_{ss} = 6.6243 nF	C_{ss} = 6.8 nF
Parallel compensation on the sending side	C_{sp} = 6.6227 nF	C_{sp} = 6.8 nF
Series compensation on the receiving side	C_{rs} = 2.7628 nF	C_{rs} = 2.2 nF
Parallel compensation on the receiving side	C_{rp} = 1.3814	C_{rp} = 1.5 nF

The obtained curves in Fig. 7.5, which are represented by solid lines, show the experimental results of the power at the load. In accordance with the numeric simulation results, the PP compensation topology has the highest power at the load at perfect alignment and at lateral misalignment cases that varies from 0% to 84% of a sending coil's diameter. Experimentally, the multi-coil system with PP compensation topology is able to

transfer 72 mW at perfect alignment, 62 mW at 10 mm of lateral misalignment and 32 mW at 25 mm of lateral misalignment.

As it is expected, good performance is given by the PP topology followed by the SP one. The obtained results of the multi-coil system are similar to the investigations performed with two-coil system in [112-114] that prove that the SP and PP topologies offer the best performance, respectively.

Deviation between the analytical and experimental results of the power at the load is caused by the small difference between the analytical and experimental values of the used capacitors as shown in Table 7.3. There are also other factors that could affect the experimental study of the multi-coil system such as the heat loses of the wires forming the coils, the neighbouring coils, and the magnetic field interference of the four active sending coils

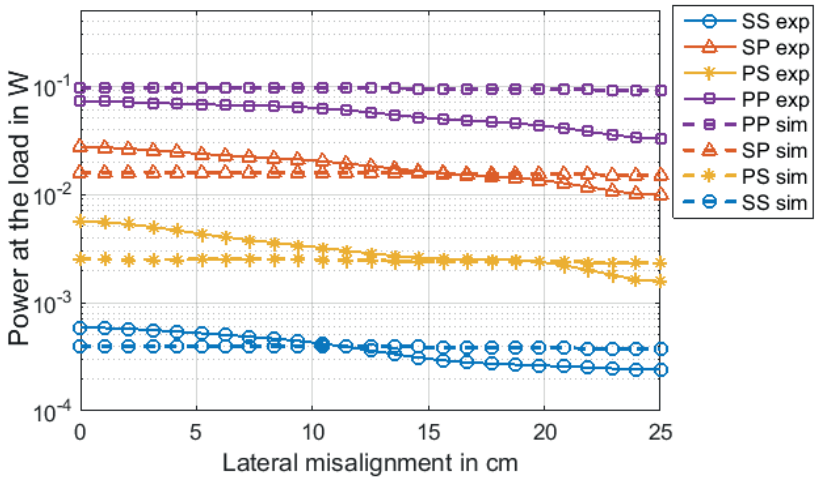

Fig. 7.5: Experimental (exp) and analytical results (sim) of the power at the load for different topologies

7.2 Load impedance

The transmitted power is not only dependent on the topology of the system, but also on the load value. In this section, the effect of the load value on the transmitted power for different system topology has been investigated. The load value should fulfil the condition (5.64). Two resistances values representing low resistive loads at 15 Ω and high resistive loads at 330 Ω have been chosen. Simulation results are shown in Fig. 7.6 and Fig. 7.7.

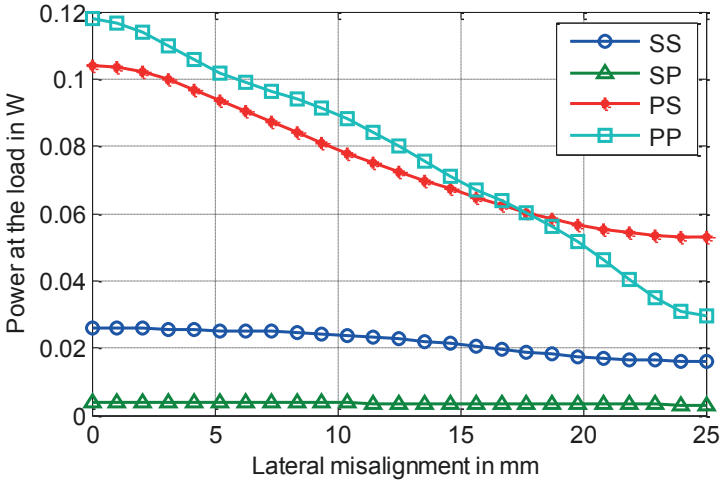

Fig. 7.6: Power at a 15 Ω pure resistive load

As can be seen in Fig. 7.6, until 18 mm of lateral misalignment, maximum power at the load is reached by PP topology. For a higher degree of misalignment, more than 18 mm, PS topology becomes better. Despite their good transmitted power to the load, PP and PS topologies show a high dependency on lateral misalignment unlike SS and SP topologies that show a small decrease of power at the load along the receiver misalignment.

For higher load value, depicted in Fig. 7.7, the maximum power at the load is reached by PP topology followed by SP topology. For both topologies, the power level is sharply decreased by increasing the lateral misalignment between the sending and receiving coils. On the other hand, the lateral misalignment has a small effect on SS and PS topologies.

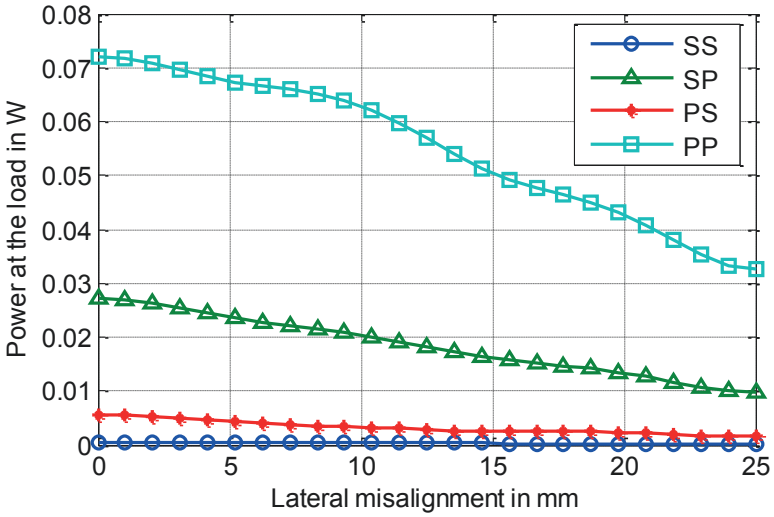

Fig. 7.7: Power at a 330 Ω pure resistive load

A comparison between the received power at the load for different system topologies and load values is provided in Fig. 7.8. It shows that the highest power at the load is achieved by PP and PS topologies at small load value and by PP topology for high load value that fulfils condition (Eq. 5.64).

The obtained results show that the optimal configuration is the PP topology because it gives the highest amount of power for both low and high load value. It gives also more flexibility to the user for the choice of the load value. SP topology can also be chosen but only for low load value.

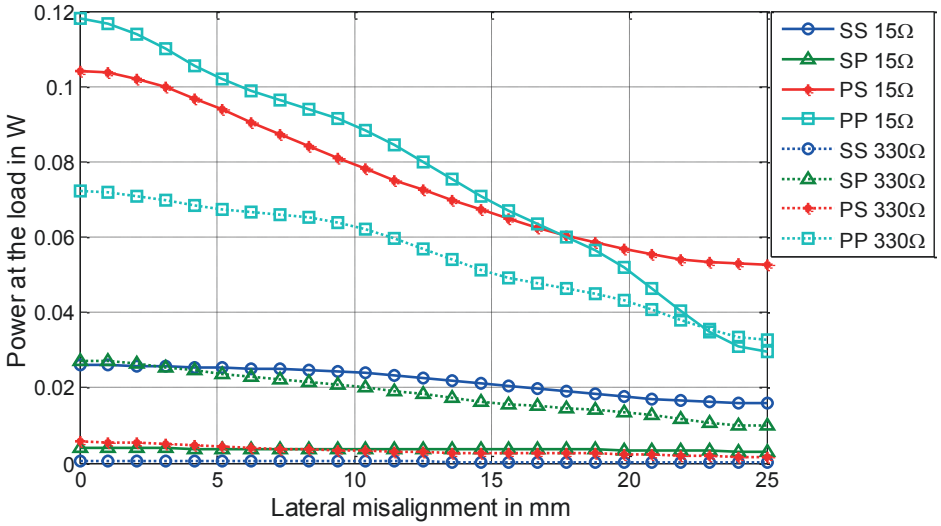

Fig. 7.8: Power comparison at 15 Ω and 330 Ω of purely resistive loads

7.3 Discussions

Different system topologies are studied to optimize the transmitted power at the load. Base on the simulation and the experimental results, we conclude that the system topology has an important impact on the transmitted power to the load.

Despite of its dependency on the lateral position of the receiver, the PP topology offers higher transmitted power at the load comparing to the other system topologies in case of high and low load impedance values fulfilling condition (5.64). Only in case of low load value and at large lateral misalignment corresponding to 58% of the sending coil's diameter, the parallel-series PS topology presents higher power at the load than the PP topology. This is due to the double dependency of the compensation capacitors of the PP

topology on the mutual inductance and the load impedance value. On the other hand, the compensation capacitors of the PS topology are dependent only on the load impedance values (see Table 7.1).

At low load impedance value, the SS and the SP topologies are less sensitive to misalignment between the sending side and the receiving coil. The investigation shows that the SS and the PS topologies are less sensitive to misalignment between the sending side and the receiving coil in case of high load impedance values.

7.4 Quantitative evaluation

The transmitted power and the transmission efficiency of the inductive systems depends on the following parameters: The vertical coil-to-coil distance, the lateral misalignment between the sending side and the receiving side, the properties of the implemented coils, the circuit's topology, the position and the type of the receiver, the power source, the frequency, the interfaces on the sending and on the receiving side. Most of the investigations have concentrated on the optimization of IPT systems by studying one or two influencing parameters and ignoring the others or they kept them in perfect conditions. The investigation carried out in this thesis has taken the majority of these parameters into consideration and proposes a novel system that is able to operate, even under non-perfect conditions.

The novel system proposal has many improvements in comparison to the state of the art. The main one is the proposal of a multi-coil system in which the conventional big sending coil is replaced by multiple smaller sending coils occupying almost the same surface in an hexagonal arrangement. Furthermore, the proposed system is able to orientate the magnetic field lines by powering the two nearest neighbouring coils of the active ones with a weak current in the opposite direction. The system offers therefore more flexibility in case of a lateral misalignment occurring often in inductive power transmission systems.

We proved that the multi-coil inductive systems with orientated magnetic field are more efficient than the conventional two-coil systems to transmit power at a large air gap between the sending and the receiving coils and beginning with a lateral misalignment of 29% of the sending coil diameter.

Table 7.4: Comparison between the proposed system and selected SOA systems

Criteria		References														
		22	23	24	25	14	27	28	31 32	33	34	35	36	37	38 39	This work
Large air-gap		x			x	x	x					x	x	x		x
Misalignment tolerance		x	x	x				x	x	x		x			x	x
Movable receiver											x	x	x	x		x
Dependency on receiver		x	x	x	x	x	x			x						
Free positioning								x	x		x	x	x	x	x	x
Receiver detection									x					x	x	x
Sending coils	Selection								x					x	x	x
	Activation strategy															x
Design complexity		-	+	++	-	-	-	+	+	+	++	+	+	++	++	-
Control complexity		-	+	+	-	++	+	-	++	+	++	+	-	+	++	-
Cost		-	-	+	-	+	-	+	+	+	+	+	-	+	+	-

In order to evaluate the proposed system, a comparison of the conventional two-coil system and the most promising proposed solutions for multi-coil system from literature [22- 78], is carried out. Table 7.4 and Table 7.5 show a quantitative improvement of the proposed solution in comparison that of the state of the art.

The proposed system is less sensitive to lateral misalignment even at lateral misalignment that equals to 50% and is able to transmit sufficiently power even at a large air gap. This represents a significant achievement because the usual lateral misalignment is in the range of 5% to 10% of the sending coil diameter and a high misalignment has been reported as 20% of the sending coil diameter [31-39]. The proposed system shows almost no dependency on small angular deviations or small misalignments of the receiver and can be realized at low costs.

The novel activation strategy of the sending coils shows an improvement of the mutual inductance of 94.15% and an improvement of the induced voltage of 15.15% in comparison to conventional systems.

Table 7. 5: Comparison between the proposed system and selected SOA systems with air core and circular shape in terms of efficiency, load power and the proportion of the coil diameter over the coils distance τ

τ	Frequency	Transmitted power	Efficiency in %	Reference
0.3	9.9 MHz	60 W	40	[71]
1	6 MHz	95 W	-	[79]
1.27	742 kHz	-	24	[56]
2	700 kHz	24 mW	72	[55]
3	4.5 MHz	10 mW	54	[75]
2	700 kHz	50 mW	36	[76]
2	2 MHz	-	40	[78]
0,6	1.2 MHz	43 mW	29.2	This work

In order to realize a high system efficiency, τ should be higher than 2. For a lower value of τ, the efficiency drops dramatically below 20%. An exception was made by MIT for high power range [71], where they succeeded to reach more than 40% efficiency at $\tau = 0.3$. In this work, we focus more on low-power applications. At $\tau = 0.6$, the efficiency of the designed inductive system equals 29.2%, which represents a significant improvement of efficiency in comparison to [56], which reached only 24% of efficiency at a high proportion of the coil diameter over the coils distance $\tau = 1.27$.

In terms of transmitted power, the proposed multi-coil system is able to transmit 43 mW to the receiving side at $\tau = 0.6$, which is a good value if we compare it to the results in [55, 75] that reported about only 24 mW at $\tau = 2$ and 10 mW at $\tau = 3$, respectively.

Chapter 8
Conclusion

Inductive power transfer is very useful as a safe, low-maintenance and reliable wireless power transmission technique. It is also very important for low-power applications such as wireless sensor systems and biomedical implants that have power consumption in the typical range between μW to tens of mW. In the practical use, a misalignment between the sending and the receiving coils is often unavoidable. It results in a sharp decrease of the transmitted energy and consequently to a decrease of the power transmission efficiency. At a large coil-to-coil vertical distance, the magnetic field issued by the sending coils is not completely enclosed by the receiving coil and consequently the transmitted power becomes not sufficient.

The main focus of this thesis is the improvement of the transmitted power, the mutual inductance, the power at the load, and consequently the power transmission efficiency of the inductive system in case of lateral misalignment between the sending and receiving sides and at large coil-to-coil vertical distance. For that, a multi-coil inductive system with optimized coil's size and arrangement is designed. The idea is to orientate the magnetic field of the sending coils by powering the nearest neighbouring coils of the active ones with a weak current and in the opposite direction.

Simulation and experimental results show that, beginning with an air-gap corresponding to 50% of the sending coil diameter and a lateral misalignment corresponding to 29% of the sending coil diameter, the proposed MISO coil system with oriented magnetic field shows a better performance than the conventional two-coil system (SISO). At 50 mm air gap, corresponding to 166% of the sending coil diameter, and at perfect alignment, the proposed solution offers 110% of the transmitted power reached by the SISO coil system. At a lateral misalignment corresponding to 33% of the sending coil diameter, it reaches the double of the transmitted power as the SISO coil system

Suitable models for the self-inductance, the resistance, the self-capacitance and the quality factor are proposed in order to extract the important parameter of the multi coil inductive system such as the equivalent mutual inductance and the coupling factor. Experimental results show that Wheeler' model is suitable for modelling of self-inductance, Ericson's model is suitable for the modelling of the resistance and Palermo's model is suitable for modelling of the self-capacitance.

In order to avoid the excessive emission of magnetic field and to increase the power transmission efficiency of the system, a receiver detection method and an activation strategy are proposed to activate, in a suitable manner, only the sending coils, which are above the receiver and switch off inactive coils. The novel detection solution is based on the measurement of the AC current peak of every sending coil and its comparison to a given detection threshold. The proposed detection method can be used for large air gap, is low cost as in needs simple electronic components and no communication between the sending side and the receiving side. It can differentiate between the receiver coil and the case of other conductive materials or no receiver. The novel activation strategy for the active sending coils guarantees a good magnetic field distribution along the active sending coils and high equivalent mutual inductance between the sending side and the receiving side at every lateral position of the receiver. Simulation results show an improvement of more than 94% of the mutual inductance and 15% of the induced voltage comparing to the system without the selected activation strategy.

Energy management of the multi-coil inductive system is also very important to reach high system efficiency through by maintaining resonance conditions and realizing impedance matching. For this purpose, compensation capacitors in Series-Series (SS), Series-Parallel (SP), Parallel-Series (PS) and Parallel-Parallel (PP) topologies are investigated. Simulation and experimental results prove that the multi-coil inductive system with Parallel-Parallel compensation topology with high or low load impedance value reaches a higher transmitted power compared to other system topologies in both coaxial and lateral misalignment cases.

The proposed multi-coil inductive system is suitable for low-power systems, such as wireless sensors and biomedical implants, but can be also applied to higher range of power at a flexible position of the receiver.

Appendix A

Complete elliptic integrals of the first and the second kinds

A.1 **Definition of elliptic integral**

If

$$R(x,y) = R_1(x) + \frac{R_2(x)}{y} \tag{A1}$$

is a rational function of x and y in which y^2 equals to a cubic or quartic polynomial in x, the integral:

$$\int R(x,y)\,dx \tag{A.2}$$

is called an elliptic integral.

A.2 **Complete elliptic integral of the first kind**

The complete integral of the first kind noted *K(k)* can be defined as follows

$$K(k) = F(\frac{1}{2}\pi, k) \tag{A.3}$$

$$= \frac{\pi}{2}\sum_{n=0}^{\infty}\left[\frac{(2n-1)!!}{(2n)!!}\right]^2 k^{2n} \tag{A.4}$$

$$= \frac{1}{2}\pi\ {}_2F_1(\frac{1}{2},\frac{1}{2};1:k^2) \tag{A.5}$$

Where k is the elliptic modulus, $F(\frac{1}{2}\pi, k)$ is the incomplete integral of the first kind and ${}_2F_1(\frac{1}{2},\frac{1}{2};1:k^2)$ is the hypergeometric function [119-121].

The complete elliptic integral of the first order satisfies the following identity

$$\frac{\pi}{2\sqrt{1-k^2}} P_{-1/2}\left(\frac{1+k^2}{1-k^2}\right) = \frac{1}{\sqrt{1-k^2}} K\left(\sqrt{\frac{k^2}{1-k^2}}\right) \tag{A.6}$$

Where $P_{-1/2}\left(\frac{1+k^2}{1-k^2}\right)$ is a Legendre polynomial [87-89].

A.3 **Complete elliptic integral of the second kind**

The complete integral of the first second noted *E(k)* can be defined as follows

$$E(k) = E(\frac{1}{2}\pi, k) \tag{A.7}$$

$$= \frac{\pi}{2}\left\{1 - \sum_{n=1}^{\infty}\left[\frac{(2n-1)!!}{(2n)!!}\right]^2 \frac{k^{2n}}{2n-1}\right\} \tag{A.8}$$

$$= \frac{1}{2}\pi \ {}_2F_1(-\frac{1}{2}, \frac{1}{2}; 1 : k^2) \tag{A.9}$$

$$= \int_0^{K(k)} dn^2(u,k)\, du \tag{A.10}$$

Where $E(\frac{1}{2}\pi, k)$, ${}_2F_1(-\frac{1}{2}, \frac{1}{2}; 1 : k^2)$ and $dn(u,k)$ are the incomplete elliptic integral of the second kind, the hypergeometric function, and the Jacobi elliptic function, respectively [119-121].

The complete elliptic integral of the second kind satisfies the following Legendre relation

$$E(k)K'(k) + E'(k)K(k) - K(k)K'(k) = \frac{1}{2}\pi \tag{A.11}$$

Where *K(k),E(k),K'(k)* and *E'(k)*are respectively the complete elliptic integral of the first kind, the complete elliptic integral of the second kind, and the complementary integrals [119-121].

The complete integral of the second kind is related to the complete elliptic integral by the following mathematical expression

$$\frac{dE}{dk} = \frac{E(k) - K(k)}{k} \tag{A.12}$$

To measure the complete elliptic integral of the first and the second kind, we define the parameter *m* satisfying $m \equiv k^2$ [119-121].

Figure A.1 depicts the numerical value of the complete elliptic integrals of the first and second kind.

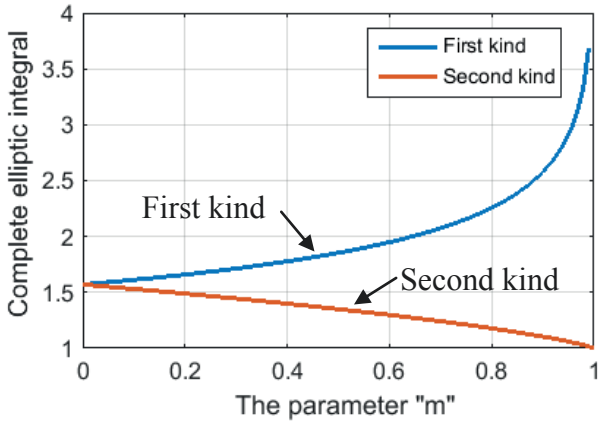

Fig. A.1: Complete elliptic integrals of the first and second kind

References

[1] N. Tesla: ‘Apparatus for transmitting electrical energy’, US patent 1119732 A, December 1914.

[2] S. Stephanie, S. Latifi: ‘Wireless power transmission’, University of Nevada, Department of electrical and computer engineering, Las Vegas, 2011.

[3] S. De Grandis, E. Finzi, C. Lombardi, et al.: ‘A feasibility study of an integral PWR for space applications’, International congress on advances in nuclear power plants, Pittsburgh, USA, June 2004.

[4] E. Finzi, C. Lombardi, L. Summerer: ‘A lunar IPWR: A pre-feasibility study’, International astronautical congress, Valencia, Spain, October 2006.

[5] U. Ortabasi, H. Friedman: ‘Powersphere: a photovoltaic cavity converter for wireless power transmission using high power lasers’, IEEE 4th world conference on photovoltaic energy conference, pp. 4, May 2006.

[6] W. H. Ko, S. P. Liang, C. D. F. Fung: ‘Design of radio-frequency powered coils for implant instruments’, Medical and biological engineering and computing, vol. 15, pp. 634–640, 1977.

[7] J. J. Schlesak, A. Alden, T. Ohno: ‘A microwave powered high altitude platform’, In proceedings of IEEE MTT-S international microwave symposium, pp.283–286, 1988.

[8] M. W. Baker, R. Sarpeshkar: ‘Feedback analysis and design of RF power links for low-power bionic systems’, IEEE Transaction on biomedical circuits and systems, vol. 1, no. 1, pp. 28–38, March 2007.

[9] N. N. Donaldson, T. A. Perkins: ‘Analysis of resonant coupled coils in the design of radio frequency transcutaneous links’, Medical and biological engineering and computing, vol. 21, no. 5, pp. 612–627, September 1983.

[10] C. Liu, A. P. Hu, X. Dai: ‘A contactless power transfer system with capacitively coupled matrix pad’, IEEE Energy conversion congress and exposition (ECCE), pp. 3488–3494, 2011.

[11] C. Liu, A. P. Hu, N. K. C. Nair, et al.: ‘2-D alignment analysis of capacitively coupled contactless power transfer systems’, IEEE Energy conversion congress and exposition (ECCE), pp. 652–657, 2010.

[12] U. M. Jow, M. Ghovanloo: ‘Design and optimization of printed spiral coils for efficient transcutaneous inductive power transmission’, IEEE Transactions on biomedical circuits systems, vol. 1, no. 3, pp. 193–202, September 2007.

[13] A. P. Sample, D. A. Meyer, J. R. Smith: ‘Analysis, experimental results, and range adaptation of magnetically coupled resonators for wireless power transfer’, IEEE Transactions on industrial electronics, vol. 58, pp. 544–554, 2011.

[14] C. Zierhofer, E. Hochmair: ‘High-efficiency coupling-in sensitive transcutaneous power and data transmission via an inductive link’, IEEE Transactions on biomedical engineering, vol. 37, no. 7, pp. 716-722, Jul. 1990.

[15] C. R. Neagu, H. V. Jansen, A. Smith, et al.: ‘Characterization of a planar microcoil for implantable microsystems’, Sensors and actuators A, vol. 62, pp. 599-611, July 1997.

[16] X. Liu, F. Zhang, S. A. Hackworth, et al.: ‘Modeling and simulation of a thin film power transfer cell for medical devices and implants’, IEEE International symposium on circuits and systems, pp.3086–3089, May 2009.

[17] X. T. García, J. Vázquez, P. R. Sánchez: ‘Design, implementation issues and performance of an inductive power transfer system for electric vehicle chargers with series–series compensation’, IET Power electronics, vol. 8, no. 10, pp. 1920–1930, 2015.

[18] F. Musavi, W. Eberle: ‘Overview of wireless power transfer technologies for electric vehicle battery charging’, IET Power electronics, vol. 7, no. 1, pp. 60–66, 2014.

[19] C. S. Wang, O. H. Stielau, G. A. Covic: ‘Design considerations for a contactless electric vehicle battery charger’, IEEE Transactions on industrial electronics, vol. 52, pp. 1308–1314, 2005.

[20] S. Lee, J. Huh, C. Park, et al.: ‘On-line electric vehicle using inductive power transfer system’, IEEE Energy conversion congress and exposition (ECCE), pp. 1598–1601, 2010.

[21] M. Moghaddami, A. Sundararajan, A. I. Sarwat: ‘Sensorless electric vehicle detection in inductive charging stations using self-tuning controllers’, IEEE Transportation electrification conference (ITEC-India), Pune, India, December 2017.

[22] S. Ahn, J. Kim: ‘Magnetic field design for high efficient and low EMF wireless power transfer in on-line electric vehicle’, In Proceedings of the Fifth european conference on antennas and propagation (EUCAP), pp. 3979–3982, 2011.

[23] Q. Xu, H. Wang, Z. Gao, et al.: ‘A novel mat-based system for position-varying wireless power transfer to biomedical implants’, IEEE Transaction on magnetics, vol. 49, no. 8, pp. 4774–4779, 2013.

[24] S. R. Khan, G. Choi: ‘Optimization of planar strongly coupled wireless power transfer system for biomedical applications’, Microwaves and optical technology letters, vol. 58, no. 8, pp. 1861–1866, 2016.

[25] S. Atluri, M. Ghovanloo: ‘Design of a wideband power-efficient inductive wireless link for implantable biomedical devices using multiple carriers’, in Proceedings of IEEE Conference on neural engineering, pp. 533–537, March 2005.

[26] D. Ahn, S. Hong: ‘Wireless power transmission with self-regulated output voltage for biomedical implant’, IEEE Transactions on industrial electronics, vol. 61, no. 5, pp. 2225–2235, May 2014.

[27] V. Boscaino, F. Pellitteri, L. Rosa, et al.: ‘Wireless battery chargers for portable applications: design and test of a high-efficiency power receiver’, IET Power electronics, vol. 6, no. 1, pp. 20–29, 2013.

[28] X. Z. Jian, H. Z. Yu: ‘A novel wireless charging system for movable telephone with printed-circuit-board windings of different structure and shape respectively’, Proceedings of international conference on electrical machines and systems, pp. 1283–1285, Seoul, Korea, 8–11 October 2007.

[29] Y. Jang, M. M. Jovanovic: ‘A contactless electrical energy transmission system for portable-telephone battery chargers’, IEEE Transaction on industrial electronics, vol. 50, no. 3, pp. 520–527, June 2003.

[30] J. Taylor, X. N. Low, J. Casanova et al.: ‘A wireless power station for laptop computers’, IEEE Radio and wireless symposium (RWS), pp. 625–628, 2010.

[31] A. Madhja, S. Nikoletseas, T. P. Raptis: ‘Distributed wireless power transfer in sensor networks with multiple mobile chargers’, Computer networks, vol 80, pp. 89–108, April 2015.

[32] B. Kallel, T. Keutel, O. Kanoun: ‘MISO configuration efficiency in inductive power transmission for supplying wireless sensors’, IEEE 11th International multi-conference on systems, signals & devices, Barcelona, Spain, pp. 1–5, February 2014.

[33] C. Liu, K. Chau, Z. Zhang, et al.: ‘Multiple-receptor wireless power transfer for magnetic sensors charging on Mars via magnetic resonant coupling’, Journal of applied physics, vol.117, pp. 17A743- 17A743-4, 2015.

[34] F. Zhang, J. Liu, Z. Mao, et al.: ‘Mid-Range wireless power transfer and its application to body sensor networks’, Open journal on applied sciences, vol. 2, pp. 35-46, 2012.

[35] S. Y. R. Hui, W. Zhong, C. K. Lee: ‘A critical review of recent progress in mid-range wireless power transfer’, IEEE Transaction on Power Electronics, vol. 29, no. 9, pp. 4500–4511, 2014.

[36] M. Sato, G. Yamamoto, D. Gunji, et al.: ‘Development of wireless in-wheel motor using magnetic resonance coupling’, IEEE Transaction on power electronics, vol. 31, no.7, pp. 5270–5278, 2016.

[37] M. Kiani, M. Ghovanloo: 'An RFID-based closed loop wireless power transmission system for biomedical applications', IEEE Transactions on circuits and systems II: express briefs, vol. 57, no. 4, pp. 260–264, April 2010.

[38] J. Garnica, R. A. Chinga, J. Lin: 'Wireless power transmission: From far field to near field', Proceedings of the IEEE, vol. 101, no. 6, pp. 1321–1331, June 2013.

[39] G. A. Covic, J. T. Boys, M. L. G. Kissin, et al.: 'A three-phase inductive power transfer system for roadway-powered vehicles', IEEE Transaction on industrial electronics, vol. 54, pp. 3370–3378, 2007.

[40] T. Imura, H. Okabe, Y. Hori: 'Basic experimental study on helical antennas of wireless power transfer for Electric Vehicles by using magnetic resonant couplings', IEEE Vehicle power and propulsion Conf. (VPPC), pp. 936–940, 2009.

[41] Z. Yang, W. Liu, E. Basham: 'Inductor modeling in wireless links for implantable electronics', IEEE Transactions on magnetics, vol. 43, no. 10, pp. 3851–3860, Oct. 2007.

[42] D. Fleisch: 'A Student's guide to Maxwell's equations', Cambridge, 2008.

[43] S. Ramo, J. R. Whinnery, T. VanDuzer: 'Fields and waves in communication electronics', 3rd edition, New York: Wiley, 1994.

[44] W. R. Smythe: 'Static and dynamic electricity', 2nd edition, New York: McGraw-Hill, 1950.

[45] R. H. Good: 'Elliptic integrals, the forgotten functions', Eur. J. Phys., vol. 22, pp. 119–126, 2001.

[46] M. Soma, D.C. Galbrath, R. L. White: 'Radio-frequency coils in implantable devices: misalignment analysis and design procedure', IEEE Transaction on biomedical engineering, vol.BME-34, no. 4, pp. 276–282, 1987.

[47] M. Abramowitz, I. A. Stegun (Eds.): 'Elliptic Integrals', 'Handbook of mathematical functions with formulas, graphs, and mathematical tables', (New York: Dover, 9th edn.), pp.587–607, 1972.

[48] E. B. Rosa, F. W. Grover: 'Formulas and tables for the calculation of mutual and self-inductance (revised)', 3rd edition, Bulletin of the bureau of standard, vol. 8, no. 1, US, 1916.

[49] ICNIRP International Commission on Non-Ionizing Radiation Protection: 'Guidelines for limiting exposure to time-varying electric, magnetic, and electro-magnetic fields (Up to 300 GHz)', Health physics, vol. 74, no. 4, pp. 494-522, 1998. January, 7. 2012.

[50] European Communities: 'council recommendation of 12 July 1999 on the limitation of exposure of the general public to electromagnetic fields (0 Hz to 300 GHz)', Official journal of the european communities, L199, pp.59–70, 30-07-1999.

[51] C. H. Durney, H. Massoudi, M. F. Iskander: 'Radio frequency radiation dosimetry handbook', Brooks air force base, TX: U.S. air force school of aerospace, medical division, Reg. No. SAM-TR-85-73, 1985.

[52] R. E. Hamam, A. Karalis, J. Joannopoulos: 'Efficient weakly-radiative wireless energy transfer: An EIT-like approach', Annals of physics, vol. 324, no. 8, pp.1783-1795, 2009.

[53] N. Oodachi, K. Ogawa, h. Kudo, et al.: 'Efficiency improvement of wireless power transfer via magnetic resonance using transmission coil array', IEEE International symposium on antennas and propagation, Spokane, Washington, USA, pp. 1707–1710, July 2011.

[54] J. P. W. Chow, N. Chen, H. S. H. Chung, et al.: 'Misalignment tolerable coil structure for biomedical applications with wireless power transfer', IEEE International conference of the engineering in medicine and biology society, Osaka, pp. 775–778, July 2013.

[55] A. K. RamRakhyani, S. Mirabbasi, M. Chiao: 'Design and optimization of resonance-based efficient wireless power delivery systems for biomedical implants', IEEE Transaction on biomedical circuits and systems, vol. 5, no.1, pp. 48–63, 2011.

[56] X. Li, H. Zhang, F. Peng, et al.: 'Wireless magnetic resonance energy transfer system for micro implantable medical sensors', Sensors, vol. 12, pp.10292–10308, 2012.

[57] S. C. Moon, G. W. Moon: ‘Wireless power transfer system with an asymmetric four-coil resonator for electric vehicle battery chargers’, IEEE transaction on power electronics, vol. 31, no. 10, pp. 6844–6854, 2016.

[58] W. X. Zhong, X. Liu, S. Y. R. Hui: ‘A novel single-layer winding array and receiver coil structure for contactless battery charging systems with free-positioning and localized cha rging features’, IEEE Transaction on industrial electronics, vol. 58, no. 9, pp. 4136–4144, 2011.

[59] D. Ahn, S. Hong: ‘Effect of coupling between multiple transmitters or multiple receivers on wireless power transfer’, IEEE Transaction on industrial electronics, vol. 60, no. 7, pp. 2602–2613, 2013.

[60] S. Kong, B. Bae, D. H. Jung, et al.: ‘An investigation of electromagnetic radiated emission and interference from multi-coil wireless power transfer systems using resonant magnetic field coupling’, IEEE Transaction on microwave theory and techniques, vol. 63, no. 3, pp. 833–846, 2015.

[61] S. Y. R. Hui: ‘Inductive battery charger system with primary transformer windings formed in a multi-layer structure’, U.S. Patent 7 164 255, Jan. 16, 2007.

[62] S. Y. R. Hui, W. C. Ho, X. Liu, et al.: ‘Localized charging, load identification and bi-directional communication methods for a planar inductive battery charging pad’, U.S. Patent 7915858, March 29, 2011.

[63] H. R. Ahn, M. S. Kim, Z. J. Kim: ‘Inductor array for minimising transfer efficiency decrease of wireless power transmission components at misalignment’, Electronics letters, vol. 50 no. 5 pp. 393–394, 2014.

[64] C. Joffe, A. Robkopf, S. Ehrlich, et al.: ‘Design and optimization of a multi-coil system for inductive charging with small air gap’, IEEE Applied power electronics conference and exposition, pp. 1741–1747, Tampa, Florida, March 2016.

[65] Z. Zhang, K. T. Chau: ‘Homogeneous wireless power transfer for move-and-charge’, IEEE transaction on power electronics, vol.30, no. 11, pp. 6213–6220, 2015.

[66] B. Kallel, K. Sasmal, O. Kanoun, et al.: ‘Analytical modeling of multi-coil system for inductive powering of movable wireless low-power devices’, IEEE 12th International multi-conference on systems, signals and devices (SSD'15), Mahdia, Tunisia, March 2015.

[67] K. Sasmal: ‘Energy management for an inductive coil system with detection of the receiving coil’ Master thesis, Chemnitz University of Technology, October 2015.

[68] C. L. W. Sonntag, J. L. Duarte, A. J. M. Pemen: ‘Load position detection and validation on variable-phase contactless energy transfer desktops’, IEEE Energy conversion congress and exposition, pp. 1818–1825, San Jose, USA, 2009.

[69] C. L. W. Sonntag, E. A. Lomonova, J. L. Duarte: ‘Variable-phase contactless energy transfer desktop part I: design’, International conference on electrical machines and systems, pp. 4460–4465, Hankou Wuhan, China, 2008.

[70] J. Albesa: ‘Monitoring switch-type sensors and powering autonomous sensors via inductive coupling. Application to removable seats in vehicles’, PhD thesis, Polytechnic University of Catalonia, 2012.

[71] A. Kurs, A. Karalis, R. Moffatt, et al.: ‘Wireless power transfer via strongly coupled magnetic resonances’, Science, vol. 317, no. 5834, pp. 83–86, 2007.

[72] K. M. Silay, C. Dehollaini, M. Declercq: ‘Improvement of power efficiency of inductive links for implantable devices’, Ph.D. research in microelectronics and electronics, Istanbul, Turkey, pp. 229–232, April 2008.

[73] K. M. Silay, D. Dondi, L. Larcher, et al.: ‘Load optimization of an inductive power link for remote powering of biomedical implants’, IEEE International symposium on circuits and systems, pp. 533–536, Taipei, Taiwan, May 2009.

[74] E. Waffenschmidt: ‘Wireless power for mobile devices’, IEEE 33rd International telecommunications energy conference, pp. 1–9, Amsterdam, Netherlands, 2011.

[75] M. W. Baker, R. Sarpeshkar: ‘Feedback analysis and design of RF power links for low-power bionic systems’, IEEE Transaction on biomedical circuits and systems, vol. 1, no. 1, pp. 28–38, March 2007.

[76] M. Catrysse, B. Hermans, R. Puers: 'An inductive power system with integrated bidirectional data transmission', in Proceedings of Eurosensors XVII, pp. 843–846, September 2003.

[77] R. Harrison: 'Designing efficient inductive power links for implantable devices', in Proceedings of International symposium on circuits and systems, pp. 2080–2083, 2007.

[78] C. Zierhofer, E. Hochmair: 'Geometric approach for coupling enhancement of magnetically coupled coils', IEEE Transactions on biomedical engineering, vol. 43, no. 7, pp. 708–714, July 1996.

[79] M. Pinuela, D. C. Yates, S. Lucyszyn, et al.: 'Maximizing DC-to-load efficiency for inductive power transfer', IEEE transactions on power electronics, vol. 28, no. 5, pp. 2437–2447, May 2013.

[80] E. Waffenschmidt, T. Staring: 'Limitation of inductive power transfer for consumer applications'. European conference on power electronics and applications, pp. 1–10, Barcelona, Spain, September 2009.

[81] W. W. Parker: 'Self induction formulas', Bachelor of science thesis, university of Illinois library, book P22, 1908.

[82] F. W. Grover: 'Inductance calculations: working formulas and tables', Dover publications, Inc., New York, pp.143, 1946.

[83] M. T. Thompson: 'Inductance calculation techniques - Part II: approximations and handbook methods', Power control and intelligent motion, December 1999.

[84] Rayleigh's collected papers, vol. 2, pp. 15, 1881-1919.

[85] H. A. Wheeler: 'Formulas for the skin effect' Proceedings of the institute of radio engineers, vol. 30, no. 9, pp.412–424, September 1942.

[86] H. A. Wheeler: 'Simple inductance formulas for radio coils', Proceedings of the institute of radio engineers, vol. 16, no. 10, pp. 1398-1400, October 1928.

[87] B. B. Babani: ‘Coil design and construction manual’, Bernards LTD, The grampians western gate London, published in July 1960, revised in August 1974

[88] Online source: Coilgun systems, Inductance Equation. Available on: http://www.coilgun.eclipse.co.uk/math_1.html#inductance_equation, accessed on 04.03.2015.

[89] S. Butterworth: ‘Eddy-current losses in cylindrical conductors, with special applications to the alternating current resistance of short coils’, Philosophical transactions of the royal society of London. Series A, containing papers of a mathematical or physical Character, vol. 222, pp. 57–100, 1922.

[90] S. Butterworth: ‘On the Alternating current resistance of single layer coils’, Proceedings of the royal society of London A, vol. 107, pp. 693–715, 1925.

[91] S. Butterworth: ‘Note on the alternating current resistance of single layer coils’, Physical review, vol. 23, pp. 752, 1924.

[92] W. Jackson: ‘Measurements of the high frequency resistance of single layer solenoids’, Journal of the institution of electrical engineers (London), vol. 80, no. 484, pp. 440–445, 1937.

[93] C. A. Balanis: ‘Antenna theory: analysis and design’, 3rd edition, New York: Wiley, 2005.

[94] F. Terman: ‘Radio engineers handbook’ McGraw Hill, 1943.

[95] K. Van Schuylenberd, R. Puers: ‘Inductive powering. Basic theory and applications to biomedical systems’, Springer, 2009.

[96] Online source: Coilgun systems, Coil resistance formula. Available on: http://www.coilgun.eclipse.co.uk/coil_resistance_formula.html, accessed on 04.03.2015.

[97] R. Ericsson: ‘Fundamentals of Power Electronics’, Kluwer academic publications, 2000.

[98] N. Mohan, T. M. Undeland, W. P. Robbins: 'Power electronics converter, applications and design', Media enhanced 3rd edition, 2009.

[99] A. J. Palermo: 'Distributed capacity of single-layer coils', Proceedings of the institute of radio engineers, vol. 22, no. 7, pp. 897–905, July 1934.

[100] R. G. Medhurst: 'H. F. Resistance and self-capacitance of single-layer solenoids', Wireless engineer, pp. 35-43, Feb. 1947.

[101] G. Grandi, M. K. Kazimierczuk, A. Massarini, et al.: 'Stray capacitances of single-layer solenoid air-core inductors', IEEE Transactions on industry applications, vol. 35, no. 5, pp. 1162–1168, September/October 1999.

[102] S. Raju, R. Wu, M. Chan, et al.: 'Modeling of mutual coupling between planar inductors in wireless power applications', IEEE Transaction on power electronics, vol.29, no.1, pp.481–490, January 2014.

[103] M. Soma, D. C. Galbrath, R. L. White: 'Radio-frequency coils in implantable devices: misalignment analysis and design procedure', IEEE Transaction on biomedical engineering, vol. 34, no.4, pp. 276–282, 1987.

[104] E. S. Hochmair, "System optimization for improved accuracy in transcutaneous signal and power transmission," IEEE Transaction on biomedical engineering, vol. 31, no. 2, pp. 177–186, 1984.

[105] G. Bouattour, B. Kallel, O. Kanoun, et al.: 'Comparative study of resonant circuit for power transmission via inductive link', IEEE 12th International multi-conference on systems, signals & devices, Mahdia, Tunisia, pp. 1–6, March 2015.

[106] Y. H. Sohn, B. H. Choi, E. S. Lee, et al.: 'General unified analyses of two-capacitor inductive power transfer systems: equivalence of current-source SS and SP compensations', IEEE Transaction on power electronics, vol. 30, no. 11, pp. 6030–6045, November 2015.

[107] Z. N. Low, J. J. Casanova, P. H. Maier, et al.: 'Method of load/fault detection for loosely coupled planar wireless power transfer system with power delivery tracking', IEEE Transaction on industrial electronics, vol. 57, pp.1478–1486, 2010.

[108] C. L. W. Sonntag, J. L. Duarte, A. J. M. Pemen: ‘Load position detection and validation on variable-phase contactless energy transfer desktops’, IEEE Energy conversion congress and exposition, pp.15–27, 2009.

[109] B. kallel, O. Kanoun, H. Trabelsi, et al.: ‘Sensing movable receiving coils by detection of AC current changes on the primary side of a multi-coil system’, Procedia engineering, vol. 168, pp. 991–994, 2016.

[110] B. Kallel, O. Kanoun, T. Keutel, et al.: ‘Improvement of the efficiency of MISO configuration in inductive power transmission in case of coils misalignment’, 2014 IEEE International instrumentation and measurement technology conference, I2MTC, Montevideo, Uruguay, May 2014.

[111] B. Kallel, O. Kanoun, H. Trabelsi: ‘Large air gap misalignment tolerable multi-coil inductive power transfer for wireless sensors’, IET Power Electronics, vol.9, no.8, pp.1768-1774, 2016.

[112] N. Jamal, S. Saat, Y. Yusmarnita, et al.: ‘Investigations on capacitor compensation topologies effects of different inductive coupling links configurations’, International Journal of power electronics and drive systems, vol. 6, no.2, pp. 274–281, 2015.

[113] M. E. Halpern, D. C. Ng: ‘Optimal tuning of inductive wireless power Links: limits of performance’, IEEE Transaction on circuits and systems I, regular papers, vol. 62, no. 3, pp. 725–732, 2015.

[114] T. Campi, S. Cruciani, F. Palandrani, et al.: ‘Wireless power transfer charging system for AIMDs and pacemakers’, IEEE Transaction on microwave theory and techniques, vol. 64, no. 2, pp. 633–642, 2016.

[115] Y. Liao, X. Yuan: ‘Compensation topology for flat spiral coil inductive power transfer systems’, IET Power electronics, vol. 8, no. 10, pp. 1893–1901, 2015.

[116] W. Zhou, H. Ma: ‘Design considerations of compensation topologies in ICPT system’, IEEE Applied power electronics conference and exposition, pp. 985 – 990, Anaheim, CA, USA, Feb. 2007.

[117] C. Zheng, H. Ma, J. S. Lai, et al.: ‘Design considerations to reduce gap variation and misalignment effects for the inductive power transfer system’, IEEE Transaction on power electronics, vol. 30, no. 11, pp. 6108–6119, 2015.

[118] G. Bouattour, B. kallel, O. Kanoun, et al.: ‘Primary side circuit design for a multi-coil inductive system’, Procedia engineering, vol. 168, pp. 920–923, 2016.

[119] M. Abramowitz, I. A. Stegun: ‘Handbook of mathematical functions with formulas, graphs, and mathematical tables’, 9th printing. New York: Dover, 1972.

[120] D. Zwillinger; ‘Handbook of differential equations’, 3rd edition, Boston, MA: Academic press, p. 122, 1997.

[121] I. S. Gradshteyn, I. M. Ryzhik: ‘Tables of integrals, series, and products’, 6th edition, San Diego, CA: Academic Press, 2000.

List of figures

Chapter 1

Chapter 2

Chapter3

Chapter 4

Chapter 5

Chapter 6

Chapter 7

List of tables

Chapter 5

Chapter 6

Chapter 7

Scientific Reports on Measurement and Sensor Technology

1. Bouchaala, Dhouha (2016)
Investigation of Current Excitation for Personal Health and Biological Tissues Monitoring
ISBN 978-3-941003-96-9
Volltext: http://nbn-resolving.de/urn:nbn:de:bsz:ch1-qucosa-204801

2. Heidary Dastjerdi, Maral (2016)
Ein Beitrag zur Verbesserung der Eigenschaften magnetisch-induktiver Tastspulen
ISBN 978-3-944640-98-3
Volltext: http://nbn-resolving.de/urn:nbn:de:bsz:ch1-qucosa-207628

3. Guermazi, Mahdi (2016)
In-Vitro Biological Tissue State Monitoring based on Impedance Spectroscopy
ISBN 978-3-96100-003-6
Volltext: http://nbn-resolving.de/urn:nbn:de:bsz:ch1-qucosa-206710

4. Viehweger, Christian (2017)
Modellbasiertes Energiemanagement für die intelligente Steuerung solarversorgter drahtloser Sensorsysteme
ISBN 978-3-96100-022-7
Volltext: http://nbn-resolving.de/urn:nbn:de:bsz:ch1-qucosa-224040

5. Gerlach, Carina (2017)
Dispersionsoptimierung von Kohlenstoffnanoröhren für die Herstellung von Polymer-Komposit-Drucksensoren
ISBN 978-3-96100-025-8
Volltext: http://nbn-resolving.de/urn:nbn:de:bsz:ch1-qucosa-226222

6. Sanli, Abdulkadir (2018)
Synthesis and Characterization of Strain Sensitive Multi-walled Carbon Nanotubes/Epoxy based Nanocomposites
ISBN 978-3-96100-047-0
Volltext: http://nbn-resolving.de/urn:nbn:de:bsz:ch1-qucosa-233763

7. Weber, Christian (2018)
Entwicklung eines Verfahrens zur Anhaftungserkennung und Trennung von Einflussgrößen bei kapazitiven Näherungsschaltern mit Hilfe der Impedanzspektroskopie

ISBN 978-3-96100-056-2
Volltext: http://nbn-resolving.de/urn:nbn:de:bsz:ch1-qucosa2-234856

8. Benchirouf, Abderrahmane (2018)
Carbonaceous Nanofillers and Poly (3,4- ethylenedioxythiophene) Poly(styrenesulfonate) Nanocomposites for Wireless Sensing Applications
ISBN 978-3-96100-068-5
Volltext: http://nbn-resolving.de/urn:nbn:de:bsz:ch1-qucosa2-319037

9. Naifar, Slim (2019)
Model based Design of a Magnetoelectric Vibration Converter from Weak Kinetic Sources
ISBN 978-3-96100-079-1
Volltext: http://nbn-resolving.de/urn:nbn:de:bsz:ch1-qucosa2-327748

10. Bouhamed, Ayda (2019)
Investigation of Stress Distribution and Adhesion Effects of Strain Sensitive Epoxy/MWCNT Nanocomposite Films
ISBN 978-3-96100-080-7
Volltext: http://nbn-resolving.de/urn:nbn:de:bsz:ch1-qucosa2-327817

11. Bradai, Sonia (2019)
Design and Modelling of a Novel Hybrid Vibration Converter based on Electromagnetic and Magnetoelectric Principles
ISBN 978-3-96100-081-4
Volltext: http://nbn-resolving.de/urn:nbn:de:bsz:ch1-qucosa2-327874

12. Kallel, Bilel (2019)
Design of Inductive Power Transmission System for Low Power Application with Movable Receiver and Large Air Gap
ISBN 978-3-96100-083-8
Volltext: http://nbn-resolving.de/urn:nbn:de:bsz:ch1-qucosa2-329759